REPORT DOCUMENTATION PAGE

AFRL-SR-AR-TR-04-

0223

1. REPORT DATE (DD-MM-YYYY)	2. REPORT TYPE	3. DATES COVERED (From - To)
29-03-2004	Final Technical	1-1-2001 to 31-12-2003

4. TITLE AND SUBTITLE
Optimal Large Eddy Simulation of Turbulence

Final Report for Contract F49620-01-1-0181

5a. CONTRACT NUMBER
F49620-01-1-0181

5b. GRANT NUMBER
F49620-01-1-0181

5c. PROGRAM ELEMENT NUMBER

6. AUTHOR(S)
R. D. Moser

S. Balachandar

R. J. Adrian

5d. PROJECT NUMBER

5e. TASK NUMBER

5f. WORK UNIT NUMBER

7. PERFORMING ORGANIZATION NAME(S) AND ADDRESS(ES)
University of Illinois at Urbana-Champaign
Department of Theoretical and Applied Mechanics, 216 Talbot
104 S. Wright, Urbana, IL 61801

8. PERFORMING ORGANIZATION REPORT NUMBER

9. SPONSORING / MONITORING AGENCY NAME(S) AND ADDRESS(ES)
AFOSR/NA
4015 Wilson Boulevard
Arlington, VA 22203-1954

10. SPONSOR/MONITOR'S ACRONYM(S)

11. SPONSOR/MONITOR'S REPORT NUMBER(S)

12. DISTRIBUTION / AVAILABILITY STATEMENT
Unrestricted

13. SUPPLEMENTARY NOTES

20040426 070

14. ABSTRACT
Optimal LES modeling is a new approach to the development of subgrid models of turbulence. It has been found to produce accurate LES simulations when based on reliable statistical information. Now, the primary effort in optimal model development is the determination of this statistical information from theoretical considerations, with minimal empirical input. The validity of the theoretically determined statistics is being tested against experimental and DNS data. When small-scales are isotropic, Kolmogorov theory, the quasi-normal approximation and a dynamic procedure allow optimal models to be constructed with no empirical input. Such models have been found to perform well, though the dynamic procedure has not yet been tested in this context. Tests using channel flow DNS show that, except for a region very near the wall, the quasi-normal approximation is valid. Further, for the log-region, a representation for the anisotropy and inhomogeneity of the statistics is being developed. Thus, the above modeling approach can be adapted to near-wall turbulence, except for the thin viscous region. To handle this wall layer, a filtered boundary optimal LES model is being developed and tested.

15. SUBJECT TERMS
Turbulence, Large Eddy Simulation, Turbulence Modeling

16. SECURITY CLASSIFICATION OF:			17. LIMITATION OF ABSTRACT	18. NUMBER OF PAGES	19a. NAME OF RESPONSIBLE PERSON
a. REPORT	b. ABSTRACT	c. THIS PAGE			Robert D. Moser
U	U	U		71	19b. TELEPHONE NUMBER (include area code) 217-244-5707

DISTRIBUTION STATEMENT A
Approved for Public Release
Distribution Unlimited

OPTIMAL LARGE EDDY SIMULATION OF TURBULENCE

Final Report for Contract F49620-01-1-0181

R. D. Moser, S. Balachandar and R. J. Adrian
Department of Theoretical and Applied Mechanics
University of Illinois, Urbana-Champaign

1 Motivation and Objectives

One of the most promising techniques for the prediction of turbulent flows is that of Large Eddy Simulation (LES), in which an under-resolved representation of the turbulence is simulated numerically by modeling the effects of the unresolved small-scales on the simulation. Such simulations have been applied in several flows with reasonable success. However, there are several outstanding problems that need to be addressed before LES can fulfill its promise as a tool for turbulence prediction in engineering flows. The most serious problems limiting the usefulness of LES is the representation of turbulence near walls and other strong inhomogeneities and the dependence of models on the filter and/or numerical discretization. Also important are the treatment of inhomogeneous filters and the lack of understanding of the modeling errors and their impact.

The optimal LES formulation [9, 10] provides a rigorous framework in which to address these issues and to develop and analyze LES models and simulations. The objective of this research is to develop new LES modeling techniques to address the difficulties cited above by using the optimal LES formulation.

2 Background & Approach

The starting point for the development of LES is the definition of a spatial filter $\tilde{\cdot}$, which can be applied to the Navier-stokes equations to obtain an equation for the filtered velocity $\tilde{u}_i$:

$$\frac{\partial \tilde{u}_i}{\partial t} = -\frac{\partial \tilde{u}_i \tilde{u}_j}{\partial x_j} - \frac{\partial \tilde{p}}{\partial x_i} + \frac{1}{\mathrm{Re}} \frac{\partial^2 \tilde{u}_i}{\partial x_j \partial x_j} + M_i, \tag{1}$$

Where M_i is the sub-grid model (force) term, which includes the divergence of the sub-grid stress as well as terms that arise when the filter does not commute with differentiation. The problem in LES of course is to model M_i. A very important result of our research [9] is that an LES w will match the one-time statistics of filtered turbulence $\tilde{u}$ if and only if the model $m_i(w)$ of M_i is given by

$$m_i(w) = \langle M_i(u) | \tilde{u} = w \rangle \tag{2}$$

This model also minimizes the difference between M_i and m_i (in the mean-square sense), and so this model has all the properties that one could ask of a sub-grid model. We therefore call it the ideal sub-grid model.

Unfortunately, the conditional average in (2) cannot practically be determined, since the conditions are that the entire filtered velocity field match the entire LES field. However, it can be estimated using stochastic estimation [2] which is a well-established technique for estimating conditional averages. The result is a class of estimation based LES models as first proposed by Adrian [1] To perform stochastic estimation one requires large quantities of two-point correlation data. For example, in linear estimation one needs $\langle \tilde{u}_j(\mathbf{x}')\tilde{u}_k(\mathbf{x}'')\rangle$ and $\langle M_i(\mathbf{x})\tilde{u}_k(\mathbf{x}'')\rangle$.

To obtain the required data, we resort to direct numerical simulation (DNS), which is limited to low Reynolds numbers, and experimental velocity field measurements, which are currently limited to two-dimensional measurements. By using reliable empirical data for the required correlations, the optimal modeling approach can be developed, tested and validated in the absence of uncertainties associated with modeling the correlations theoretically. Once the formulations has been developed and validated, truly predictive, generally applicable models can be developed based on theoretical approximations to the required correlations.

3 Supported Research

To pursue the objectives defined above, a number of research activities were pursued under the current grant. These are described briefly below and in more detail in the following subsections, and the referenced publications.

1. **Correlation Data Acquisition**: To develop and test the optimal LES formulation, extensive multi-point correlation information was needed. Since the wall-modeling problem is of prime importance, we concentrate on near-wall correlations from turbulent channel flow. Data was generated both experimentally, using a novel PIV technique [6], and numerically, using direct numerical simulation (DNS).[8] This data is also being used to formulate and check theoretical descriptions of the two-point correlation (see item 5 below).

2. **Development and Testing of Optimal LES Formulations**: It had previously been shown that optimal LES based on Fourier cut-off filters performed very well. But, Fourier cutoff filters are not practical for use in complex geometries. So, an optimal LES formulation based on finite volume filters was developed and tested (see [16] and Appendix A). Further, for several reasons, it would be advantageous to develop optimal models based on finite difference discretizations, rather than finite volume, and such formulations have also been developed and tested.

3. **Filtered Wall Treatment**: One of the difficulties associated with wall-bounded flows is that if one sharply defines the wall and the no-slip boundary condition, it requires that the filter be extremely inhomogeneous near the wall. This causes a number of problems. Alternatively, the boundary can itself be filtered, producing the LES analog of an embedded boundary method. Wall models for this approach have been developed using optimization techniques.

4. **Theoretical Optimal LES for Isotropic Turbulence**: To eliminate the need for extensive empirical input to optimal modeling, the required correlations need to be determined theoretically. Using a combination of Kolmogorov scaling, small-scale isotropy, the quasi-normal approximation and a dynamic approach, theoretical optimal LES models for the finite volume formulation were developed. The resulting models are valid provided the Reynolds number is sufficiently large, and small-scale isotropy is a valid approximation. These models have also been tested.

5. **Theoretical Correlations for Wall-Bounded Turbulence**: Near walls, the assumption of small-scale isotropy and filter widths in the inertial range are invalid. A representation for the inhomogeneity and anisotropy of the multi-point correlations in wall-bounded turbulence (particularly in the log-layer) is needed for use in the development of optimal models. Such a representation is being pursued based on the developments by Procaccia's group[4, 3, 11], the similarity forms of Oberlack,[13] consistency with the Navier-Stokes equations and the quasi-normal approximation. Further, the DNS and experimental data described in (1) are being used for guidance.

3.1 Correlation Data Acquisition

To acquire the correlation data needed to address the modeling of wall-bounded turbulence, a new DNS of turbulent channel flow, and a laboratory experiment on turbulent channel flow were conducted.

3.1.1 Channel Flow DNS

A turbulent channel flow at $Re_\tau = 940$ in a very large spatial domain ($L_x = 8\pi h$, $L_z = 3.25\pi h$, where h is the channel half-width) was conducted. The large spatial domain allows more reliable statistics to be gathered, and facilitates the study of large length-scale phenomena known to be present in the near-wall region. Further, this large-domain channel provides a valuable validation target for wall-bounded turbulence LES. In particular the capture of long wavelength phenomena by the LES can be assessed.

The simulations were performed at the San Diego Supercomputer facility and at the DOD HPC facility at NAVO. The simulation produced a library of approximately 100 DNS fields which are currently being post-processed for a number of purposes, including the correlation representation discussed in section 3.5. Furthermore the data is in the process of being made available to researchers in the turbulence community through the website `http://davinci.tam.uiuc.edu`. Finally, the first paper published on the data has appeared [8].

3.1.2 Channel Flow Experiments

To support the development of optimal LES models, detailed PIV measurements of turbulent channel flow were made. In addition to standard velocity measurements, which are used to determine

the multi-point velocity correlations required in the formulation velocity time-derivative measurements were made using a novel PIV technique, and correlations of the time-derivative were computed also to support modeling of LES dynamics. The experimental technique is described briefly below, and in more detail in [6].

Measurements of instantaneous time- and bulk-convective-derivative fields have been made over a broad range of Reynolds numbers to support the development of optimal LES models. A two-CCD-camera PIV arrangement was designed to acquire large ensembles of time-resolved velocity data at moderate-to-high Reynolds numbers in the streamwise–wall-normal plane of fully developed turbulent channel flow. The cameras are focused on the same field of view (temporal derivative) or shifted in the streamwise direction (bulk convective derivative), and the acquisition of the second is delayed in time by τ (typically a fraction of the Kolmogorov time scale, t_k), to allow the computation of the associated time derivative. Polarization filtering is used to separate the particle images viewed by each camera. Rigorous techniques have been developed to compensate for the noise inherent in the PIV velocity measurements.

Recent effort has focused on the bulk convective derivative because comparison of the streamwise spectra of $\partial u_i/\partial t$ and $\mathrm{D}u_i/\mathrm{D}t$ indicates that, at all scales, the temporal derivative of velocity is dominated by bulk convection, not evolution. These convection effects mask the underlying dynamics of interest in optimal LES development.

Reynolds-number scaling of the bulk convective derivative statistics has been assessed for both unfiltered and filtered data. The intent of this analysis is to determine the most appropriate time scale for achieving Reynolds-number similarity in the bulk convective derivative statistics. Figure 1(a) shows the root-mean-square of $\mathrm{D}_b v/\mathrm{D}t$ (unfiltered) scaled with the friction velocity (u_*) and the outer time scale ($t_o = u_*/h$) as a function of wall-normal position ($\mathrm{D}_b v/\mathrm{D}t$ has the strongest Reynolds number dependence). Near the wall, this scaling does not remove the strong Reynolds-number dependence in the RMS, but further from the wall ($y/h > 0.4$), this scaling works well. This is the best scaling found for this quantity. In figure 1(b) the RMS time derivative of the filtered fields is shown (top-hat filter of width $\Delta = 0.2h$). The strong Reynolds-number dependence noted in the unfiltered profiles is now absent. Scaling of the two-point correlation functions of $\mathrm{D}_b u_i/\mathrm{D}t$ yields similar results: unfiltered correlations show Reynolds-number dependence when scaled with t_o, while filtering removes this dependence, yielding a consistent scaling of the correlations. It is the time derivative of the filtered velocity that is of interest in LES, so the scalings based upon t_o are appropriate for the optimal LES formulation. This information will be used to develop a comprehensive Reynolds-number-scaling framework for extending optimal formulations to higher Reynolds numbers.

3.2 Development and Testing of Optimal LES Formulations

A finite volume formulation of optimal LES was developed previously [10], but had not been tested. This formulations has been tested and refined. Also, it was recognized that a finite difference formulation of optimal LES would be advantageous, and this has also been developed and tested, though more work on refinement remains to be done. These activities are discussed below.

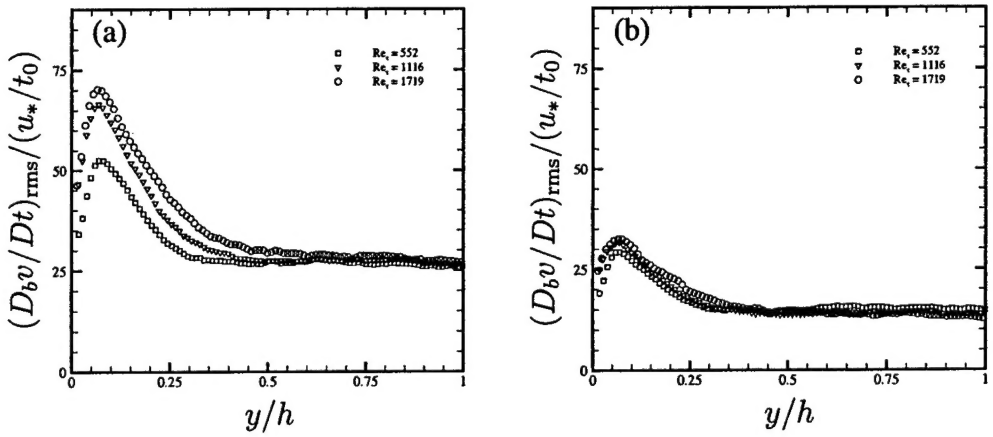

Figure 1: Scaling of $D_b v/Dt_{RMS}$ profiles with u_* and t_o. (a) Unfiltered, (b) Filtered.

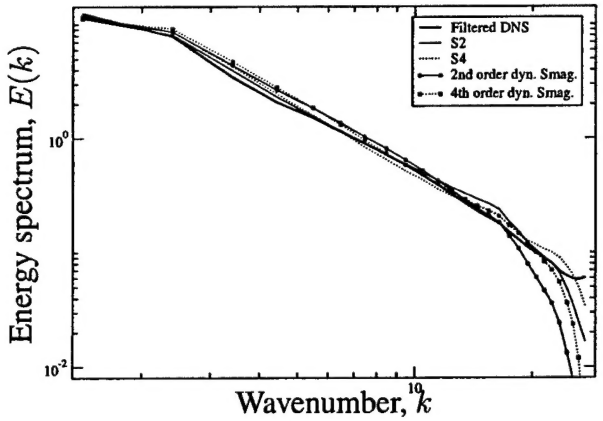

Figure 2: Three-dimensional energy spectrum E(k), filtered DNS compared with *optimal* LES with 2-cell (S2) and 4-cell (S4) stencils and dynamic Smagorinsky.

3.2.1 Finite Volume Optimal LES

In the finite volume LES formulation of Langford [10], the "filter" is defined to be the average over discrete volumes. As in a standard finite volume numerical discretization, the evolution of the volume averaged velocity requires the evaluation of momentum fluxes through the boundaries of each discrete volume. In the LES context, these cannot be estimate using standard finite volume reconstruction techniques because the cell size (filter width) is not small compared to the smallest scales over which the velocity varies (the Kolmogorov scale). In short, the velocity is not smooth on the scale of the volumes. Instead, we use the optimal LES technique to estimate the fluxes. Thus, the usual convergence considerations normally used to develop numerical methods are replaced with the requirement that the flux estimates be consistent with the statistical properties of turbulence.

This finite volume LES formulation was tested in isotropic turbulence using DNS data to determine the required correlations. The results are quite good as shown by the spectra plotted in figure 3.2.1. It was found that a simple stencil in which two cells on either side of a face are used to estimate

the flux is adequate to yield very good results. It was also found that a staggered grid formulation produces a much better LES. The details of this study are provided in [16], a preprint of which is included as Appendix A.

3.2.2 Finite Difference Optimal LES

One issue which must always be addressed in LES is that it is generally not the filtered turbulence that is of interest, but rather the real unfiltered turbulence. Thus, when interpreting LES results, it is necessary to account for the missing small-scales. For example, the turbulent kinetic energy will be missing the contribution from the unresolved small scales.

If one is interested in statistical correlations of the velocity, then an LES definition that preserves the statistics of the velocity would be particularly useful, since it would avoid these difficulties. One such LES filter definition is just a sampling of the turbulence on a grid of points. This is a non-invertible linear transformation that can be used as an LES "filter," though it does not have the usual filter properties of eliminating small-scale fluctuations. Indeed, such a mapping can be considered to exhibit aliasing of the small scales. None-the-less, the ability to preserve velocity statistics in this formulation make it an attractive target for LES development.

The evolution equations for the point-sampled velocity are given by

$$\frac{\partial u^{\mathbf{j}}_i}{\partial t} = - \left. \frac{\partial u_i u_k}{\partial x_k} \right|^{\mathbf{j}} - \left. \frac{\partial p}{\partial x_i} \right|^{\mathbf{j}} + \nu \left. \frac{\partial^2 u_i}{\partial x_k \partial x_k} \right|^{\mathbf{j}} \tag{3}$$

where $\mathbf{j}$ is the index for the grid of points. Note that the terms on the right hand side all involve spatial derivatives, which cannot be directly evaluated from the point sampled fields. Because the grid spacing is assumed to be large compared to the smallest turbulence scale, the usual finite difference approximations of the derivative are invalid. Instead, we use optimal LES modeling to estimate these derivatives. This is very like the finite volume formulation, though we are estimating derivatives in this case, rather than fluxes.

There were several subtleties that needed to be addressed in developing the optimal estimates of the derivatives. First among these is that the nonlinear term is energy conserving in this formulation. All energy dissipation occurs through the viscous term. It was necessary for stability and robustness that the estimated nonlinear term be constrained to be energy conserving as well. This was easily accommodated as part of the estimation procedure. Another issue is the enforcement of continuity. The presence of significant aliasing in the LES filter definition makes continuity a very weak constraint on the point sampled velocity. Thus, imposing a continuity constraint on the sampled velocity is apparently not valid. But the pressure must still be determined. For our preliminary studies, an approximate continuity constraint was applied and the pressure was determined from this constraint. Better approaches are being explored.

A preliminary result for the spectrum of the sampled velocity is shown in figure 3, along with that for the sampled DNS of isotropic turbulence. The results are not nearly as impressive as the finite volume results discussed above, but at least part of this can be attributed to the treatment of continuity. The finite difference optimal LES approach is continuing to be refined.

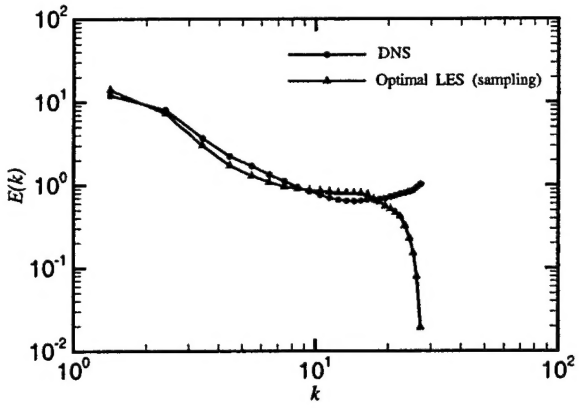

Figure 3: Three dimensional energy spectrum in forced isotropic turbulence with a point-sampled LES filter. Shown are filtered DNS and LES results.

3.3 Filtered Wall Treatment

It was pointed out by Das & Moser[7] that the wall of a wall bounded flow could be filtered to avoid the use of strongly inhomogeneous filters near the wall. In this approach, a homogeneous (or nearly homogeneous) filter is applied to an extended domain including a region exterior to the wall in which $u = 0$. When such a filter is applied to the Navier-Stokes equations (extended in to the interior), the result is

$$\frac{\partial \tilde{u}_i}{\partial t} + \tilde{u}_j \frac{\partial \tilde{u}_i}{\partial x_j} = -\frac{\partial \tilde{p}}{\partial x_i} + \frac{1}{Re} \frac{\partial^2 \tilde{u}_i}{\partial x_j \partial x_j} + b_i + \frac{\partial \tau_{ij}}{\partial x_j} \tag{4}$$

where b_i is the boundary term arising from the filtering of the boundary and τ_{ij} is the usual subgrid stress term. The boundary term is expressed as

$$b_i(\mathbf{x}) = \int_{\partial R} \sigma_{ij}(\mathbf{x}') n_j G(\mathbf{x} - \mathbf{x}')\, d\mathbf{x}'$$

where σ is the stress at the boundary, including pressure and viscous stress, ∂R is the boundary of the fluid region R and n_j is the unit normal to the boundary. To determine the stresses, we note that the velocities should remain zero exterior to the flow domain. The stresses can thus be determined to minimize the velocities in the exterior. In particular, we minimize the cost function: $E = \int |\tilde{u}_i|^2 + \alpha \left| \frac{\partial \tilde{u}_i}{\partial t} \right|^2 dy$, where α is a numerical constant selected to be of order Δt^2.

To test this approach, a filtered boundary simulation of the turbulence in a channel at $Re_\tau = 180$ was performed, with no filtering in the horizontal directions, and a Fourier cutoff filter with $k_c = 371/\delta$ in the wall-normal direction ($\Delta y^+ = 1.5$). This is a sufficiently fine filter that the primary effect is to smear the boundaries, so it could be considered to be a filtered-boundary DNS. The results of this simulation are compared to those of [12] in figure 4, and the agreement is excellent.

These results indicate that the filtering and wall-modeling approach are viable, at least in the context of a well resolved simulation. However, the real application for this approach is in LES, where the filter width will be large in wall units. In this case, the wall model must represent significantly more of the near-wall physics, particularly the near-wall production process. To evaluate

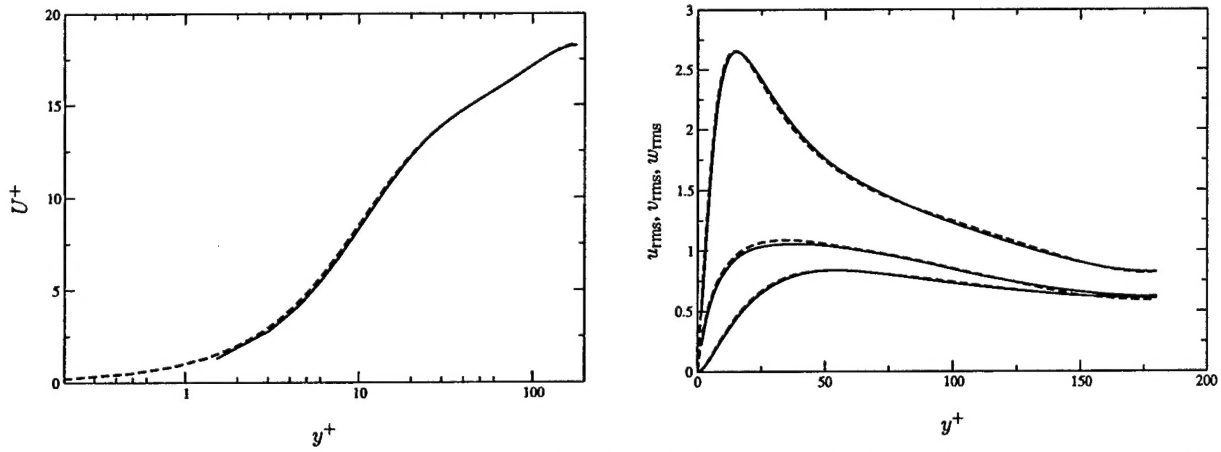

Figure 4: Mean velocity (left) and rms velocities (right) in a turbulent channel at $Re_\tau = 180$; – – –, DNS of [12]; ——filtered boundary DNS using a Fourier cutoff filter with $k_c = 371/\delta$ ($\Delta y^+ = 1.5$). On the right, streamwise (top curves), spanwise (middle curves) and wall-normal (lower curves) rms velocities are shown.

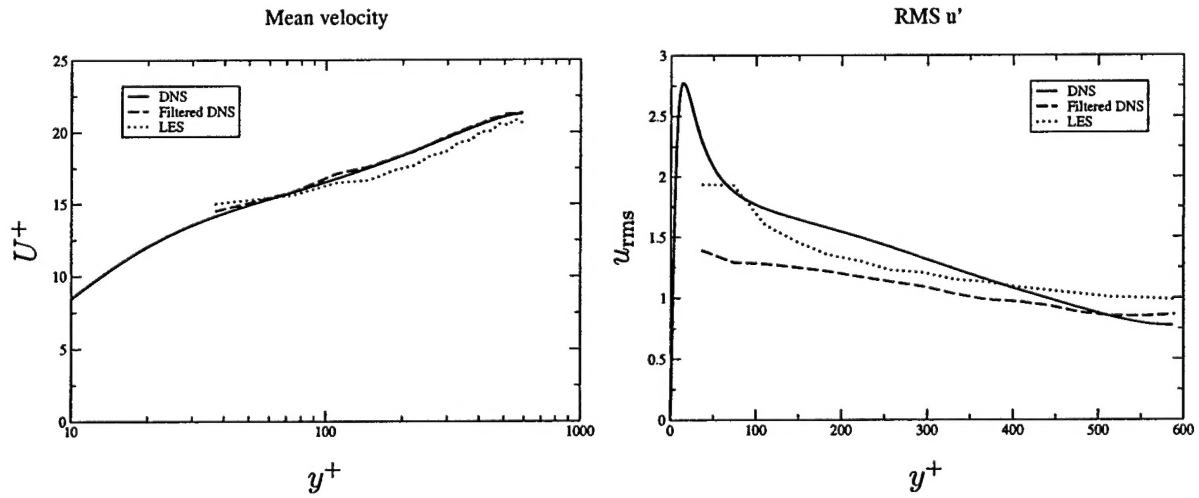

Figure 5: Mean velocity and streamwise rms velocity for LES of channel flow at $Re_\tau = 590$. with Fourier cutoff filters in a spatial directions, thus the walls are also filtered. Shown are the DNS data, the filtered DNS and the LES. Filter widths were: $\Delta_x^+ = 116$, $\Delta_y = 37^+$ and $\Delta_z^+ = 58$.

the ability of the model described above to represent the near-wall process, an channel flow LES was formulated using a Fourier cutoff filter in the wall normal direction, in addition to the homogeneous directions. In plus units the filter widths in the streamwise wall-normal and spanwise directions were $\Delta_x^+ = 116$, $\Delta_y = 37^+$ and $\Delta_z^+ = 58$. The Reynolds number was $Re_\tau = 590$, the same case investigated by Voelker *et al*[15]. An optimal LES model based on the DNS data of [12] was used for the interior, with the same formulation suggested by Voelker *et al.* The wall treatment discussed above was also used. The results are shown in figure 5. The mean velocity is in only fair agreement with the filtered DNS data, and the rms streamwise velocity is systematically over-predicted, particularly near the wall.

It appears that these shortcomings arise because the wall model is optimized to minimize "leakage" of energy and momentum into the exterior, rather than the transport of energy (or Reynolds stress) into the fluid domain, as suggested by the results of Voelker. Both these requirements are important, so a hybrid approach in which both are minimized simultaneously is being developed.

3.4 Theoretical Optimal LES for Isotropic Turbulence

We seek to develop the correlations required to do finite volume LES analytically based on the assumption of a Kolmogorov inertial range and standard two-point modeling assumptions, particularly the quasi-normal approximation. The finite volume optimal LES is selected as a target here because the goal is a generally applicable modeling approach, which makes spectral representations and filters inappropriate.

In the finite volume optimal LES formalism, we need to estimate the integrated fluxes through a surface in terms of the velocities averaged over discrete volumes, and these estimates must be at least quadratic to represent the Navier-Stokes-like terms of the LES. Thus, our estimate is of the form:

$$\int_s u_i(\mathbf{x}) u_s(\mathbf{x})\, d\mathbf{x} = \sum_v L_{ij}(s,v) \int_v u_j(\mathbf{x})\, d\mathbf{x} \tag{5}$$

$$+ \sum_{v1,v2} Q_{ijk}(s,v_1,v_2) \int_{v_1} u_j(\mathbf{x}^1)\, d\mathbf{x}^1 \int_{v2} u_k(\mathbf{x}^2)\, d\mathbf{x}^2 \tag{6}$$

where s is a surface (volume face) and v a volume, and u_s is the (outward directed) component of u normal to the surface s. To determine the estimation coefficients L and Q, we solve a system of equations in terms of the integrated multi-point correlations:

$$I^1_{li}(v',s) = \sum_v L_{ij}(s,v) I^2_{lj}(v',v) + \sum_{v_1,v_2} Q_{ijk}(s,v_1,v_2) I^3_{ljk}(v',v_1,v_2) \tag{7}$$

$$I^4_{lmi}(v'_1,v'_2,s) = \sum_v L_{ij}(s,v) I^3_{lmj}(v'_1,v'_2,v) + \sum_{v_1,v_2} Q_{ijk}(s,v_1,v_2) I^5_{lmjk}(v'_1,v'_2,v_1,v_2) \tag{8}$$

where the integrated correlations I^1 to I^5 are given by

$$I^1_{li}(v',s) = \int_{v'} \int_s \langle u_l(\mathbf{x}') u_i(\mathbf{x}) u_s(\mathbf{x}) \rangle\, d\mathbf{x}\, d\mathbf{x}' \tag{9}$$

$$I^2_{lj}(v',v) = \int_{v'} \int_v \langle u_l(\mathbf{x}') u_j(\mathbf{x}) \rangle\, d\mathbf{x}\, d\mathbf{x}' \tag{10}$$

$$I^3_{ljk}(v', v_1, v_2) = \int_{v'}\int_{v_1}\int_{v_2} \langle u_l(\mathbf{x}')u_j(\mathbf{x}^1)u_k(\mathbf{x}^2)\rangle \, d\mathbf{x}^2 \, d\mathbf{x}^1 \, d\mathbf{x}' \quad (11)$$

$$I^4_{lmij}(v'_1, v'_2, s) = \int_{v'_1}\int_{v'_2}\int_{s} \langle u_l(\mathbf{x}^{1\prime})u_m(\mathbf{x}^{2\prime})u_i(\mathbf{x})u_s(\mathbf{x})\rangle \, d\mathbf{x} \, d\mathbf{x}^{2\prime} \, d\mathbf{x}^{1\prime} \quad (12)$$

$$I^5_{lmjk}(v'_1, v'_2, v_1, v_2) = \int_{v'_1}\int_{v'_2}\int_{v_1}\int_{v_2} \langle u_l(\mathbf{x}^{1\prime})u_m(\mathbf{x}^{2\prime})u_j(\mathbf{x}^1)u_k(\mathbf{x}^2)\rangle \, d\mathbf{x}^2 \, d\mathbf{x}^1 \, d\mathbf{x}^{2\prime} \, d\mathbf{x}^{1\prime} \quad (13)$$

Thus, there are three correlation tensors needed to determine the estimation coefficients:

$$R_{ij}(\mathbf{r}^1) = \langle u_i(\mathbf{x})u_j(\mathbf{x}^1)\rangle \quad (14)$$

$$T_{ijk}(\mathbf{r}^1, \mathbf{r}^2) = \langle u_i(\mathbf{x})u_j(\mathbf{x}^1)u_k(\mathbf{x}^2)\rangle \quad (15)$$

$$F_{ijkl}(\mathbf{r}^1, \mathbf{r}^2, \mathbf{r}^3) = \langle u_i(\mathbf{x})u_j(\mathbf{x}^1)u_k(\mathbf{x}^2)u_l(\mathbf{x}^3)\rangle, \quad (16)$$

where we have used homogeneity to express the dependence of the correlation on location differences, $\mathbf{r}^i = \mathbf{x} - \mathbf{x}^i$.

3.4.1 Correlations

To determine these correlations, we can make use of the isotropy of the tensors, and we will assume that all the spatial separations are small enough to be in the Kolmogorov inertial range of an infinite Reynolds number isotropic turbulence. From this assumption, we can determine the second and third-order longitudinal structure functions:

$$S2(r^1) = \langle (u_\parallel(\mathbf{x}) - u_\parallel(\mathbf{x}^1))^2\rangle = C_1\epsilon^{2/3}(r^1)^{2/3} \quad (17)$$

$$S3(r^1) = \langle (u_\parallel(\mathbf{x}) - u_\parallel(\mathbf{x}^1))^3\rangle = -\frac{4}{5}\epsilon r^1 \quad (18)$$

where $r^i = |\mathbf{r}^i|$ is the magnitude of the separation vector, $u_\parallel$ is the velocity component in the direction of the separation vector and C_1 is the Kolmogorov constant.

The structure function relations along with isotropy allow us to determine two useful correlations. First, the most general isotropic two-point correlation R_{ij} that is consistent with (17) is given by

$$R_{ij}(\mathbf{r}^1) = u^2\delta_{ij} + \frac{C_1}{6}\epsilon^{2/3}(r^1)^{-4/3}(r^1_i r^1_j - 4(r^1)^2\delta_{ij}) \quad (19)$$

Similarly, $S3$ is related to the third-order two-point correlation:

$$b_{ijk}(\mathbf{r}^1) = \langle u_i(\mathbf{x})u_j(\mathbf{x})u_k(\mathbf{x}^1)\rangle = T_{ijk}(0, \mathbf{r}^1). \quad (20)$$

and the most general isotropic form consistent with (18) and continuity is:

$$b_{ijk}(\mathbf{r}^1) = \frac{\epsilon}{15}\left(\delta_{ij}r^1_k - \frac{3}{2}(\delta_{ik}r^1_j + \delta_{jk}r^1_i)\right) \quad (21)$$

This is precisely the correlation needed for the integral I^1 (9). However, the more general third-order three-point correlation is needed for I^3 (11). And the fourth order four-point correlation is

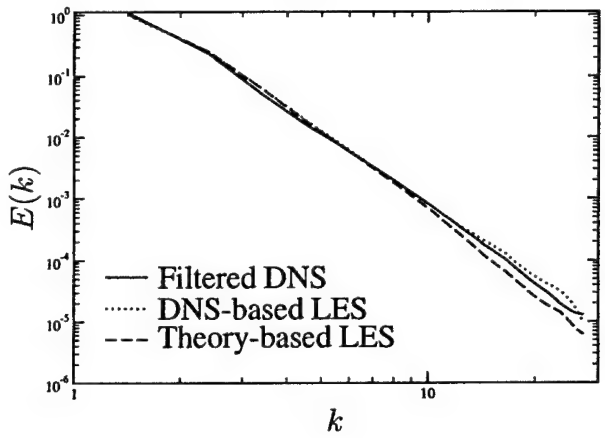

Figure 6: Three-dimensional energy spectrum E(k), filtered DNS compared with *Optimal* LES with 4-cell stencils, developed from theory and from DNS statistical data.

needed for I^4 (12) and I^5 (13). Further modeling assumptions will be required. Particularly, the quasi-normal approximation can be used to determine F_{ijkl} in terms of R_{ij}. The result is:

$$F_{ijkl}(\mathbf{r}^1, \mathbf{r}^2, \mathbf{r}^3) = R_{ij}(\mathbf{r}^1)R_{kl}(\mathbf{r}^3 - \mathbf{r}^2) + R_{ik}(\mathbf{r}^2)R_{jl}(\mathbf{r}^3 - \mathbf{r}^1) + R_{il}(\mathbf{r}^3)R_{jk}(\mathbf{r}^2 - \mathbf{r}^1). \quad (22)$$

While it is commonly used, the quasi-normal approximation has had mixed success in turbulence modeling. Particularly, when used as a model to close the third-order spectrum equations, the quasi-normal approximation leads to an unrealizable energy spectrum. The reason is that the small errors in the quasi-normal approximation accumulate, and realizability of the energy spectrum is sensitive. Fortunately, in the current case, there is no analog to the realizability constraint. Our model is for the filtered fluctuating velocity equation, which can be used to determine the spectrum directly in a way that is inherently realizable (because it is computed from the velocities). Whether the errors in the quasi-normal approximation are significant for the current purposes can only be determined by testing the resulting models.

The third-order three-point correlation is problematic. It cannot be determined theoretically from the considerations discussed above. Instead we observe that I^3 (as well as I^2 and I^5) can be recast as a correlation among the LES state variable (volume averaged velocities). Thus it is possible to determine I^2, I^3 and I^5 from a running LES. This allows for the possibility that these quantities can be determined dynamically as a simulation is running. This is the approach that is currently being pursued for I^3.

While this approach is being refined, a test of the modeling approximations described above was conducted by computing I^3 from DNS while using the models described above to determine the remaining terms. The resulting model was tested in isotropic turbulence using the same case and same filter size used in [16] (see Appendix A). The results are shown in figure 6, with comparison to filtered DNS and to the DNS-based model discussed in [16]. The results with this model are not quite as good as the DNS-based model, but there is a small inconsistency associated with using the DNS data for I^3, and the high-Reynolds number theory for the rest. This may well be responsible for the this somewhat degraded performance. None-the-less, the results suggest that the approach to modeling the correlations discussed here is viable.

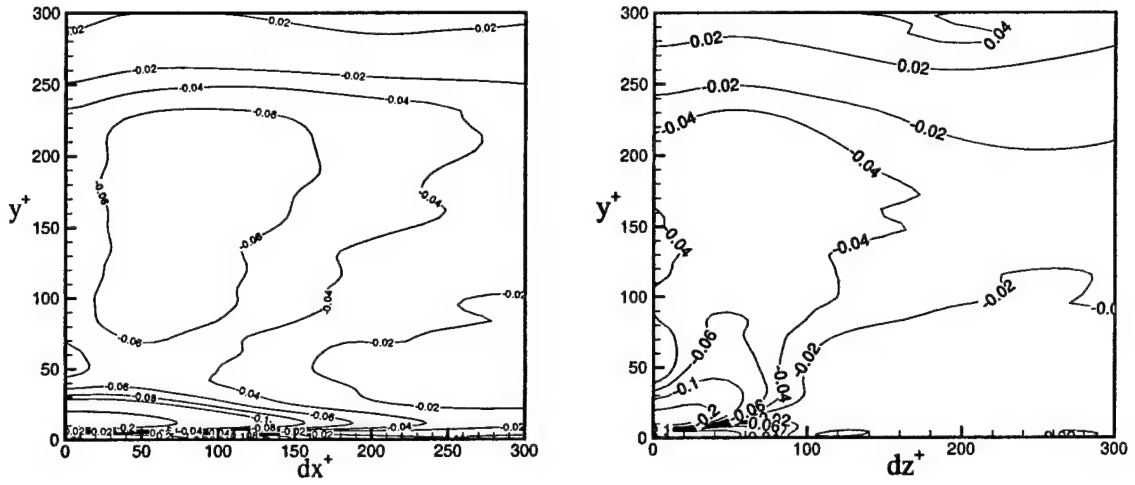

Figure 7: Contours of normalized error, $\phi_{11,11}$, as a function of the (left) streamwise separations and (right) spanwise separations (along horizontal coordinate) and wall normal coordinate (vertical coordinate). The axes are scaled by wall units.

3.5 Theoretical Correlations for Wall-Bounded Turbulence

The modeling approaches described in section 3.4 are clearly not applicable to wall-bounded turbulence. The turbulence cannot be considered isotropic or homogeneous, and the assumption of filter widths in the inertial range are clearly not justified. However, we do have a number of tools available for modeling the correlations in wall bounded flows. In particular, there is the representation theory developed by Procaccia's group [4, 3, 11] to represent anisotropy and the similarity theory of Oberlack for the log-layer. Further the quasi-normal approximation may still be valid, and the Navier-Stokes equations constrain the possible properties of the two-point third-order correlation. Finally, it is still the case the I^2, I^3 and I^5 are correlations between the LES state variables, so they are candidates to be determined dynamically.

To date, the application of the theory of Procaccia and of Oberlack as well as the quasi-normal approximation have been explored by appeal to DNS channel data. The results of these investigations are given in the following subsections.

3.5.1 Applicability of the Quasi-Normal Approximation

To determine whether the quasi-normal approximation is applicable in the near-wall of a wall-bounded flow, it was directly tested in a turbulent channel flow using DNS data at $Re_\tau = 590$. Various restrictions of the full four-point fourth ranked tensor were computed directly from the data and via the quasi-normal approximation and the second order correlations computed from the DNS. The results suggested that the approximation is remarkably accurate except for a region very near the wall ($y^+ < 50$). An example result is shown in figure 7. At high Re, the region with $y^+ < 50$ will need to be treated as part of the boundary treatment discussed in section 3.3, so the quasi-normal approximation appears to be valid where the interior models will need to be formulated. Details of the test of the quasi-normal approximation are provided in [14], a preprint

of which appears as Appendix B.

3.5.2 Procaccia and Oberlack Theory

The main objective of the study is to get a representation for the difference between the two point velocity fluctuation correlation and the Reynolds stress $\Delta R_{\alpha\beta}(\mathbf{x},\mathbf{r}) = \langle u_\alpha(\mathbf{x})u_\beta(\mathbf{x}+\mathbf{r})\rangle - \langle u_\alpha(\mathbf{x})u_\beta(\mathbf{x})\rangle$ in the different regions of the turbulent channel flow. The particular representation to be looked at is given by [4], and has the following form

$$\Delta R_{\alpha\beta}(\mathbf{x},\mathbf{r}) = \sum_{l=0}^{\infty}\sum_{m=-l}^{l}\sum_{q=1}^{q_{max}(l)} c_{qlm}(\mathbf{x},r)\, B_{\alpha\beta}^{qlm}(\hat{\mathbf{r}}) \tag{23}$$

Here, the basis tensors $\mathbf{B}^{qlm}$ form an irreducible representation of the rotation group, implying that applying a rotational transformation to a basis tensor gives back a linear combination of basis tensors with the same l indices. In the special case of homogeneous turbulence, it has been shown by [4] that this quality of the basis tensors along with the isotropy of the governing equations of the two point correlations implies that it is possible for the coefficients $c_{qlm}(\mathbf{x},r)$ having the same l to be proportional to $r^{\xi(l)}$. Based on experimental and theoretical evidence (e.g. [4], [11]) that $\xi(l)$ increases with l, it can be justified that $\mathbf{B}^{qlm}$ with higher l should have lesser importance as the separation r goes down. This property is obviously useful, because it gives a clear hierarchy of basis tensors for the representation of any two-point correlation tensor.

In the log-layer of the channel, [13] has shown that $R_{\alpha\beta}(\mathbf{x},\mathbf{r})$ depends on the similarity variable $\mathbf{r}/y$, where y is the distance from the channel wall. Thus, the two-point correlation at only one y in the log-layer is required to get the representation in the whole log-layer.

Some of the objectives of this study are to calculate the components $c_{qlm}(\mathbf{x},r)$ of the basis tensors and
- Verify whether it decreases in importance with l
- Find out the number of l's up to which it needs to be retained
- Check if in the log-layer they depend only on $\mathbf{r}/y$ and if this self-similarity can be used to simplify the representation

Properties of the full representation: The representation of the two point correlation containing terms only up to $l = l_{max}$ is given by

$$\Delta R_{\alpha\beta}^{(l_{max})}(\mathbf{x},\mathbf{r}) = \sum_{l=0}^{l_{max}}\sum_{m=-l}^{l}\sum_{q=1}^{q_{max}(l)} c_{qlm}(\mathbf{x},r)\, B_{\alpha\beta}^{qlm}(\hat{\mathbf{r}}) \tag{24}$$

The fractional error between $\Delta\mathbf{R}^{(l_{max})}$ and the exact $\Delta\mathbf{R}$ is given by

$$E^{l_{max}} = \sqrt{\frac{\int_0^{r_{max}} \langle \Delta\mathbf{R}^{(l_{max})} - \Delta\mathbf{R} | \Delta\mathbf{R}^{(l_{max})} - \Delta\mathbf{R}\rangle\, r^2 dr}{\int_0^{r_{max}} \langle \Delta\mathbf{R}|\Delta\mathbf{R}\rangle\, r^2 dr}} \tag{25}$$

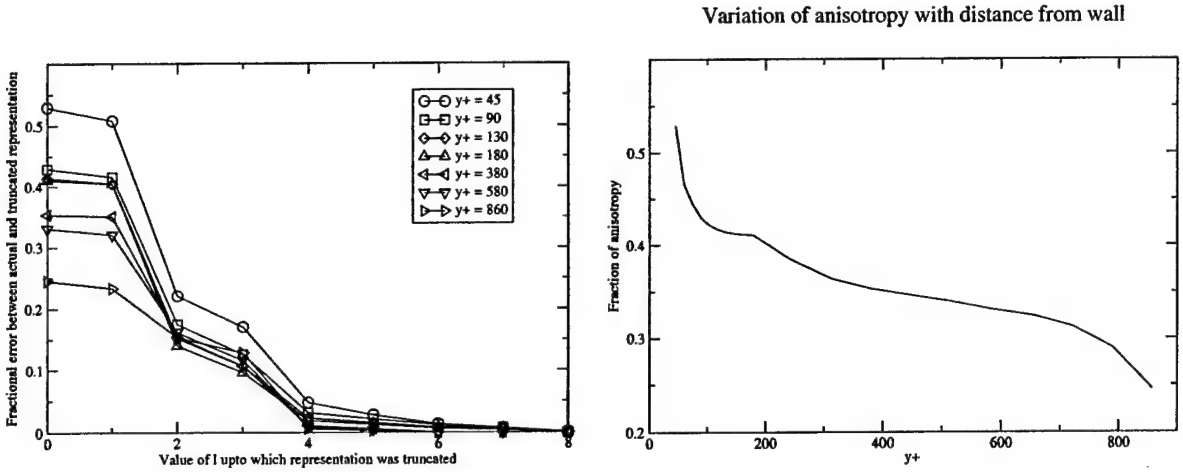

Figure 8: Relative error in the representation of ΔR (left) as a function of truncation index l for various y^+, and (right) when truncated at $l = 0$ (isotropic term) as a function of y^+. The error is measured in DNS of turbulent channel flow at $Re_\tau = 940$.

With r_{max}/h varying from 0.05 near the wall to 0.2 at the center. The inner product between any two tensors G and H is given by

$$\langle \mathbf{G}(\mathbf{r}) \mid \mathbf{H}(\mathbf{r}) \rangle = \int_0^{2\pi} \int_0^{\pi} G^*_{\alpha\beta}(r,\theta,\phi)\, H_{\alpha\beta}(r,\theta,\phi) \sin\theta d\theta d\phi \tag{26}$$

The two-point correlations have been obtained for channel flow of $Re_\tau = 934$. Figure 8(a) compares the values of $E^{l_{max}}$ for various y^+ ranging from near wall to the center of the channel. Clearly, for all points, a very good representation can be obtained for values of $l_{max} = 4$ while for $l_{max} = 2$ we get a maximum error of close to 20%. The odd l values do not contribute as much as the even l values. Therefore if we include only the $l = 0$ and $l = 2$ components, then for homogeneous turbulence we get 10 independent non-zero c_{qlm} components, while for inhomogeneous turbulence we get 19 independent non-zero c_{qlm} components. We can also see that the curves for $90 < y^+ < 180$ collapse, due to the fact that the correlation is self-similar in the log-layer. Figure 8(b) shows the value of E^0 for different y^+ values, i.e. the percentage error in the correlation if only the isotropic part of the correlation were used for it's representation. Clearly, even for y^+ values close to the wall the isotropic part represents the majority of the correlation. Again, evidence of self-similarity can be seen by flattening of the curve between $90 < y^+ < 180$.

Self-similarity in the log-layer:

Now we try to verify the self-similarity hypothesis in the log-layer. Clearly, if $R_{\alpha\beta}(y, \mathbf{r})$ depends only on $\mathbf{r}/y$ then $c_{qlm}(y, r)$ should depend on r/y. Figure 9(a) shows the curve $c_{420}(y, r)$ plotted against r/y for different y values in the log-layer. We can clearly see very good self-similarity in this case. However, this is not seen in all the components, and a significant proportion of them do not collapse on a single curve. An example of this is seen in figure 9(b) for $c_{120}(y, r)$. This implies that the correlation can be separated into self-similar and non self-similar parts. It is not

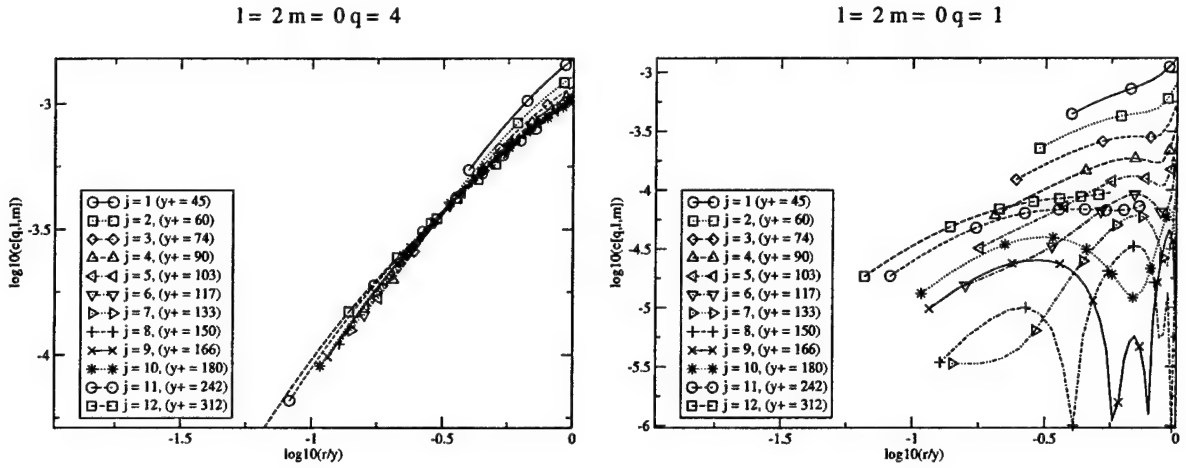

Figure 9: Angular expansion coefficients c_{qlm} for the indicated values of the indices. Coefficients are plotted as functions of r/y, consistent with similarity scaling of Oberlack [13].

clear whether there is a unique decomposition which can actually separate these parts, since it is not possible to define a unique non self-similar component. Instead, we look at some way to reduce the size of the representation, such that for each (l, m) subspace we choose an optimal tensor and a self similar scalar component which minimizes the global error between the reduced representation and the two-point correlation across the log-layer. Thus, we look for a representation of the form

$$\Delta R^{opt}_{\alpha\beta}(\eta) = \sum_{lm} a^{lm}(\eta) S^{lm}_{\alpha\beta}(\hat{\eta}) \tag{27}$$

where $\eta = \mathbf{r}/y$ and

$$S^{lm}_{\alpha\beta}(\hat{\eta}) = \sum_{q} f^{qlm} B^{qlm}_{\alpha\beta}(\hat{\eta}) \tag{28}$$

Here f^{qlm} is a set of scalar constants and is one of the variables which need to be optimized, the other being $a^{lm}(\eta)$. To formulate the optimization, we first get the orthonormal basis of $\mathbf{B}^{qlm}$ within the (l, m) subspace using the gram-schmidt orthonormalization procedure. Therefore, we get

$$\mathbf{B}'^{qlm}(\hat{\eta}) = \sum_{q'} h^{lm}_{qq'} \mathbf{B}^{q'lm}(\hat{\eta}) \tag{29}$$

so that $\left\langle B'^{qlm} \mid B'^{q'lm} \right\rangle = \delta_{qq'}$. The exact representation is now given by

$$\Delta R_{\alpha\beta}(\mathbf{x}, \mathbf{r}) = \sum_{qlm} c'^{qlm}(\mathbf{x}, r) B'^{qlm}_{\alpha\beta}(\hat{r}) \tag{30}$$

We can redefine the optimal tensors $\mathbf{S}^{lm}$ as

$$S^{lm}_{\alpha\beta}(\hat{\eta}) = \sum_{q} g^{qlm} B'^{qlm}_{\alpha\beta}(\hat{\eta}) \tag{31}$$

with the constraint

$$\sum_{q} \bar{g}^{qlm} g^{qlm} = 1 \tag{32}$$

in order to make sure that only $a^{lm}(\eta)$ contains information about the magnitude of the component. We need to minimize the error between $\Delta\mathbf{R}(\mathbf{x},\mathbf{r})$ and $\Delta\mathbf{R}^{opt}(\eta)$ over the range of the log layer $y_0 < y < y_1$. This error is given by

$$F = \frac{1}{y_1 - y_0}\int_{y_0}^{y_1}\int_{0}^{1}\left\langle \Delta\mathbf{R}(y,y\eta) - \Delta\mathbf{R}^{opt}(\eta) \mid \Delta\mathbf{R}(y,y\eta) - \Delta\mathbf{R}^{opt}(\eta)\right\rangle \eta^2 d\eta dy \tag{33}$$

Using the expansions given by equations (23) and (27) the inner product inside the integral is given by a known functional of the coefficients $\{a^{lm}(\eta)\}$, $\{g^{qlm}\}$ and $\{c^{qlm}(y,y\eta)\}$. The problem is solved using the method of Lagrange multipliers, by minimizing $F + \sum_{lm}\lambda_{lm}(\sum_{q}\bar{g}^{qlm}g^{qlm} - 1)$. This reduces to solving for

$$\frac{\partial}{\partial g^{qlm}}\left[F + \sum_{lm}\lambda_{lm}(\sum_{q}\bar{g}^{qlm}g^{qlm} - 1)\right] = 0 \tag{34}$$

$$\frac{\partial}{\partial a^{lm}}\left[F + \sum_{lm}\lambda_{lm}(\sum_{q}\bar{g}^{qlm}g^{qlm} - 1)\right] = 0 \tag{35}$$

The sets of $\{g^{qlm}\}$ which satisfy the above equations are given by the eigenvalue problem

$$\sum_{q'} C_{qq'lm}g^{q'lm} = \lambda_{lm}g^{qlm} \tag{36}$$

Here

$$C_{qq'lm} = \int_{0}^{1} I^{qlm}(\eta)\bar{I}^{q'lm}(\eta)\eta^2 d\eta \tag{37}$$

and

$$I^{qlm}(\eta) = \frac{1}{y_1 - y_0}\int_{y_0}^{y_1} c'^{qlm}(y,y\eta)dy \tag{38}$$

Where $\{c'^{qlm}(y,r)\}$ can be obtained from $\{c^{qlm}(y,r)\}$ using (23), (29) and (30). Thus $\{g^{qlm}\}$ is given by the eigenvectors of (36), with the most optimal set given by the eigenvector corresponding to the maximum λ_{lm}. The most optimal set of $\{a^{lm}(\eta)\}$ is then given by

$$a^{lm}(\eta) = \sum_{q} I^{qlm}(\eta)\bar{g}^{qlm} \tag{39}$$

Table (1) shows the degree to which the self-similar representation matches the two-point correlation in the log-layer. F_1 shows the fraction of the correlation represented by the individual mode and F_2 is the fraction of correlation represented by the sum of the first i modes. Clearly, the self-similar representation is a very good approximation of the correlation across the log-layer. The isotropic tensor itself forms the largest part of the correlation, while the $l = 2$ components come in next. Therefore, a self-similar representation using just the $l = 0$ and $l = 2$ components should be good enough, even though the region is highly inhomogeneous. Figure 10 shows the comparison of the fully reconstructed self-similar representation with correlations in a higher Reynolds number flow taken from experiments [6]. The self-similar representation gives a reasonable estimate of the streamwise correlation across the log-layer.

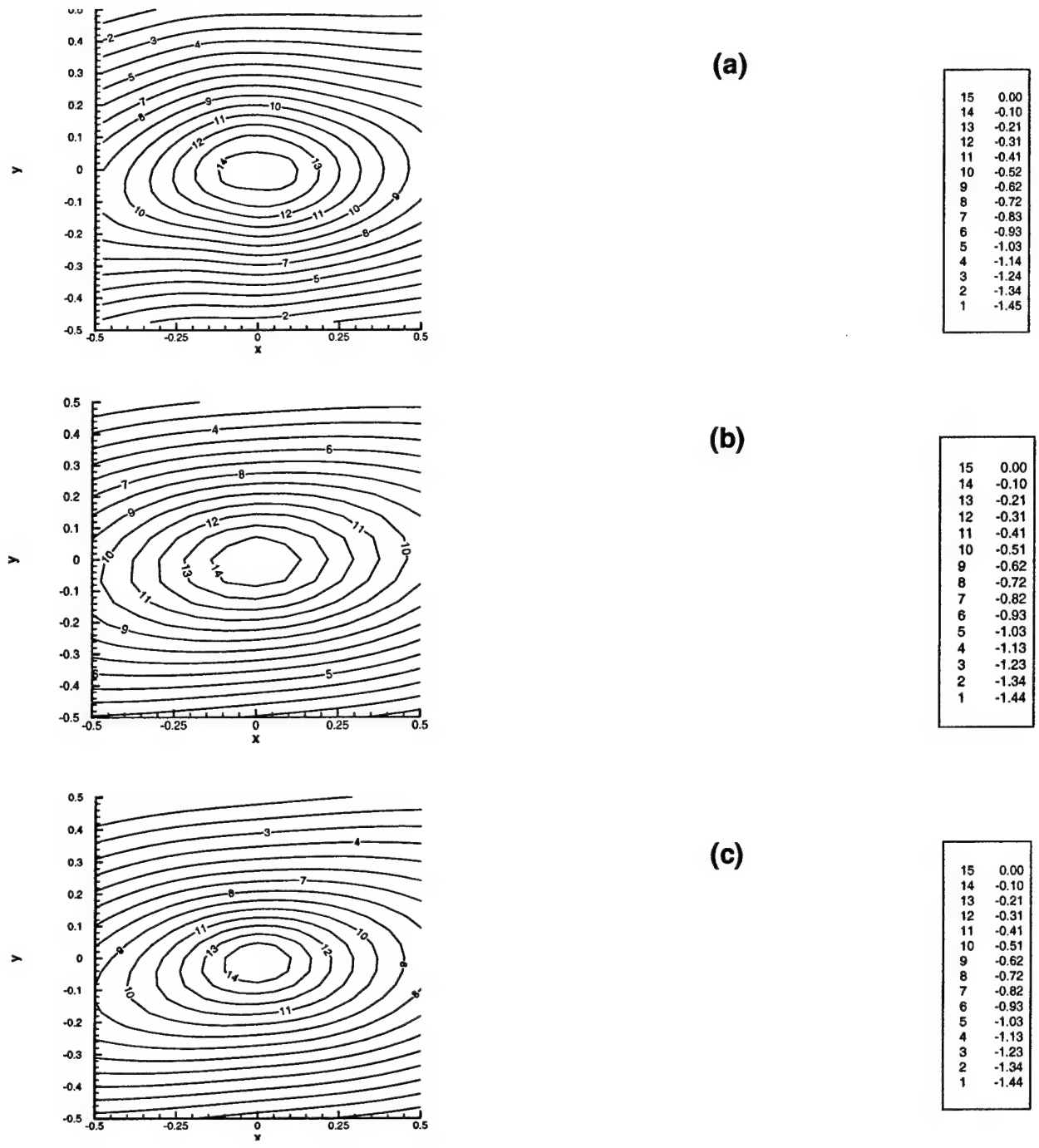

Figure 10: Comparison between the self-similar part of $R_{11}(y, \mathbf{r})$ calculated from DNS with actual correlations in channel flow with $Re_\tau = 2433$ (Experimental data). (a) shows the self-similar part of the correlation calculated from DNS, (b) & (c) show correlation taken from experiment for $y/h = 0.15$ and $y/h = 0.25$, both in the log-layer. The correlations are in the x-y plane, and the separations in the x and y directions have been normalized with respect to distance from the wall

Table 1: The modes in the self-similar representation sorted according to decreasing order of importance. $F_1 = \frac{\|a^{l(i)m(i)}(\eta)\mathbf{S}^{l(i)m(i)}(\tilde{\eta})\|^2}{\|\Delta\mathbf{R}(y,y\eta)\|^2}$ and $F_2 = \frac{\|\sum_{i'=1}^{i} a^{l(i')m(i')}(\eta)\mathbf{S}^{l(i')m(i')}(\tilde{\eta})\|}{\|\Delta\mathbf{R}(y,y\eta)\|}$, where $\|\mathbf{M}(y,\eta)\|^2 = \int_{y_0}^{y_1}\int_0^1 \langle \mathbf{M}|\mathbf{M}\rangle\, \eta^2 d\eta dy$

i	l(i)	m(i)	F_1	F_2
1	0	0	0.815	0.903
2	2	1	0.066	0.939
3	2	0	0.045	0.963
4	2	2	0.024	0.975
5	3	1	0.014	0.982
6	4	0	0.012	0.988
7	1	1	0.007	0.992
8	1	0	0.003	0.993
9	4	3	0.002	0.994
10	3	2	0.001	0.995

4 Other Information

This project was jointly funded by AFOSR under the subject grant and NSF under grant NSF-CTS-001435. The following personnel were supported by these grants:

John Wu	Graduate student, University of Illinois, Urbana-Champaign
Arup Das	Graduate student, University of Illinois, Urbana-Champaign
Amitabh Bhattacharya	Graduate student, University of Illinois, Urbana-Champaign
Ken Christensen	Postdoc, University of Illinois, Urbana-Champaign Current Position: Professor, University of Illinois, Urbana-Champaign
Prakash Vedula	Postdoc, University of Illinois, Urbana-Champaign
Robert D. Moser	Professor, University of Illinois, Urbana-Champaign
S. Balachandar	Professor, University of Illinois, Urbana-Champaign
Ron J. Adrian	Professor, University of Illinois, Urbana-Champaign

A number of papers were published during the grant period based on research undertaken under this grant, and its predecessor. These are listed below:

Publications

Balachandar, S. and Najjar, F. M. 2001 Optimal two-dimensional models for wake flows, *Phys. of Fluids*, **13**, 157-176.

Christensen, K. T. & Adrian, R. J. 2001 Statistical Evidence of Hairpin Vortex Packets in Wall Turbulence, *J. Fluid Mech.* **431**, 433-443.

Christensen, K. T. & Adrian, R. J. 2001 Measurement of Instantaneous Acceleration Fields using PIV, *Proc. 4th International Symposium on Particle Image Velocimetry.*

Christensen, K. T. & Adrian, R. J. 2001 The Small-Scale Structure of Acceleration in Wall Turbulence. *Proc. 2nd International Symposium on Turbulent Shear Flow Phenomena*, Stockholm.

Moser, R. D., Langford, J. A. & Volker, S. 2001 A Radical Approach to Large Eddy Simulation. AIAA paper *AIAA 2001-2835.*

Langford, J. A. & Moser, R. D. 2001 Breakdown of continuity in large-eddy simulation. *Phys. Fluids* **13**, 1524-1527.

Moser, R. D. & Volker, S. 2001 Characterization of Optimal LES in Turbulent Channel Flow. Proceedings of the Third AFOSR International Conference on LES/DNS, Arlington VA.

Das, A. & Moser, R. D. 2001 Filtering Boundary Conditions for LES and Embedded Boundary Simulations. Proceedings of the Third AFOSR International Conference on LES/DNS, Arlington VA.

Adrian, R. J. 2002 Information and the study of turbulence and complex flow, *JSME J. Ser. B*, **45**, 2-8.

Adrian, R. J., Balachandar, S. & Liu, Z. C., 2001 Spanwise growth of vortex structure in wall turbulence, *KSME Intl. J.*, **15**, 1741-1749.

Adrian, R. J. & Liu, Z. C. 2002 Observation of vortex packets in direct numerical simulation of fully turbulent channel flow, *J. Vis.*, **5**, 9-19.

Christensen, K. T. & Adrian, R. J. 2002 The velocity and acceleration signatures of small-scale vortices in turbulent channel flow, *J. Turbulence.*

Liu Z. C., Adrian R. J. & Hanratty T. J. 2001 Large-scale modes of turbulent channel flow: Transport and structure, *J. Fluid Mech.* **448**, 53-80.

Das, A. & Moser, R. D. 2002 Optimal Large eddy simulation of forced Burger's equation, *Phys. of Fluids*, **14**, 4344.

Volker, S., Venugopal, P. & Moser, R. D. 2002 Optimal large eddy simulation of turbulent channel flow based on direct numerical simulation statistical data, *Phys. of Fluids* **14**, 3675.

Christensen, K. T. & Adrian R. J. 2002 Measurement of instantaneous Eulerian acceleration fields by particle image accelerometry: method and accuracy *Exp. Fluids* **33** (6), 759-769.

Moser, R. D. & Zandonade, P. 2003 Development of High Reynolds Number Optimal LES Models, in *Reynolds Number Scaling in Turbulent Flow*, Smits, A. J. (Ed.) Kluwer, Dordrecht, The Netherlands, 169-174.

de Alamo, J. C., Jimenez, J., Zandonade, P. & Moser, R. D. 2004 Scaling of the energy spectra of turbulent channels, *J. Fluid Mech.* **500**, 135-144.

Zandonade, P. S., Langford, J. A. & Moser, R. D. 2004 Finite volume optimal large-eddy simulation of isotropic turbulence, To appear *Phys. of Fluids.*

Acknowledgment/Disclaimer

This work is jointly sponsored by the National Science Foundation and the Air Force Office of Scientific Research, USAF, under grant/contract numbers NSF-CTS-001435 and F49620-01-0181. The views and conclusions contained herein are those of the authors and should not be interpreted as necessarily representing the official policies or endorsements, either expressed or implied, of the Air Force Office of Scientific Research or the U. S. Government.

References

[1] R. Adrian. Stochastic estimation of sub-grid scale motions. *Applied Mechanics Review*, 43(5):214–218, 1990.

[2] R. Adrian, B. Jones, M. Chung, Y. Hassan, C. Nithianandan, and A. Tung. Approximation of turbulent conditional averages by stochastic estimation. *Physics of Fluids*, 1(6):992–998, 1989.

[3] I. Arad, B. Dhruva, S. Kurien, V. S. L'vov, I. Procaccia, and K.R. Sreenivasan. Extraction of anisotropic contributions in turbulent flows. *Phys Rev. Lett*, 81:5330–5333, 1998.

[4] I. Arad, V.S. L'vov, and I. Procaccia. Correlation functions in isotropic and anisotropic turbulence: The role of the symmetry group. *Phys Rev. E*, 59:6753–6765, 1999.

[5] K. T. Christensen and R. J. Adrian. Statistical evidence of hairpin vortex packets in wall turbulence. *Journal of Fluid Mechanics*, 431:433–443, 2001.

[6] K. T. Christensen and Adrian R. J. Measurement of instantaneous eulerian acceleration fields by particle image accelerometry: method and accuracy. *Exp. Fluids*, 33:759–769, 2002.

[7] A. Das and R. D. Moser. Filtering boundary conditions for les and embedded boundary simulations. In *Proceedings of the Third AFOSR International Conference on LES/DNS, Arlington VA*, 2001.

[8] J. C. del Álamo, J. Jiménez, P. Zandonade, and R. D. Moser. Scaling of the energy spectra of turbulent channels. *J. Fluid Mech.*, 500:135–144, 2004.

[9] J. Langford and R. Moser. Optimal LES formulations for isotropic turbulence. *Journal of Fluid Mechanics*, 398:321–346, 1999.

[10] J.A. Langford. *Toward Ideal Large-Eddy Simulation.* PhD thesis, University of Illinois at Urbana-Champaign, 2000.

[11] V. S. L'vov, I. Procaccia, and V. Tiberkevich. Scaling exponents in anisotropic hydrodynamic turbulence. *Phys. Rev. E*, 67:026312, 2003.

[12] R.D. Moser, J. Kim, and N.N. Mansour. Direct numerical simulation of turbulent channel flow up to $Re_\tau = 590$. *Physics of Fluids*, 11(4):943–945, April 1999.

[13] M Oberlack. A unified approach for symmetries in plane parallel turbulent shear flows. *Journal of Fluid Mechanics*, 427:299–328, 2001.

[14] P. Vedula and R. D. Moser. On the validity of quasi-normal approximation in turbulent channel flow. Submitted to *Phys. of Fluids*, 2004.

[15] S. Volker, P. Venugopal, and R. D. Moser. Optimal large eddy simulation of turbulent channel flow based on direct numerical simulation statistical data. *Phys. of Fluids*, 14:3675, 2002.

[16] P. S. Zandonade, J. A. Langford, and R. D. Moser. Finite-volume optimal large-eddy simulation of isotropic turbulence. To appear in *Phys. of Fluids*, 2004.

APPENDIX A

Preprint of Zandonade, P. S., Langford, J. A. & Moser, R. D. 2003 Finite volume optimal large-eddy simulation of isotropic turbulence, To appear *Phys. of Fluids.*

Finite-Volume Optimal Large-Eddy Simulation of Isotropic Turbulence

Paulo S. Zandonade, Jacob A. Langford, and Robert D. Moser

Department of Theoretical and Applied Mechanics,

University of Illinois at Urbana-Champaign

(Dated: March 5, 2004)

Abstract

The feasibility of an *optimal* finite-volume large-eddy simulation (LES) model for isotropic turbulence is evaluated. This modeling approach is based on the approximation of the *ideal* LES by a stochastic estimate of the fluxes in a finite-volume representation of the Navier-Stokes equation. Stochastic estimation of the fluxes allows for the simultaneous treatment of Navier-Stokes, discretization and subgrid effects, yielding a compact, yet accurate scheme for the large eddy simulation of isotropic turbulence. Both global and local models based on *optimal* finite-volume LES are developed and used in *a priori* tests guiding the choice of stencil geometry and model inputs. The most promising models in the *a priori* exams are tested in actual simulations (i.e. *a posteriori*) and the results compared with those for filtered DNS and the dynamic Smagorinsky model. The *a posteriori* performance of the *optimal* finite-volume LES models, evaluated by the energy spectrum and third-order structure function, is superior to that of the dynamic Smagorinsky model on a coarse grid. While applicability to other cases is currently limited by the dependence of the present approach on direct numerical simulation (DNS) statistical data, research is underway to remove this requirement.

I. INTRODUCTION

In large-eddy simulation (LES), one simulates turbulence by resolving only the large scales while modeling the small ones. This approach is justified by the observation that the large scales usually dominate the dynamics of the flow, whereas the small scales are important only to the extent to which they affect the large scales. The small scales of turbulence are believed to be more universal and, therefore, more amenable to modeling, which should allow for a prediction method that can be used, with little change, in a wide range of flows. For reviews of LES see Rogallo & Moin [1], Lesieur & Métais [2] and Meneveau & Katz [3]. Despite its great promise as a turbulence prediction technique, current LES practice suffers from many shortcomings (e.g. near-wall modeling, and effect of numerical discretization errors) which hamper the use of LES as a reliable engineering prediction tool. Several active research efforts [4–9] are underway to improve LES modeling, and, in particular, *optimal* LES models [10, 11] as those reported here are being pursued to address these issues.

Development of *optimal* LES has benefited from a careful reexamination of the formalism underlying LES. Because of the continuous range of scales present in a high Reynolds number turbulent flow, it is necessary to define with some precision the large scales to be simulated and the small scales to be discarded in an LES. This is accomplished through spatial filtering. Filtered quantities, denoted by $\widetilde{(.)}$, represent the large (or resolved) scales, and can be defined through the operation of a filter kernel on the original variable. As an example, the filtered velocity field $\widetilde{u}_i$ is defined through the filter kernel g (in general g could be a distribution) operating on the velocity u_i:

$$\widetilde{u}_i(\boldsymbol{x}) = \int g(\boldsymbol{x}', \boldsymbol{x})\, u_i(\boldsymbol{x}')\, \mathrm{d}\boldsymbol{x}' \tag{1}$$

The small scales in the LES, e.g. $u_i' = u_i - \widetilde{u}_i$, are commonly called subgrid scales.

The standard LES practice is to apply the filter to the Navier-Stokes and continuity equations, yielding the governing equations for the resolved scales:

$$\frac{\partial \widetilde{u}_i}{\partial x_i} + C = 0 \tag{2}$$

$$\frac{\partial \widetilde{u}_i}{\partial t} = -\frac{\partial \widetilde{\widetilde{u}_i \widetilde{u}_j}}{\partial x_j} - \frac{\partial \widetilde{p}}{\partial x_i} + \frac{1}{\mathrm{Re}} \frac{\partial^2 \widetilde{u}_i}{\partial x_j \partial x_j} + M_i \tag{3}$$

where

$$M_i = -\frac{\partial \tau_{ij}}{\partial x_j} + C_i \tag{4}$$

$$\tau_{ij} = \widetilde{u_i u_j} - \widetilde{u}_i \widetilde{u}_j \tag{5}$$

and C and C_i are commutation terms that arise when the filter does not commute with spatial differentiation. The term τ_{ij} is the subgrid stress term, which represents the effect of the subgrid scales on the resolved scales.

Most current LES formulations use discretized versions of (2) and (3) as evolution equations, with the modeling effort focused on determining the correct representation of the subgrid stress term τ_{ij}. These subgrid stress models, such as the Smagorinsky [12], dynamic [13], scale-similarity [6, 14], stretched vortex [5] and defiltering models [8, 15–17] have been used to simulate a variety of turbulent flows, but are derived assuming that errors due to numerical discretization of the remaining terms in the evolution equation are negligible.

The introduction of numerical discretization in LES raises both a fundamental and practical issue. The fundamental issue arises because continuous filters used in LES are commonly invertible, or nearly so. For example, the Gaussian filter is formally invertible, and a top-hat filter can be inverted with the addition of only boundary information. With invertible filters and in the absence of numerical discretization, the filtered velocity can be evolved exactly by inverse filtering, computing the terms in the Navier-Stokes equations, then filtering the result. However, numerical discretization actually eliminates critical small-scale information, making this impossible, and thus it is the presence of numerical discretization that makes LES modeling necessary in these cases. Because of this, it seems desirable that LES models be formulated in the context of the numerical representation with which they will be used.

As a practical matter, the numerical discretization errors introduced by standard low-order numerical schemes are of the same order as the LES model terms [18–20], leading to solutions that are contaminated by numerical errors. Two different approaches are currently used to avoid such large numerical errors: high-order discretization schemes (or spectral methods) and/or grid refinement while keeping the filter width Δ constant. Both of these approaches have been successfully applied to yield accurate LES solutions [21, 22], but their use is limited by practical considerations. The application of high-order methods is usually difficult in complex geometries, while the cost of adequate grid refinement is generally prohibitive. Since neither of these options is acceptable in complex turbulent flows, another

approach seems necessary. In particular, if subgrid models could be formulated to account for the numerical discretization, accurate low-cost LES would be possible.

In the development of *optimal* LES, the above considerations have led to an approach in which the numerical discretization is considered to be part of a generalized "filter." In this way, the filter is viewed as a mapping from the infinite dimensional space of Navier-Stokes solutions to a finite dimensional LES space, which can be represented computationally without further truncation. The many-to-one nature of the mapping leads to an analysis of the subgrid turbulence and its effects as stochastic, and the use of stochastic modeling tools in the development of *optimal* LES models, which are deterministic [10]. This filtering approach also leads to other differences in the current development relative to other LES formulations. For example, in our formulation, there is no distinction between the grid scale and the filter scale, or between numerical errors and modeling errors. It would also be possible to formulate *optimal* LES based on appropriate non-invertible filters which are distinct from the numerical discretization, but that is not the approach taken here.

In this paper, we examine the feasibility of using *optimal* LES techniques to develop models for use with a coarse finite-volume representation of turbulence. Finite volume representations are used because of their general applicability to flows with complex geometries, in contrast to the spectral representations used in previous *optimal* LES studies [10, 11]. To this end, an *optimal* finite-volume LES model that simultaneously represents Navier-Stokes dynamics, numerical and subgrid effects is constructed and evaluated. It is important to point out that, in the current study, the correlations needed for the *optimal* modeling approach are supplied from DNS statistical data, rendering the model specific to the isotropic flow for which it is constructed. This is not an inherent shortcoming of the *optimal* LES approach, but rather a choice which was made to evaluate the procedure in isolation of further modeling which is necessary for a complete and general LES model. While research is underway to generalize the *optimal* finite-volume LES model, specifically the modeling of the correlations which are currently computed from DNS data, it is important to verify if the *optimal* procedure, by itself, is adequate for constructing the compact, accurate models proposed above. A promising approach to modeling the required correlations is discussed briefly in section IV.

II. OPTIMAL FINITE-VOLUME LES

The existence of a model defining the limiting accuracy of an LES simulation has been noted previously [10, 23]. This *ideal* LES model reproduces all single-time, multi-point statistics exactly and minimizes the error of the large-scale dynamics. The evolution of this *ideal* LES is defined by the following conditional average:

$$\frac{\mathrm{d}\boldsymbol{w}}{\mathrm{d}t} = \left\langle \widetilde{\frac{\mathrm{d}\boldsymbol{u}}{\mathrm{d}t}} \middle| \widetilde{\boldsymbol{u}} = \boldsymbol{w} \right\rangle \tag{6}$$

where $\boldsymbol{w}$ represents an LES field and $\boldsymbol{u}$ represents a real turbulent field (notice that these are entire fields). This expression for the *ideal* LES is perfectly general. In the case when the filter is invertible, $\widetilde{\frac{\mathrm{d}\boldsymbol{u}}{\mathrm{d}t}}$ is not stochastic, and the *ideal* LES evolution reduces to $\frac{\mathrm{d}\boldsymbol{w}}{\mathrm{d}t} = \widetilde{\frac{\mathrm{d}\boldsymbol{u}}{\mathrm{d}t}}$, indicating that the filtered field evolution can be determined exactly in terms of just the filtered field. Such a simulation is equivalent to a DNS, with the same resolution requirements. Only when the filter is a many-to-one mapping as described in section I does this formalism correspond to an LES, and this is the case of interest here.

Unfortunately, direct computation of the *ideal* model is not practical, because of the immense amount of statistical information contained in (6). *Optimal* LES is a formal approximation of the *ideal* LES using stochastic estimation, a well-known technique for approximating the conditional average with a manageable amount of data [24–26]. *Optimal* LES has been previously applied to model the subgrid term with spectral numerical representations of the Navier-Stokes-like terms in the filtered equation[10, 11]. In these previous studies, the focus was the analysis of the resulting *optimal* subgrid model in order to identify the fundamental properties a subgrid model should have in isotropic [10] and wall-bounded [11] turbulence. The authors made no attempt to construct a general *optimal* LES model for use in a range of complex turbulent flows.

One of the primary impediments to the broad application of the *optimal* LES approach developed in these previous studies is their reliance on spectral numerical representations, which are not easily applied to flows in complex geometries. In the present study, the applicability of *optimal* LES to finite volume representations is explored. This is more challenging than spectral methods, since exact derivative operators cannot be defined. To avoid the numerical errors inherent in a finite-volume representation of the Navier-Stokes terms, the *optimal* modeling procedure is applied to the filtered Navier-Stokes equation as

a whole, rather than just the subgrid stress as was done in [10, 11]. A generally applicable *optimal* finite-volume model requires modeling of the small-separation second-, third- and fourth-order velocity correlations appearing in section II B 3. For the current study, this requirement is being bypassed through the use of DNS statistical data, allowing us to focus on the viability of the finite-volume *optimal* LES modeling procedure.

A. Finite-volume formulation of LES

To evaluate the feasibility of applying the *optimal* LES procedure directly to a finite volume representation, a coarse finite-volume representation of homogeneous isotropic turbulence is explored. In this case, the domain is a periodic cube of dimension 2π, with the numerical grid for each velocity component composed of N^3 cubes of dimension $\Delta = 2\pi/N$. To allow for staggered as well as collocated grids, the cubes are labeled as Ω_{ji}, each with center located at $\boldsymbol{x}^{ji} = \boldsymbol{x}^{j0} + \boldsymbol{i}\Delta$, where $\boldsymbol{x}^{j0}$ is the origin of each grid. For collocated grids $\boldsymbol{x}^{j0} = \boldsymbol{0}$, and for staggered grids $\boldsymbol{x}^{j0} = -\frac{\Delta}{2}\boldsymbol{e}^j$, where $\boldsymbol{e}^j$ is the unit vector in the j direction. The j indices refer to the grid associated with the j^{th} component of velocity, while $\boldsymbol{i}$ is a vector of integers which establishes the position of the cube.

The finite-volume filter kernel, $g(\boldsymbol{x} - \boldsymbol{\xi})$ as defined in (1) is a top-hat filter sampled on a grid and is given by:

$$g^{ji}(\boldsymbol{x} - \boldsymbol{\xi}) = \delta(\boldsymbol{x}^{ji} - \boldsymbol{x}) G(x_1 - \xi_1) G(x_2 - \xi_2) G(x_3 - \xi_3) \tag{7}$$

where δ is the Dirac delta function and $G(x_i - \xi_i)$ is the one-dimensional box or top-hat filter:

$$G(x_i - \xi_i) = \begin{cases} \frac{1}{\Delta} & \text{if } |x_i - \xi_i| \leq \frac{\Delta}{2}, \\ 0 & \text{otherwise.} \end{cases} \tag{8}$$

Note that, to support staggered grids, the filter kernel depends on which velocity component is being filtered.

The finite-volume filtered velocity is, therefore, defined as:

$$w_j^{\boldsymbol{i}} = \frac{1}{\Delta^3} \int_{\Omega_{ji}} u_j(\boldsymbol{x})\, \mathrm{d}\boldsymbol{x}. \tag{9}$$

The evolution equations for the filtered velocity are found by filtering the Navier-Stokes

equations with g, yielding the control-volume form of these equations:

$$\int_{\Omega_{ji}} \frac{\partial u_j}{\partial t} \mathrm{d}\boldsymbol{x}' + \int_{\Omega_{ji}} \frac{\partial u_j u_k}{\partial x'_k} \mathrm{d}\boldsymbol{x}' = -\int_{\Omega_{ji}} \frac{\partial p}{\partial x'_j} \mathrm{d}\boldsymbol{x}' + \frac{1}{\mathrm{Re}} \int_{\Omega_{ji}} \frac{\partial^2 u_j}{\partial x'_k \partial x'_k} \mathrm{d}\boldsymbol{x}' \tag{10}$$

$$\int_{\Omega_{ji}} \frac{\partial u_j}{\partial x'_j} \mathrm{d}\boldsymbol{x}' = 0. \tag{11}$$

The divergence theorem is used to convert the volume integrals to surface integrals:

$$\Delta^3 \frac{\mathrm{d}w_j^{\boldsymbol{i}}}{\mathrm{d}t} + \int_{\partial\Omega_{ji}} u_j u_k n_k \mathrm{d}\boldsymbol{x}' = -\int_{\partial\Omega_{ji}} p n_j \mathrm{d}\boldsymbol{x}' + \frac{1}{\mathrm{Re}} \int_{\partial\Omega_{ji}} \frac{\partial u_j}{\partial x'_k} n_k \mathrm{d}\boldsymbol{x}' \tag{12}$$

$$\int_{\partial\Omega_{ji}} u_j n_j \mathrm{d}\boldsymbol{x}' = 0 \tag{13}$$

where n_j is the outward pointing normal of the volume boundary $\partial\Omega_{ji}$.

The evolution of the LES field now depends only on the surface fluxes in each volume. In a standard finite-volume scheme, the fluxes would be approximated numerically through reconstruction techniques, yielding approximations which converge as the grid size tends to zero, $\Delta \to 0$. However, such convergence considerations are not applicable, for the LES considered here, since $\Delta \gg \eta$ (η is the Kolmogorov scale). Instead, the convective and diffusive fluxes in equation (12) will be modeled using stochastic estimation. One could also subject the pressure flux term to the same modeling technique, but, as pointed out by Langford & Moser [27], such a representation would be inherently non-local and thus impractical in complex applications. An alternative is to use an approximate continuity constraint to determine the pressure fluctuation, as in traditional finite-volume methods. Langford & Moser [27] have shown that an *optimal* scheme for pressure is only slightly more accurate than the traditional schemes, especially in the staggered grid case.

The task of modeling the surface fluxes appearing in the exact LES equations (12) can be simplified considerably. The flux across a particular face appears in the momentum equation of two neighboring cells; to ensure conservation, the two cells must have identical representations of the flux. In isotropic turbulence, homogeneity dictates that a model for the flux through a given face must not depend on the location of the face. These two requirements imply that a model need only be provided for three of the six faces of the cube.

Further simplifications are introduced by isotropy. The symmetry of the grid requires that the equations for the LES evolution be invariant to reflections and rotations in the coordinate system. This basic requirement imposes a symmetry on the flux models, and

implies that each flux term can be constructed from rotations and reflections of four (4) basic fluxes. The terms M^i_{ww}, M^i_{uw}, $M^i_{\partial w/\partial z}$ and $M^i_{\partial u/\partial z}$ are used to denote these basic fluxes, which are averages of ww, uw, $\partial w/\partial z$, and $\partial u/\partial z$ (for the remainder of this paper, u, v, and w are used to denote components of $\boldsymbol{w}$), respectively, over a face of dimension $\Delta \times \Delta$ oriented with normal in the z-direction and located at the top (positive z side) of the $\boldsymbol{i}^{\text{th}}$ volume element. For M_{ww} and $M_{\partial w/\partial z}$, the relevant volume element is for the w-component of velocity, and for the other fluxes, the relevant volume is for the u-component of velocity. The four fluxes to be modeled are

$$M^i_{ww} = \frac{1}{\Delta^2} \int_{x_2^{3i}-\Delta/2}^{x_2^{3i}+\Delta/2} \int_{x_1^{3i}-\Delta/2}^{x_1^{3i}+\Delta/2} u_1 u_3 \mathrm{d}x\mathrm{d}y \tag{14}$$

$$M^i_{uw} = \frac{1}{\Delta^2} \int_{x_2^{1i}-\Delta/2}^{x_2^{1i}+\Delta/2} \int_{x_1^{1i}-\Delta/2}^{x_1^{1i}+\Delta/2} u_3 u_3 \mathrm{d}x\mathrm{d}y \tag{15}$$

$$M^i_{\partial w/\partial z} = \frac{1}{\Delta^2} \int_{x_2^{3i}-\Delta/2}^{x_2^{3i}+\Delta/2} \int_{x_1^{3i}-\Delta/2}^{x_1^{3i}+\Delta/2} \frac{\partial u_1}{\partial z} \mathrm{d}x\mathrm{d}y \tag{16}$$

$$M^i_{\partial u/\partial z} = \frac{1}{\Delta^2} \int_{x_2^{1i}-\Delta/2}^{x_2^{1i}+\Delta/2} \int_{x_1^{1i}-\Delta/2}^{x_1^{1i}+\Delta/2} \frac{\partial u_3}{\partial z} \mathrm{d}x\mathrm{d}y \tag{17}$$

To actually perform a simulation, the models for these fluxes must be rotated and reflected appropriately to generate all the terms in (12).

B. Stochastic estimation technique

In stochastic estimation, which is the basis for *optimal* LES models, one begins by defining a restricted functional form (e.g. linear or quadratic) for the model. The stochastic estimate is then determined by minimizing the mean-square difference between the model and the exact quantity being modeled. The application of this technique to the finite volume fluxes is discussed below, followed by a brief discussion of the sense in which such model can be considered to "converge."

1. Model definition

The stochastic estimation model $m^{\boldsymbol{i}}$ of a particular flux term $M^{\boldsymbol{i}}$, is expressed as a sum of linear and quadratic products of filtered velocities:

$$m^{\boldsymbol{i}} = A + \sum_{\boldsymbol{m}} B_j^{\boldsymbol{m}} w_j^{\boldsymbol{i}+\boldsymbol{m}} + \sum_{\boldsymbol{m}} \sum_{\boldsymbol{n}} C_{jk}^{\boldsymbol{m}\boldsymbol{n}} w_j^{\boldsymbol{i}+\boldsymbol{m}} w_k^{\boldsymbol{i}+\boldsymbol{n}}. \tag{18}$$

More elaborate model forms are possible, but at least a quadratic dependence is needed, since the convective fluxes are quadratic. Note that $\boldsymbol{m}$ and $\boldsymbol{n}$ are vectors representing the separation between the face being modeled (face $\boldsymbol{i}$) and the velocity term used in the sum. One can extend the summation over all volumes, generating a global model, or restrict $\boldsymbol{m}$ and $\boldsymbol{n}$ to a certain stencil of volumes, generating a local model.

The geometry of the stencils for local models is described through the following notation:

$$N_x^u \times N_y^u \times N_z^u - N_x^v \times N_y^v \times N_z^v - N_x^w \times N_y^w \times N_z^w$$

where N_x, N_y and N_z define the number of volumes in the stencil in each direction. In our convention, the fluxes are estimated on a face with surface normal pointing in the positive z-direction, with the stencil centered about this face. The u, v and w superscripts specify the component of velocity for which the stencil is used. This distinction is necessary since, in general, different velocity components will have different stencils for a given flux. When referring to a stencil for a single velocity component, the simpler notation

$$N_x \times N_y \times N_z$$

can be used. In Fig. 1, examples of single velocity stencils are shown.

2. Defining the minimization

In the stochastic estimation technique, the model coefficients A, B and C are determined by minimizing the mean-square error with respect to the model's inputs or *events* ($w_j^{\boldsymbol{i}+\boldsymbol{m}}$ and $w_j^{\boldsymbol{i}+\boldsymbol{m}} w_k^{\boldsymbol{i}+\boldsymbol{n}}$ in the model defined by equation (18)). The stochastic estimate is intended to approximate the conditional average constituting the ideal LES (in this case $m_{\text{ideal}}^{\boldsymbol{i}} = \langle M^{\boldsymbol{i}} | \tilde{\boldsymbol{u}} = \boldsymbol{w} \rangle$), so it is the mean-square error in reproducing $m_{\text{ideal}}^{\boldsymbol{i}}$ that is to be minimized, even though $m_{\text{ideal}}^{\boldsymbol{i}}$ is not known. However, it can be shown [11] that this error is also

minimized when the mean-square difference between $M^{\boldsymbol{i}}$ and $m^{\boldsymbol{i}}$ is minimized. Thus, it is this mean-square difference

$$d^{\boldsymbol{i}} = M^{\boldsymbol{i}} - m^{\boldsymbol{i}} \tag{19}$$

that is directly minimized in developing the estimates. We refrain from labeling d as an error since it cannot, even in principle, be made to approach zero. Its mean square is bounded from below by the variance of $M^{\boldsymbol{i}}$ about $m^{\boldsymbol{i}}_{\text{ideal}}$. Instead d will be called the "variation" of the model.

However, there are at least two different ways to define the variation when estimating the fluxes. The single-flux variation measures the difference between the model and the flux at a single face, and is defined as

$$d^{\boldsymbol{i}}_{|} = M^{\boldsymbol{i}} - m^{\boldsymbol{i}} \tag{20}$$

While this is the most straightforward definition of the model's variation, it is not the most relevant to the dynamics of the LES evolution. For example, if the flux contributes to the momentum equation for the w component of velocity, as for M_{ww} and $M_{\partial w/\partial z}$, then the model appears in the momentum evolution equation as follows:

$$\frac{\mathrm{d}w^{\boldsymbol{i}}_3}{\mathrm{d}t} = \cdots + m^{\boldsymbol{i}} - m^{\boldsymbol{i}-(0,0,1)} \tag{21}$$

The contribution of the model to the variation in the momentum evolution is the dual-flux variation of the estimate, defined as

$$d^{\boldsymbol{i}}_{||} = \left(M^{\boldsymbol{i}} - m^{\boldsymbol{i}}\right) - \left(M^{\boldsymbol{i}+(0,0,1)} - m^{\boldsymbol{i}+(0,0,1)}\right) \tag{22}$$

In general, the dual-flux variation $d_{||}$ is different from the single-flux variation $d_{|}$, because there are stochastic portions of the exact flux term $M^{\boldsymbol{i}}$ that exactly cancel portions of the flux term on the opposing face. The single-flux variation $d_{|}$ includes contribution from the cancellation, and may thus overpredict variation in the momentum equation. Whenever the variation is plotted or tabulated, $d_{||}$ is used, since this non-canceling portion of the variation is most relevant to the dynamics of the LES, due to its explicit appearance in the momentum equations.

In reporting *a priori* variations, it is clearly $d_{||}$ that is of interest, but one of the other variations may be most appropriate to minimize to determine the modeling coefficients A, B and C. When local estimates are used, somewhat different models will result depending

on which variation is minimized, and the differences can be important. For example, it is shown in Appendix A that minimizing $d_|$ results in a model that conserves momentum, and correctly predicts dissipation in the *a priori* sense. Whereas, minimizing $d_{||}$ results in models that are either conservative or have correct *a priori* dissipation, but not both. Local estimates were computed using both the single-flux, $d_|$, and dual-flux, $d_{||}$, variations, and it was found that the increase in $d_{||}$ due to minimizing the mean-square of $d_|$ is small, but that the error in predicting *a priori* dissipation is significant when the mean-square of $d_{||}$ is minimized. For these reasons, the local models developed here were determined by minimizing $d_|$.

3. Determining Optimal Estimates

In order for a linear estimate to minimize $d_|$, the following conditions should be met [28]:

$$\langle M^{\boldsymbol{i}} \rangle = \langle m^{\boldsymbol{i}} \rangle \tag{23}$$

$$\langle (M^{\boldsymbol{i}} - m^{\boldsymbol{i}}) E_l^{\boldsymbol{i}} \rangle = 0 \tag{24}$$

where $\boldsymbol{E}$ is the event vector, consisting of all events used in the model equation (18). For an *optimal* linear estimate ($C = 0$ in (18)) the event vector is given by:

$$\boldsymbol{E} = \left(w_j^{\boldsymbol{i}+\boldsymbol{m}} \right) \tag{25}$$

while the event vector for the *optimal* quadratic model is

$$\boldsymbol{E} = \begin{pmatrix} w_j^{\boldsymbol{i}+\boldsymbol{m}} \\ w_j^{\boldsymbol{i}+\boldsymbol{m}} w_k^{\boldsymbol{i}+\boldsymbol{n}} \end{pmatrix} \tag{26}$$

where $\boldsymbol{m}$ and $\boldsymbol{n}$ vary over all separations defined by the stencil for a specific model.

Therefore, to determine the *optimal* linear estimates and the associated variation, the following correlations are required:

$$\langle MM \rangle \,,\ \langle M w_i^{\boldsymbol{n}} \rangle \,,\ \langle w_i^{\boldsymbol{m}} w_j^{\boldsymbol{n}} \rangle \tag{27}$$

The $\boldsymbol{i}$ superscripts have been removed since the correlations are averaged over all volumes. To compute the *optimal* quadratic estimate, the following additional correlations are required:

$$\langle M w_i^{\boldsymbol{n}} w_j^{\boldsymbol{p}} \rangle \,,\ \langle w_i^{\boldsymbol{m}} w_j^{\boldsymbol{n}} w_k^{\boldsymbol{p}} \rangle \,,\ \langle w_i^{\boldsymbol{m}} w_j^{\boldsymbol{n}} w_k^{\boldsymbol{p}} w_l^{\boldsymbol{q}} \rangle \tag{28}$$

The data requirement for representing the entire fourth-order correlation function in (28) is prohibitive. To ease the requirement, quadratic products in the model (18) are restricted to nearby separations ($|\boldsymbol{m} - \boldsymbol{n}| \leq 1$).

The linear *optimal* estimate is determined using the following estimation equations:

$$\langle M \rangle = A \tag{29}$$

$$\langle M w_i^{\boldsymbol{p}} \rangle = \sum_{\boldsymbol{m}} B_j^{\boldsymbol{m}} \langle w_j^{\boldsymbol{m}} w_i^{\boldsymbol{p}} \rangle \tag{30}$$

For the quadratic *optimal* estimate, the following set of estimation equations must be solved:

$$\langle M \rangle = A + \sum_{\boldsymbol{m}} \sum_{\boldsymbol{n}} C_{jk}^{\boldsymbol{mn}} \langle w_j^{\boldsymbol{m}} w_k^{\boldsymbol{n}} \rangle \tag{31}$$

$$\langle M w_i^{\boldsymbol{p}} \rangle = \sum_{\boldsymbol{m}} B_j^{\boldsymbol{m}} \langle w_j^{\boldsymbol{m}} w_i^{\boldsymbol{p}} \rangle + \sum_{\boldsymbol{m}} \sum_{\boldsymbol{n}} C_{jk}^{\boldsymbol{mn}} \langle w_j^{\boldsymbol{m}} w_k^{\boldsymbol{n}} w_i^{\boldsymbol{p}} \rangle \tag{32}$$

$$\langle M w_i^{\boldsymbol{p}} w_l^{\boldsymbol{q}} \rangle = A \langle w_i^{\boldsymbol{p}} w_l^{\boldsymbol{q}} \rangle + \sum_{\boldsymbol{m}} B_j^{\boldsymbol{m}} \langle w_j^{\boldsymbol{m}} w_i^{\boldsymbol{p}} w_l^{\boldsymbol{q}} \rangle + \sum_{\boldsymbol{m}} \sum_{\boldsymbol{n}} C_{jk}^{\boldsymbol{mn}} \langle w_j^{\boldsymbol{m}} w_k^{\boldsymbol{n}} w_i^{\boldsymbol{p}} w_l^{\boldsymbol{q}} \rangle \tag{33}$$

In this work, the correlations are computed using filtered DNS fields from a well-resolved pseudo-spectral 256^3 simulation of forced isotropic turbulence. Numerical details of the simulation can be found in Rogallo [29]. In the arbitrary units of the simulation code, the DNS data has the following characteristics: turbulent kinetic energy $q^2/2 = 41.1$, dissipation $\epsilon = 62.9$, Taylor microscale $\lambda = 0.209$, and microscale Reynolds number $R_\lambda = 164$. The three-dimensional energy spectrum of the DNS is displayed in Fig. 2, with the filter width clearly indicated. This is the same DNS used by Langford & Moser [10] for computing their *optimal* subgrid stress model. Note that due to the relatively low Reynolds number of the DNS, the filter width Δ could not be either much larger or much smaller in this flow if it is to remain in the approximate inertial range.

The correlations were gathered from 15 DNS fields, each separated by approximately one-half of an eddy-turnover time. To increase the statistical sample, each of the 48 possible reflections and rotations of the field were also included in the averaging. Note that the mapping from a single DNS field to a filtered field is not unique, because the volume elements can be positioned at many different locations. When mapping from a 256^3 DNS field to a 32^3 LES field, 8^3 linearly independent choices exist for the mapping. By averaging over all the possibilities, one ensures the highest quality correlations. In this work, a choice was made to consider only 2^3 LES mappings for each DNS field. This number was chosen to allow a data set that could be stored and managed on available equipment.

4. Convergence

In traditional finite-volume schemes for incompressible flows, the flux model is derived from a reconstruction of the flux function from the cell-averaged velocity data. A reconstruction based on a Taylor series expansion is usually appropriate because it can be assumed that the underlying function is smooth and that the grid separation, Δ, is small when compared to the smallest lengthscales of the velocity field. The resulting approximation then converges in the usual sense, in that the errors decrease with decreasing Δ, and can be made arbitrarily small, limited only by the precision of the arithmetic used in the calculations. For example, order of accuracy considerations in traditional finite-volume schemes results in an error decaying as Δ^2 (a second order scheme) for a $1\times1\times2$ stencil, while a $1\times1\times4$ stencil yields a fourth-order accurate scheme.

The ideas of convergence and order of accuracy of the numerical model must be reexamined in the current *optimal* finite-volume LES approach. In this case, Δ is by definition not small compared to the smallest scales of the velocity field. Furthermore, in the LES formulation considered here, the filter definition and numerical discretization are identical, so the grid size Δ cannot be small compared to the filtered velocity either. Reconstruction of the fluxes based on Taylor series or other numerical procedure would clearly be invalid in this case, as are our usual notions of convergence.

In *optimal* finite volume LES, two senses of convergence should be considered, though neither will be of direct utility in the current work. First, at fixed Δ we can ask whether a sequence of increasingly complex models converges to the *ideal* model. For the model defined in (18), the complexity can be increased by increasing the size of the stencil. But this clearly does not yield convergence to the ideal model, since (18) is restricted to quadratic dependence on $\boldsymbol{w}$. While this does not yield convergence to the ideal, the way local models approach the corresponding global model as the stencil is expanded, is of interest [30]. In addition, adding higher order terms, (cubic, fourth order etc.) to (18) could in principle result in convergence to the ideal, though this would be difficult to prove, and impractical to implement.

The second sense of convergence is statistical. For a given non-ideal model, we are interested in the convergence of statistical quantities representative of the large scales with decreasing Δ. This is the sense of convergence defined by Pope (private communication,

2002; see also Meneveau [31]). In this case, Δ is considered to always be much larger than the Kolmogorov scale (formally $Re \to \infty$ as $\Delta \to 0$), so the usual convergence to a DNS does not apply. To capture the large scale statistics, it is clearly necessary for Δ to be small compared to the large scales of turbulence (which are of order q^3/ϵ, where q^2 is twice the turbulent kinetic energy and ϵ is the dissipation), thus $\Delta\epsilon/q^3$ should be small (it is 0.017 for the case considered in section III). For comparison purposes, the ratio of Δ to the Kolmogorov lengthscale, Δ/η, is 23.7, and the ratio of Δ to the longitudinal integral lengthscale, Δ/L_{11}, is 0.195. Convergence in this sense clearly depends on the statistical quantity considered. For the purposes of this paper, we will consider the low-wavenumber spectrum and the large-separation third-order structure function. However, because of the reliance on moderate Reynolds number DNS for the statistical data needed in the *optimal* model, it is not possible to empirically explore statistical convergence in the limit defined above.

III. RESULTS

Diagnostics of LES models are usually divided into two distinct categories: *a priori* and *a posteriori*. In *a priori* tests one evaluates the model's performance by comparing the modeled terms with actual terms obtained from DNS (or experiments, where possible). Notice that this kind of diagnostic is actually an integral part of the *optimal* modeling technique, since the *optimal* model minimizes a given *a priori* variation (in our case, the single-flux variation d_1 defined by (20)).

A-priori testing of LES models has often revealed that the modeled term correlates rather poorly with the actual term determined from real turbulence realizations. In the language of the current study, the variation associated with the model is large. As was mentioned in section II B 2, it is inappropriate to label this variation "error," because much of this commonly identified "error" is actually due to the stochastic nature of the filtered field evolution. Due to the many-to-one nature of the filter mapping, a filtered field does not include enough information to uniquely determine its evolution, or for a finite volume filter, the fluxes. The variability in the possible filtered evolutions is responsible for the irreducible variance about the *ideal* LES evolution given by (6).

Ideally, one should separate the variation measured *a-priori* for any model into two

components; the deterministic error of the model and the stochastic variance. The stochastic variance is intrinsic to the LES and is the variation attained by the *ideal* LES model. This portion of the *a-priori* variation is only dependent on the characteristics of the filter and the turbulent flow. The deterministic error reflects modeling errors and quantifies the accuracy of a given model in approximating the ideal. Unfortunately, these components of the *a-priori* variation cannot be computed separately. Only the combined variation of a given model can be determined, and it can give the false impression that the model is inaccurate when it is the stochastic variance that is large.

In many models found in the literature [32–35], the correlation between the *a priori* and *a posteriori* results has been poor, since performance commonly appears to be unsatisfactory in the former, but is acceptable in the latter. This suggests that the *a-priori* results may have been dominated by the stochastic variance component, which has no effect on single-time multi-point statistics [10, 23]. To compare LES models fairly in *a-priori* evaluation, one must be careful to keep the stochastic portion of the results consistent. In the present case, the *a-priori* results for all models are computed with the same filter and for the same turbulent flow. Therefore, the *a priori* variations for the models are indicative of relative model accuracy. In particular, the measured difference in the mean-square variation associated with two models is also the mean-square difference in the deterministic error, which can be used as a guide in selecting the best stencil geometries and model inputs.

The *a posteriori* tests measure the performance of the models in actual simulations, with emphasis on the simulation results, rather than a detailed analysis of the models' accuracy. The models with the best performance in the *a-priori* tests will be evaluated in simulations, where they will be compared with the dynamic Smagorinsky subgrid model and filtered DNS results.

A. *A Priori* Analysis of Global Estimates

Relative root mean-square variation measurements for the global estimates are shown in Table I. Shown are the *a-priori* dual-flux variations $d_{||}$, which, as noted before, are a better measure of impact on the dynamics of an LES than the single-flux variations $d_{|}$. The RMS

variations are defined as:

$$RMS = \sqrt{\frac{\left\langle d_{||}^2 \right\rangle}{\left\langle \left(M^i - M^{i+(0,0,1)}\right)^2 \right\rangle}} \tag{34}$$

Note that the difference between the mean-square variations of two models, δ_d, is a measure of the difference in the deterministic modeling error between these models. One can easily verify the relation between the variation and deterministic error differences by defining δ_d as:

$$\begin{aligned} \delta_d &= {RMS_2}^2 - {RMS_1}^2 \\ &= \frac{\left\langle d_{||}^2 \right\rangle_2 - \left\langle d_{||}^2 \right\rangle_1}{\left\langle \left(M^i - M^{i+(0,0,1)}\right)^2 \right\rangle} \end{aligned} \tag{35}$$

where the 1 and 2 subscripts refer to two different models.

Writing the dual-flux variation $d_{||}$ as the sum of the modeling error e and stochastic variance v

$$d_{||} = e + v, \tag{36}$$

substituting (36) in (35) and expanding yields

$$\delta_d = \frac{\langle e^2 \rangle_2 - \langle e^2 \rangle_1 + 2\langle ev \rangle_2 - 2\langle ev \rangle_1 + \langle v^2 \rangle_2 - \langle v^2 \rangle_1}{\left\langle \left(M^i - M^{i+(0,0,1)}\right)^2 \right\rangle} \tag{37}$$

Equation (37) can be simplified by noting that the stochastic variance is a property only of the filter and the flow, not of the model, so that $\langle v^2 \rangle_2 = \langle v^2 \rangle_1$. Furthermore, the modeling error and stochastic variance are orthogonal (see [11]); that is $\langle ev \rangle_2 = \langle ev \rangle_1 = 0$. Therefore, δ_d is the difference in mean-square modeling error between two models

$$\delta_d = \frac{\langle e^2 \rangle_2 - \langle e^2 \rangle_1}{\left\langle \left(M^i - M^{i+(0,0,1)}\right)^2 \right\rangle}. \tag{38}$$

Variation measurements can thus be used as a measure of relative modeling accuracy between the *optimal* models.

These variation measurements allow one to make comparisons of the following: linear vs. quadratic estimates; staggered vs. collocated grids; local vs. nonlocal quadratic products. Local quadratic products are those in which the velocity components forming the quadratic

event variable are located in the same or overlapping volumes. For nonlocal quadratic products, the separation between velocity components may be greater. One can also assess the importance of terms which are not similar to those in standard finite-volume schemes. These terms will be referred to as *nonstandard.* Standard terms are those that would arise in standard finite-volume schemes: w velocities for $M_{\partial w/\partial z}$; u velocities for $M_{\partial u/\partial z}$; w–w velocity products for M_{ww}; u–w velocity products for M_{uw}. Estimates having only standard terms are marked with a † in Table I. Nonstandard dependencies in the model might improve estimates because the velocity components are correlated, so that velocity components on which a quantity is not directly dependent (*e.g.* v in the the M_{ww} flux) can provide information about that quantity.

The following conclusions are supported by the variation measurements:

- Linear estimates are suitable for estimations of the viscous fluxes, $M_{\partial w/\partial z}$ and $M_{\partial u/\partial z}$, but not for the convective fluxes (as expected).

- For the convective fluxes, M_{ww} and M_{uw} on collocated grids, the inclusion of nonlocal quadratic products provides modest ($< 3\%$ of the dual flux term) reduction in error when only standard terms are used, and a larger ($> 5\%$) reduction in error when nonstandard terms are used.

- For estimates with only standard terms, there is no clear advantage to either the staggered or collocated grid. When nonstandard terms are included, the staggered grid is better for the viscous fluxes, and the collocated grid is better for the convective fluxes.

- For the viscous fluxes, including nonstandard terms provides a modest (3–4% of the dual flux term) reduction in error. For the convective fluxes, the use of nonstandard terms reduces error by up to 6%.

For estimates with only standard terms, the relative root mean-square variations are about 36% for $M_{\partial w/\partial z}$, 51% for $M_{\partial u/\partial z}$, 44% for M_{ww}, and 50% for M_{uw}. These variations are large, especially considering that they are normalized by the magnitude of the total flux term, which represents both the Navier-Stokes and subgrid effects. The large *a priori* variations of these global estimates are similar to those encountered by Langford & Moser [10] and Völker, Moser & Venugopal [11] for the subgrid terms. As pointed out previously,

such large variations are to be expected if the term being modeled is largely stochastic. Particularly, if the variance about the ideal model dominates the variation, then a large variation will not impact the accuracy of an LES.

B. *A Priori* Analysis of Local Estimates

While a global model will provide the best estimate for the fluxes, the computational cost associated with the large stencil (32×32×32 volumes for each velocity component) makes it impractical for actual simulations, and may be unnecessary. Local models may be nearly as accurate, at a fraction of the cost of a global model. A large collection of local models was computed for both staggered and collocated grids. The complete set of *a priori* results can be found in Langford [30].

The observations made in the case of global estimates still hold for the local models. For the viscous fluxes, linear estimates are sufficient. For convective fluxes the nonlocal quadratic models result in the lowest variations. There is, however, a dependence on stencil, flux and type of grid on the effect of using standard or nonstandard estimates.

The viscous terms have little sensitivity to the use of nonstandard terms, notably in the thinner stencils (the width of the stencil is related to the number of volumes in the direction parallel to the face, while the length is related to the number of volumes in the direction normal to the face). With wider stencils, accuracy improves with the use of nonstandard terms, but the improvement is small. For example, the best linear nonstandard staggered model for $M_{\partial u/\partial z}$(the 5×5×6–6×6×6–6×5×5 stencil) shows only a 7% improvement in the variation over the much thinner linear standard staggered 1×1×6–2×2×2–2×1×1 stencil. Note that the smaller stencil is composed of only 16 volumes, while the best model's stencil is composed of 516 volumes. The cost of the model increases faster than linearly with the number of volumes (N^2, or $Nlog(N)$ if a Fourier transform is used), so one must weigh the small accuracy improvement against the large increase in cost.

The effect of nonstandard terms on the convective fluxes is also stencil dependent. The effect on the thinner stencils is small, but the improvement on the wider stencils is quite significant, especially in the collocated case (up to 19% improvement). The improvement in the case of staggered grids is not as important (a maximum of 6%). Once again one must measure the cost of using a wider stencil against the reduction in error.

When extending the stencil, one must weigh the advantages of lengthening versus widening. It is clear from the *a priori* results that lengthening is preferable in almost every occasion. In the viscous flux case, widening the stencil brought little, if any, improvement to the variation, while lengthening the stencil from 2 to 6 volumes decreased the variation by as much as 22%. In the case of the convective terms, the same observation holds, with the caveat that if nonstandard terms are used, widening of the stencil does produce a noticeable decrease in variation.

The difference in variation between the best local estimates and the global estimates is small. The variation for the best estimates (with stencils which occupy approximately 1/25 of the volume occupied by the global stencil) are within 10% of the global estimates, and most of the improvement in accuracy occurs when lengthening the stencil to four (4) volumes in the direction normal to the face. This indicates that most of the information needed for the accurate estimation of the fluxes is local, and that the use of local estimates does not lead to variations which are much greater than those observed with global estimates. This is consistent with the observations of Langford [30] in spectral based optimal LES.

With these observations about local estimates in mind, one can make suggestions about the stencils to be used in actual simulations. For the viscous fluxes a standard linear model is adequate, while a quadratic model (as expected) must be used for the convective fluxes. To improve the accuracy of the models, the extension of the stencil should be primarily in the direction normal to the face. If further accuracy is desired, the stencil can be widened and, in this case only, nonstandard models should be used. This last recommendation appears more important for collocated grids than for staggered ones.

C. *A Posteriori* Analysis of Local Estimates

The choice of local models for the *a posteriori* analysis is based on the results from the previous section. The models analyzed *a posteriori* are listed in Table II with their *a-priori* variations displayed in Table III. The nomenclature of the models is the following: the first letter indicates whether the model is for a staggered or collocated grid, the second character (2, 4, 6 or w) indicates the stencil geometry and the third letter, if present, indicates the use of standard (s) or nonstandard (n) finite-volume events in the model. Model descriptors without a third-character refer to models using only standard events. Note that the stencils

are only given for four fluxes shown in Table II because by isotropy, these four fluxes can be rotated to define the stencil for any of the required fluxes (see Section II A). For this reason, there is no v-dependency in any of the standard models shown.

In *a priori* analysis, lengthening the model's stencil yielded the largest improvements in the accuracy of the flux. Widening the stencil did not bring such benefits, unless nonstandard terms were used. With these characteristics in mind, most of the models for *a posteriori* analysis were constructed with long, thin stencils. Wider models (models Cws, Cwn, Sws and Swn) were used to verify if extending the stencil in the direction parallel to the face was indeed ineffective for error reduction. Most of the *a posteriori* models only contain standard terms, but four pairs of models (model pairs C6s-C6n, Cws-Cwn, S6s-S6n and Sws-Swn), with identical stencil geometries, were simulated with standard-only and standard+nonstandard terms. These results allow the investigation of the effect of nonstandard terms on model accuracy.

The *a posteriori* results were obtained using a third-order Runge-Kutta scheme for time integration. To maintain turbulence, a negative viscosity forcing term was used to stir the flow. The forcing was identical to the one used in the original DNS [10]. The LES statistics were collected for approximately $60t$, with samplings separated by $0.15t$, where t is the eddy-turnover time defined by

$$t = \frac{q^2}{2\epsilon} \tag{39}$$

The initial fields for the simulation were obtained by filtering DNS fields.

Pressure was determined by projecting the velocity field onto a discretely divergence-free space, using an approximate divergence operator. As pointed out by Langford & Moser [27], such a projection introduces a modeling error because the filtered field does not exactly satisfy any continuity constraint. As suggested by their results, a two or three-point stencil (for staggered and collocated grids, respectively) for the approximate divergence was used, which provides an accurate approximation, at least in the staggered grid case. By symmetry, these approximate divergence operators are equivalent to the second-order divergence approximations commonly used in finite-volume methods. Unfortunately, many of the collocated models were not numerically stable and results were obtained only for few of them (models C2, C4 and Cwn). The reason for this instability appears to be connected to the treatment of pressure, leading to the commonly observed odd-even decoupling in collocated models without enough dissipation at the highest wavenumbers.

The three-dimensional energy spectrum is shown in Fig. 3. Most of the models agree very well with the filtered DNS energy spectrum, with small errors in the high wavenumber region. The smallest stencils, represented by models C2 and S2, do not seem to incorporate enough information to represent the higher wavenumbers. The collocated model C2 is especially inaccurate, only wavenumbers up to around 7 are correctly represented. The staggered model S2 is better, but there seems to be excess dissipation at the higher wavenumbers. The larger staggered stencils are remarkably better. With model S4, the LES spectrum is accurate throughout the wavenumber range, and model S6 improves upon those results only slightly. The collocated C4 model only improves slightly upon the C2 model, and is not nearly as accurate as the staggered models.

Surprisingly, widening the stencil, as in model Sws, caused a large discrepancy in the energy of the higher wavenumbers. Inspection of the stencils for the Sws model showed that the linear terms for the M_{uw} fluxes had an anti-diffusive character for large wavenumbers. This is likely to lead to poor large-wavenumber performance, and may lead to numerical instabilities. There is no *a-priori* guarantee that the *optimal* estimation procedure will produce numerical schemes that are stable. Such stability constraints could be included in the optimization and this should be explored in future research.

The models with nonstandard terms (Cwn, S6n and Swn) were markedly inaccurate when compared with the similar models which used only standard terms (S6s and Sws), especially at high wavenumbers. The value of nonstandard terms in reducing the *a priori* error is dependent on the correlations between different velocity components. Apparently in the LES, these cross correlations were not maintained causing the nonstandard terms to degrade, rather than enhance performance. An examination of the coefficients for the nonstandard terms reveals that many of them involve what appear to be discrete approximations to $\partial u/\partial x$, $\partial v/\partial y$ and/or $\partial w/\partial z$, so as to suggest that the quantities being modeled can be rewritten using continuity. Thus, it may be that modeling errors inherent to the continuity representation contribute to the poor performance of nonstandard models.

The energy transfer by the models can be analyzed by computing the third-order structure function

$$S_3(r) = \left\langle \left(u\left(x+r\right) - u\left(x\right)\right)^3 \right\rangle, \tag{40}$$

which is shown in Fig. 4. The structure function results for the smaller models (C2 and S2) are not in agreement with the DNS data for small separations. This reveals that the

energy transfer is not adequately represented by stencils smaller than 4 in the direction normal to the face, and explains the deficiencies encountered in the energy spectrum of the smaller models. The remaining staggered models reproduce S_3 quite accurately, while the C4 collocated model underpredicts it at all separations and the Cwn collocated model is quite inaccurate for small separations. For the staggered grids, the widest stencil (model Sws) is slightly better than the thin stencils (models S4 and S4s), but the difference is almost negligible. The nonstandard models are again less accurate than their standard counterparts.

In Appendix B, the model coefficients for the S2 and S4 models are given. The S4 model is given because it is the smallest stencil that produces good agreement with the filtered DNS data, for both the spectra and the structure function. The S2 model is shown for comparison with a standard second-order finite-volume scheme. One important difference between the S2 model and the standard second-order staggered approximation is that the *optimal* model is more dissipative, primarily due to the linear term in the convective fluxes. This is expected because the *optimal* model includes the effects of the subgrid turbulence, which is primarily dissipative. Also shown in Appendix B is the procedure for constructing the S2 model, that can be easily extended to all other *optimal* models discussed in this paper.

In Figs. 5 and 6, results for the *optimal* finite-volume LES models are compared with results obtained with the dynamic Smagorinsky subgrid scale model. The dynamic Smagorinsky results were obtained on staggered grids using the same code used for the *optimal* finite-volume LES cases, employing second- and fourth-order accurate discretization schemes for the fluxes and subgrid models. In Fig. 5, the dynamic Smagorinsky model dampens the high-wavenumber spectra excessively when compared to the *optimal* models and the filtered DNS results, while the spectra for *optimal* and dynamic Smagorinsky models is comparable up to wavenumbers around 18.

In Fig. 6, the structure function results indicate that the smaller stencils, S2 and the second-order accurate dynamic Smagorinsky, are not appropriate for an accurate representation of the energy transfer in this LES. For these small stencils, the dynamic Smagorinsky model is better than the *optimal* model at small separations, while overpredicting the structure function by a large margin when the separation is larger. When using the larger stencils, as in the S4 *optimal* model and the fourth-order accurate dynamic Smagorinsky model, the energy transfer of the fourth-order dynamic Smagorinsky model is slightly more accurate

than that of the second-order model, but the structure function is still overpredicted in most of the separation range. On the other hand, the *optimal* model S4 structure function is very close to the filtered DNS results for all separations. Therefore, for this example, the *optimal* model S4 is more accurate than the dynamic Smagorinsky subgrid model using a standard finite-volume discretization scheme with an identically sized stencil.

IV. DISCUSSION

An *optimal* coarse finite-volume LES modeling technique has been developed and applied to isotropic turbulence. This approach addresses some of the issues encountered in current LES modeling, namely: ambiguous definition of filtering and treatment of numerical discretization errors. While many current LES models allow the filter to be defined implicitly by the numerics, the *optimal* finite-volume LES technique rigorously defines the filter (equation (9)) and the resulting model is strongly dependent on this choice, as it must be. Numerical discretization issues usually encountered in coarse representations of LES are resolved in the *optimal* technique by handling the Navier-Stokes, discretization and subgrid effects simultaneously. In this way, the combined numerical and modeling errors are minimized.

The results obtained while testing the *optimal* finite-volume staggered models are encouraging. The energy spectra and third-order structure functions computed *a posteriori* are of comparable accuracy to those obtained by Langford [30] using a spectral numerical method, a sharp Fourier-cutoff filter and an *optimal* model for the subgrid stress. The spectral numerical method used in Langford [30] avoids the discretization errors usually encountered in LES. The current approach achieves similar results, indicating that the numerical limitations one expects in a finite-volume representation have largely been avoided. The *a-posteriori* results for the *optimal* model were more accurate than those obtained with the dynamic Smagorinsky model using either standard second- or fourth-order discretizations for the flux terms. The dynamic Smagorinsky results show high-wavenumber discrepancies in the energy spectra that are not observed in the data from the *optimal* models. This behavior is consistent with the inability of the coarse low-order standard numerical method to resolve the high-wavenumber components of the resolved field.

While the performance of the *optimal* finite volume LES evaluated here was quite promis-

ing, there are a few issues that need to be addressed. In a few isolated cases, the *optimal* estimation procedure yielded model coefficients with poor numerical properties, and in some cases the models were unstable. Methods that constrain the *optimal* procedure to produce only stable numerical schemes should be pursued in future research. Instabilities also arose in collocated models, probably due to the implementation of the continuity constraint. Traditional finite-volume schemes have similar difficulties that commonly lead to checkerboard decoupling of the pressure. In future research with collocated grids, stabilization procedures for computation of the pressure (e.g. Rhie & Chow [36]) may be useful.

The modeling procedure described here, in which DNS statistical data is used as input to the *optimal* modeling formulation, is clearly not useful for generating practical LES models, unless the need for DNS data can be eliminated. Because the results of the current study indicates that our approach can produce accurate LES, such a generalization is being pursued. A promising approach to eliminating the need for LES data is to evaluate their required statistical quantities theoretically. The correlations required as input to the modeling (see Appendix B) are surface and volume integrals of multi-point second, third and fourth order velocity correlations. Using a combination of Kolmogorov theory (the $\frac{2}{3}$ and $\frac{4}{5}$ laws for the second and third order correlations respectively), the quasi-normal approximation (fourth order correlations) and a generalized dynamic procedure, it appears that the required correlations can be determined under the assumption that filter width is in an inertial range, and that the small scales are isotropic. Once these multi-point velocity correlations are determined, they can be integrated as needed for the finite volume grid being used in any particular problem, and the *optimal* modeling coefficients specific to that grid can then be found. We envision this as a preprocessing step for a simulation, similar to constructing and storing the stencil coefficients for a standard differencing scheme on a general mesh. When the assumptions of an inertial range and small scale isotropy are not valid (*e.g.* near walls), then further modeling will be required. However, it is still a matter of modeling the small-separation multi-point velocity correlations.

It is useful to contrast the development of the finite volume *optimal* LES formulation described here with common finite volume numerical schemes and to the MILES approach introduced by Boris, *et al.* [37]. In the current formulation, the representation in terms of volume averaged velocities is identical to standard finite volume techniques. But, because the volume size is by definition large compared to the smallest scale of motion, it is not valid

to approximate fluxes using standard reconstruction techniques, which are based on the assumption that the velocity is smooth on the scale of the volume size. Another circumstance in which this assumption is violated is shock capturing. In this instance, special numerical approximations have been devised to account for the sub-grid features of the flow (the shocks), based on knowledge of the properties of shocks. Thus shock capturing schemes are designed to recover the shock jump conditions, keep the numerical shock as thin as possible on the grid (of order the grid spacing) and preserve the monotonicity of the shock solution. Subgrid turbulence is more complex and our knowledge of the properties of subgrid turbulence is only statistical. It is thus this statistical information that is used in the *optimal* LES formulation. The MILES formulation first introduced by Boris, *et al.* [37] is based on the observation that one of the statistical properties of subgrid turbulence is that, like shocks, it is dissipative. Numerical schemes similar to those designed for shock capturing are thus used in MILES, with the dissipative properties adjusted to more closely resemble those of turbulence. However, in general, subgrid turbulence has numerous statistical properties that impact large-scale dynamics, besides dissipation. In particular, with finite volume representations like those described here, the subgrid affects every aspect of the filtered dynamics. The *optimal* approach allows models to be constructed that reproduce most of the dynamically significant statistical properties *a priori* [11].

The finite volume *optimal* LES formulation described here was pursed rather than the theoretically more straight-forward formulations based on spectral representations because a spectral formulation cannot easily be applied in flows with complex geometries. While, the current study involves only a very simple flow (isotropic turbulence) on a uniform Cartesian grid, the approach is clearly applicable in general geometries on general grids. The only limitation is the availability of the required statistical data. In this study, statistical data was obtained from DNS, but current research is directed at providing this information theoretically.

Acknowledgments

The research reported here has been supported under NSF grant CTS-001435 and AFOSR grant F49620-01-1-0181, and by the Center for Simulation of Advanced Rockets, which is funded by the Department of Energy through University of California grant B341494. This

support is gratefully acknowledged. We also benefited from many discussions with Profs. Balachandar and Adrian, and Dr. Andreas Haselbacher of the Center for Simulation of Advanced Rockets.

APPENDIX A: ANALYSIS OF ESTIMATES BASED ON SINGLE AND DUAL-FLUX VARIATIONS

While the dual-flux variation $d_{||}$ is more relevant to the LES evolution, using this variation in the estimation procedure is not without problems, as demonstrated by the following one-dimensional model problem. Notation for this problem is illustrated in Fig. 7. The variable w is a scalar and M is the x-component of a vector field.

The model system is considered to be homogeneous, with a reflectional symmetry in its single spatial direction. It follows that the symmetries of this system are

$$\langle w^+ w^+ \rangle = \langle ww \rangle , \tag{A1}$$

$$\langle w^+ w \rangle = \langle w w^- \rangle , \tag{A2}$$

$$-\langle M^+ w \rangle = \langle M^+ w^+ \rangle . \tag{A3}$$

The exact evolution of the model system is $\dot{w} = M^+ - M^-$, where $\dot{w} = \mathrm{d}w/\mathrm{d}t$. Therefore, the mean dissipation ϵ in this system is

$$\begin{aligned} \epsilon &= \langle \dot{w} w \rangle \\ &= \langle M^+ w \rangle - \langle M^- w \rangle \\ &= 2 \langle M^+ w \rangle \\ &= -2 \langle M^+ w^+ \rangle . \end{aligned} \tag{A4}$$

1. Estimate based on Single-Flux Variation $(d_|)$

If the linear stochastic model of M^+ given event data w and w^+ is:

$$m^+ = \alpha w^+ + \beta w. \tag{A5}$$

The coefficients α and β can be determined by the stochastic estimation procedure. When minimizing the single-flux variation $d_| = M^+ - m^+$, the stochastic estimation procedure

yields the following linear system

$$\begin{pmatrix} \langle w^+w^+\rangle & \langle ww^+\rangle \\ \langle w^+w\rangle & \langle ww\rangle \end{pmatrix} \begin{pmatrix} \alpha \\ \beta \end{pmatrix} = \begin{pmatrix} \langle M^+w^+\rangle \\ \langle M^+w\rangle \end{pmatrix}. \tag{A6}$$

From the symmetries (A1–A3) it follows that the solution for the coefficients is

$$\alpha = -\beta = \frac{\langle M^+w^+\rangle}{\langle ww\rangle - \langle ww^+\rangle}. \tag{A7}$$

The estimated evolution of the system is $\widetilde{\dot{w}} = m^+ - m^-$, so that the estimated dissipation $\tilde{\epsilon}$ is

$$\begin{aligned} \tilde{\epsilon} &= \left\langle \widetilde{\dot{w}} w \right\rangle \\ &= \langle m^+w\rangle - \langle m^-w\rangle \\ &= \alpha\left(\langle w^+w\rangle - \langle ww\rangle\right) - \alpha\left(\langle ww\rangle - \langle w^-w\rangle\right) \\ &= 2\alpha\left(\langle ww^+\rangle - \langle ww\rangle\right). \end{aligned} \tag{A8}$$

Substituting equation (A7) into equation (A8) and comparing with the expression given by (A4), is is clear that $\tilde{\epsilon} = \epsilon$.

The shortcoming to this method of estimation is the possibility of fluctuations of M^+ that exactly cancel fluctuations of M^-. Unfortunately, part of the "effort" of computing the estimate goes to estimating the part that cancels. An improvement may be achieved by minimizing the variation in the dual-flux, $M^+ - M^-$, rather than the single-flux variation in only M^+.

2. Estimates based on the Dual-Flux variation $(d_{||})$

When using the dual-flux variation, the estimate is of the following form

$$\begin{aligned} m^+ - m^- &= \alpha w^+ + \beta w - \alpha w - \beta w^- && \text{(A9)} \\ &= \alpha w^+ + (\beta - \alpha)w - \beta w^- && \text{(A10)} \\ &= \alpha(w^+ - w) + \beta(w - w^-). && \text{(A11)} \end{aligned}$$

This can be regarded as a linear stochastic model of $(m^+ - m^-)$ given event data $(w^+ - w)$ and $(w - w^-)$.

The estimation equations in this case are given by the linear system

$$\begin{pmatrix} \langle (w^+ - w)(w^+ - w) \rangle & \langle (w - w^-)(w^+ - w) \rangle \\ \langle (w^+ - w)(w - w^-) \rangle & \langle (w - w^-)(w - w^-) \rangle \end{pmatrix} \begin{pmatrix} \alpha \\ \beta \end{pmatrix} = \begin{pmatrix} \langle (M^+ - M^-)(w^+ - w) \rangle \\ \langle (M^+ - M^-)(w - w^-) \rangle \end{pmatrix}. \tag{A12}$$

The solution for this system is

$$\alpha = -\beta = \frac{\langle (M^+ - M^-)(w^+ - w) \rangle}{\langle (w - w^-)(w - w^-) \rangle - \langle (w - w^-)(w^+ - w) \rangle}, \tag{A13}$$

and the estimated dissipation is

$$\begin{aligned} \tilde{\epsilon} &= \left\langle \tilde{\dot{w}} w \right\rangle \\ &= \langle (m^+ - m^-) w \rangle \\ &= \alpha \left(\langle (w^+ - w) w \rangle - \langle (w - w^-) w \rangle \right) \\ &= \alpha \left(\langle w w^+ \rangle - 2 \langle w w \rangle + \langle w w^- \rangle \right) \\ &= 2\alpha \left(\langle w w^+ \rangle - \langle w w \rangle \right). \end{aligned} \tag{A14}$$

Note that (A14) is identical to equation (A8) of the single-flux estimate. The value of α for the previous solution, equation (A7), was such that $\tilde{\epsilon} = \epsilon$. The value of α for the current technique, equation (A13), is different. The current solution for α given in (A13) depends on $\langle w^- w^+ \rangle$, while the previous solution, equation (A7), does not. It follows that the coefficients α for the two cases are in general different, and that for this method, $\tilde{d} \neq d$.

Therefore, a dual-flux estimate written in conservative form will not correctly match dissipation. One can, however, choose to estimate the dual-flux in a nonconservative form, i.e.

$$m^+ - m^- = \alpha w^+ + \beta w + \gamma w^-. \tag{A15}$$

In this case, the estimation equations are

$$\begin{pmatrix} \langle w^+ w^- \rangle & \langle w w^- \rangle & \langle w^- w^- \rangle \\ \langle w^+ w \rangle & \langle w w \rangle & \langle w^- w \rangle \\ \langle w^+ w^+ \rangle & \langle w w^+ \rangle & \langle w^- w^+ \rangle \end{pmatrix} \begin{pmatrix} \alpha \\ \beta \\ \gamma \end{pmatrix} = \begin{pmatrix} \langle (M^+ - M^-) w^+ \rangle \\ \langle (M^+ - M^-) w \rangle \\ \langle (M^+ - M^-) w^- \rangle \end{pmatrix}. \tag{A16}$$

Symmetries dictate that $\alpha = \gamma$, but nothing is implied about the relationship to β. Without actually solving these equations, we will simply consider the second row in (A16). It follows that

$$\begin{aligned} \langle (m^+ - m^-)w \rangle &= \langle (M^+ - M^-)w \rangle \\ \tilde{d} &= d. \end{aligned} \tag{A17}$$

This estimate does not suffer from cancellation problems, and it has the correct dissipation. However, it is not conservative.

In the three cases shown above, it was demonstrated that there are several choices for local estimation techniques, but they all suffer from a deficiency. One can construct a conservative single-flux estimate that correctly matches dissipation, but some of the estimation power goes to minimize an error in portions of the flux that trivially cancel. Or one can construct a conservative dual-flux estimate that is aware of the cancellations, but dissipation is not correctly matched. Finally, one can construct a dual-flux estimate that minimizes the most relevant error and correctly matches dissipation, but the resulting estimate is not conservative.

There is yet another alternative. One can construct a conservative dual-flux estimate, subject to the constraint that dissipation is matched, i.e. that

$$\alpha \langle (w^+ - w)w \rangle + \beta \langle (w - w^-)w \rangle = \langle (M^+ - M^-)w \rangle . \tag{A18}$$

For the simple example explored here, the procedure reduces to the conservative single-flux estimate. However, as additional nonlocal velocity data is incorporated into the estimate, the procedure yields a distinct, fourth estimation procedure. Also note that in the limit of a global estimate, all four estimation procedures are identical. This can be understood by noting that for the global estimates, one can regard the procedure as the simultaneous estimation of fluxes at all locations, not just flux at a single location. Then, the combination of fluxes at opposite faces is merely a linear transformation of the quantity being estimated.

APPENDIX B: MODELS S2 AND S4 FOR STAGGERED GRIDS

The coefficients for the *optimal* finite-volume LES models S2 and S4 as formulated in the equations below, are presented in table IV, with coefficients for the standard second-order finite-volume scheme shown for comparison. The *optimal* models are strictly valid

only for the test case presented (microscale Reynolds number $\mathrm{Re}_\lambda = 164$, Taylor microscale $\lambda = 0.209$, kinetic energy $q^2/2 = 41.1$, dissipation $\epsilon = 62.9$ and grid spacing $\Delta = \pi/16$).

$$
\begin{aligned}
\frac{\partial u}{\partial t} &= A(u_{i-1,j,k} + u_{i+1,j,k}) + B(u_{i-2,j,k} + u_{i+2,j,k}) \\
&+ C(u_{i,j-1,k} + u_{i,j,k-1} + u_{i,j,k+1} + u_{i,j+1,k}) + D(u_{i,j-2,k} + u_{i,j,k-2} + u_{i,j,k+2} + u_{i,j+2,k}) \\
&+ E(u_{i,j,k}) + F(u_{i-1,j,k}u_{i-1,j,k} - u_{i+1,j,k}u_{i+1,j,k}) + G(u_{i-1,j,k}u_{i,j,k} - u_{i,j,k}u_{i+1,j,k}) \\
&+ H(-u_{i-2,j,k}u_{i-1,j,k} + u_{i+1,j,k}u_{i+2,j,k}) + I(u_{i-2,j,k}u_{i-2,j,k} - u_{i+2,j,k}u_{i+2,j,k}) \\
&+ J(u_{i,j-1,k}v_{i-1,j,k} + u_{i,j-1,k}v_{i,j,k} + u_{i,j,k-1}w_{i-1,j,k} + u_{i,j,k-1}w_{i,j,k} \\
&- u_{i,j,k}v_{i-1,j+1,k} - u_{i,j,k}v_{i,j+1,k} - u_{i,j,k}w_{i-1,j,k+1} - u_{i,j,k}w_{i,j,k+1} \\
&+ v_{i-1,j,k}u_{i,j,k} - v_{i-1,j+1,k}u_{i,j+1,k} + v_{i,j,k}u_{i,j,k} - v_{i,j+1,k}u_{i,j+1,k} \\
&+ w_{i-1,j,k}u_{i,j,k} - w_{i-1,j,k+1}u_{i,j,k+1} + w_{i,j,k}u_{i,j,k} - w_{i,j,k+1}u_{i,j,k+1}) - p_x
\end{aligned}
$$

$$
\begin{aligned}
\frac{\partial v}{\partial t} &= A(v_{i,j-1,k} + v_{i,j+1,k}) + B(v_{i,j-2,k} + v_{i,j+2,k}) \\
&+ C(v_{i-1,j,k} + v_{i,j,k-1} + v_{i,j,k+1} + v_{i+1,j,k}) + D(v_{i-2,j,k} + v_{i,j,k-2} + v_{i,j,k+2} + v_{i+2,j,k}) \\
&+ E(v_{i,j,k}) + F(v_{i,j-1,k}v_{i,j-1,k} - v_{i,j+1,k}v_{i,j+1,k}) + G(v_{i,j-1,k}v_{i,j,k} - v_{i,j,k}v_{i,j+1,k}) \\
&+ H(-v_{i,j-2,k}v_{i,j-1,k} + v_{i,j+1,k}v_{i,j+2,k}) + I(v_{i,j-2,k}v_{i,j-2,k} - v_{i,j+2,k}v_{i,j+2,k}) \\
&+ J(u_{i,j-1,k}v_{i,j,k} + u_{i,j,k}v_{i,j,k} - u_{i+1,j-1,k}v_{i+1,j,k} - u_{i+1,j,k}v_{i+1,j,k} \\
&+ v_{i-1,j,k}u_{i,j-1,k} + v_{i-1,j,k}u_{i,j,k} + v_{i,j,k-1}w_{i,j-1,k} + v_{i,j,k-1}w_{i,j,k} \\
&- v_{i,j,k}u_{i+1,j-1,k} - v_{i,j,k}u_{i+1,j,k} - v_{i,j,k}w_{i,j-1,k+1} - v_{i,j,k}w_{i,j,k+1} \\
&+ w_{i,j-1,k}v_{i,j,k} - w_{i,j-1,k+1}v_{i,j,k+1} + w_{i,j,k}v_{i,j,k} - w_{i,j,k+1}v_{i,j,k+1}) - p_y
\end{aligned}
$$

$$\frac{\partial w}{\partial t} = A(w_{i,j,k-1} + w_{i,j,k+1}) + B(w_{i,j,k-2} + w_{i,j,k+2})$$
$$+ C(w_{i-1,j,k} + w_{i,j-1,k} + w_{i,j+1,k} + w_{i+1,j,k}) + D(w_{i-2,j,k} + w_{i,j-2,k} + w_{i,j+2,k} + w_{i+2,j,k})$$
$$+ E(w_{i,j,k}) + F(w_{i,j,k-1}w_{i,j,k-1} - w_{i,j,k+1}w_{i,j,k+1}) + G(w_{i,j,k-1}w_{i,j,k} - w_{i,j,k}w_{i,j,k+1})$$
$$+ H(-w_{i,j,k-2}w_{i,j,k-1} + w_{i,j,k+1}w_{i,j,k+2}) + I(w_{i,j,k-2}w_{i,j,k-2} - w_{i,j,k+2}w_{i,j,k+2})$$
$$+ J(u_{i,j,k-1}w_{i,j,k} + u_{i,j,k}w_{i,j,k} - u_{i+1,j,k-1}w_{i+1,j,k} - u_{i+1,j,k}w_{i+1,j,k}$$
$$+ v_{i,j,k-1}w_{i,j,k} + v_{i,j,k}w_{i,j,k} - v_{i,j+1,k-1}w_{i,j+1,k} - v_{i,j+1,k}w_{i,j+1,k}$$
$$+ w_{i-1,j,k}u_{i,j,k-1} + w_{i-1,j,k}u_{i,j,k} + w_{i,j-1,k}v_{i,j,k-1} + w_{i,j-1,k}v_{i,j,k}$$
$$- w_{i,j,k}u_{i+1,j,k-1} - w_{i,j,k}u_{i+1,j,k} - w_{i,j,k}v_{i,j+1,k-1} - w_{i,j,k}v_{i,j+1,k}) - p_z$$

The procedure for computing model S2 is described below, the extension to the other models is straight forward. Each of the basic fluxes (M_{uw}, M_{ww}, $M_{\partial u/\partial z}$ and $M_{\partial w/\partial z}$) must obey the stochastic estimation equations (23) and (24), which are repeated here for convenience:

$$\langle M^i \rangle = \langle m^i \rangle \tag{B1}$$
$$\langle (M^i - m^i) E_l^i \rangle = 0 \tag{B2}$$

Note that the mean-preserving condition (B1) may be incorporated into (B2) by adding a constant term to the event vector $\boldsymbol{E}^i$ and, therefore, the estimation equations can be expressed as:

$$\langle m E_l \rangle = \langle M E_l \rangle \tag{B3}$$

The i superscripts may be removed since the correlations are averaged over all volumes. For clarity's sake, the following notation will be used for the filtered velocity components:

$$u_- = u(\boldsymbol{x}) \tag{B4}$$
$$u_+ = u(\boldsymbol{x} + (0, 0, \Delta)) \tag{B5}$$
$$w_- = w(\boldsymbol{x}) \tag{B6}$$
$$w_+ = w(\boldsymbol{x} + (0, 0, \Delta)) \tag{B7}$$
$$w_l = w\left(\boldsymbol{x} + \left(-\frac{\Delta}{2}, 0, \frac{\Delta}{2}\right)\right) \tag{B8}$$
$$w_r = w\left(\boldsymbol{x} + \left(\frac{\Delta}{2}, 0, \frac{\Delta}{2}\right)\right) \tag{B9}$$

The event vectors for each basic flux are:

M_{uw}:

$$\boldsymbol{E} = \begin{pmatrix} 1 \\ u_- \\ u_+ \\ u_- w_r \\ u_- w_l \\ u_+ w_r \\ u_+ w_l \end{pmatrix} \tag{B10}$$

M_{ww}:

$$\boldsymbol{E} = \begin{pmatrix} 1 \\ w_- \\ w_+ \\ w_- w_- \\ w_+ w_+ \\ w_- w_+ \end{pmatrix} \tag{B11}$$

$M_{\partial u/\partial z}$:

$$\boldsymbol{E} = \begin{pmatrix} 1 \\ u_- \\ u_+ \end{pmatrix} \tag{B12}$$

$M_{\partial w/\partial z}$:

$$\boldsymbol{E} = \begin{pmatrix} 1 \\ w_- \\ w_+ \end{pmatrix} \tag{B13}$$

Note that the equation for the model (18) may be written in the following form (summation on repeated indices):

$$m^{\boldsymbol{i}} = C_k E_k^{\boldsymbol{i}} \tag{B14}$$

where C is a vector of coefficients. Therefore, the estimation equation (B3) may be expressed as:

$$C_k \langle E_k E_l \rangle = \langle M E_l \rangle \tag{B15}$$

or in matrix notation:

$$\begin{bmatrix} \langle E_1E_1\rangle & \langle E_1E_2\rangle & \dots & \langle E_1E_n\rangle \\ \langle E_2E_1\rangle & \langle E_2E_2\rangle & \dots & \langle E_2E_n\rangle \\ \dots & \dots & \dots & \dots \\ \langle E_nE_1\rangle & \langle E_nE_2\rangle & \dots & \langle E_nE_n\rangle \end{bmatrix} \begin{bmatrix} C_1 \\ C_2 \\ \dots \\ C_n \end{bmatrix} = \begin{bmatrix} \langle ME_1\rangle \\ \langle ME_2\rangle \\ \dots \\ \langle ME_n\rangle \end{bmatrix} \tag{B16}$$

where n is the number of events for the model. Notice that the correlation matrix is symmetric.

Therefore, for model S2, the matrix form of the estimation equations is (since the matrices are symmetric, only the upper triangle of each is shown):

M_{uw}:

$$\begin{bmatrix} 1 & \langle u_-\rangle & \langle u_+\rangle & \langle u_-w_r\rangle & \langle u_-w_l\rangle & \langle u_+w_r\rangle & \langle u_+w_l\rangle \\ & \langle u_-^2\rangle & \langle u_-u_+\rangle & \langle u_-^2w_r\rangle & \langle u_-^2w_l\rangle & \langle u_-u_+w_r\rangle & \langle u_-u_+w_l\rangle \\ & & \langle u_+^2\rangle & \langle u_+u_-w_r\rangle & \langle u_+u_-w_l\rangle & \langle u_+^2w_r\rangle & \langle u_+^2w_l\rangle \\ & & & \langle (u_-w_r)^2\rangle & \langle u_-^2w_rw_l\rangle & \langle u_-u_+w_r^2\rangle & \langle u_-w_ru_+w_l\rangle \\ & & & & \langle (u_-w_l)^2\rangle & \langle u_-w_lu_+w_r\rangle & \langle u_-u_+w_l^2\rangle \\ & & & & & \langle (u_+w_r)^2\rangle & \langle u_+^2w_rw_l\rangle \\ & & & & & & \langle (u_+w_l)^2\rangle \end{bmatrix} \begin{bmatrix} C_1^{M_{uw}} \\ C_2^{M_{uw}} \\ C_3^{M_{uw}} \\ C_4^{M_{uw}} \\ C_5^{M_{uw}} \\ C_6^{M_{uw}} \\ C_7^{M_{uw}} \end{bmatrix} = \begin{bmatrix} \langle M_{uw}\rangle \\ \langle M_{uw}u_-\rangle \\ \langle M_{uw}u_+\rangle \\ \langle M_{uw}u_-w_r\rangle \\ \langle M_{uw}u_-w_l\rangle \\ \langle M_{uw}u_+w_r\rangle \\ \langle M_{uw}u_+w_l\rangle \end{bmatrix} \tag{B17}$$

M_{ww}:

$$\begin{bmatrix} 1 & \langle w_-\rangle & \langle w_+\rangle & \langle w_-^2\rangle & \langle w_+^2\rangle & \langle w_-w_+\rangle \\ & \langle w_-^2\rangle & \langle w_-w_+\rangle & \langle w_-^3\rangle & \langle w_-w_+^2\rangle & \langle w_-^2w_+\rangle \\ & & \langle w_+^2\rangle & \langle w_+w_-^2\rangle & \langle w_+^3\rangle & \langle w_-w_+^2\rangle \\ & & & \langle w_-^4\rangle & \langle (w_-w_+)^2\rangle & \langle w_-^3w_+\rangle \\ & & & & \langle w_+^4\rangle & \langle w_-w_+^3\rangle \\ & & & & & \langle (w_-w_+)^2\rangle \end{bmatrix} \begin{bmatrix} C_1^{M_{ww}} \\ C_2^{M_{ww}} \\ C_3^{M_{ww}} \\ C_4^{M_{ww}} \\ C_5^{M_{ww}} \\ C_6^{M_{ww}} \end{bmatrix} = \begin{bmatrix} \langle M_{ww}\rangle \\ \langle M_{ww}w_-\rangle \\ \langle M_{ww}w_+\rangle \\ \langle M_{ww}w_-^2\rangle \\ \langle M_{ww}w_+^2\rangle \\ \langle M_{ww}w_-w_+\rangle \end{bmatrix} \tag{B18}$$

$M_{\partial u/\partial z}$:

$$\begin{bmatrix} 1 & \langle u_-\rangle & \langle u_+\rangle \\ & \langle u_-^2\rangle & \langle u_+u_-\rangle \\ & & \langle u_+^2\rangle \end{bmatrix} \begin{bmatrix} C_1^{M_{\partial u/\partial z}} \\ C_2^{M_{\partial u/\partial z}} \\ C_3^{M_{\partial u/\partial z}} \end{bmatrix} = \begin{bmatrix} \langle M_{\partial u/\partial z}\rangle \\ \langle M_{\partial u/\partial z}u_-\rangle \\ \langle M_{\partial u/\partial z}u_+\rangle \end{bmatrix} \tag{B19}$$

$M_{\partial w/\partial z}$:

$$\begin{bmatrix} 1 & \langle w_- \rangle & \langle w_+ \rangle \\ & \langle w_-^2 \rangle & \langle w_+ w_- \rangle \\ & & \langle w_+^2 \rangle \end{bmatrix} \begin{bmatrix} C_1^{M_{\partial w/\partial z}} \\ C_2^{M_{\partial w/\partial z}} \\ C_3^{M_{\partial w/\partial z}} \end{bmatrix} = \begin{bmatrix} \langle M_{\partial w/\partial z} \rangle \\ \langle M_{\partial w/\partial z} w_- \rangle \\ \langle M_{\partial w/\partial z} w_+ \rangle \end{bmatrix} \tag{B20}$$

The solution for these estimation systems gives us the models for the basic fluxes corresponding to model S2. Many of the correlations appearing in the estimation equations may be simplified by using homogeneity and isotropy, such as:

$$\langle u_+ \rangle = \langle u_- \rangle = \langle w_+ \rangle = \langle w_- \rangle = 0$$
$$\langle u_+^2 \rangle = \langle u_-^2 \rangle = \langle w_+^2 \rangle = \langle w_-^2 \rangle$$
$$\langle u_+ u_-^2 \rangle = -\langle u_- u_+^2 \rangle$$

The extension of the estimation procedure to other model inputs and stencils is trivial, since the estimation equations are only based on the event vector $\boldsymbol{E}$. When constructing estimation equations for a different model, all one must do is form an event vector with all model inputs, compute the correlation matrix $\langle E_i E_j \rangle$ and the right-hand side vector $\langle M E_i \rangle$, and solve the resulting linear system $(\langle E_i E_j \rangle C_j = \langle M E_i \rangle)$ for the coefficients C. In this work, Gaussian elimination was used to solve the linear system.

[1] R. S. Rogallo and P. Moin, Numerical simulation of turbulent flows, Ann. Rev. Fluid Mech. **21**, 1525 (1984).

[2] M. Lesieur and O. Métais, New trends in large-eddy simulations of turbulence, Ann. Rev. Fluid Mech. **28**, 45 (1996).

[3] C. Meneveau and J. Katz, Scale-invariance and turbulence models for large-eddy simulation, Ann. Rev. Fluid Mech. **32**, 1 (2000).

[4] F. Porté-Agel, C. Meneveau, and M. B. Parlange, A scale-dependent dynamic model for large-eddy simulation: application to a neutral atmospheric boundary layer, Journal of Fluid Mechanics **415**, 261 (2000).

[5] D. I. Pullin, A vortex-based model for the subgrid flux of a passive scalar, Physics of Fluids **13**, 2311 (2000).

[6] S. Liu, C. Meneveau, and J. Katz, On the properties of similarity subgrid-scale models as deduced from measurements in a turbulent jet, Journal of Fluid Mechanics **275**, 83 (1994).

[7] J. A. Domaradzki, K. C. Loh, and P. P. Yee, Large eddy simulations using the subgrid-scale estimation model and truncated navier-stokes dynamics, Theor. Comput. Fluid Dyn. **15**, 421 (2002).

[8] B. J. Geurts and D. D. Holm, Regularization modeling for large-eddy simulation, Physics of Fluids **15**, L13 (2003).

[9] M. Lesieur, P. Comte, Y. Dubief, E. Lamballais, O. Metais, and S. Ossia, From two-point closures of isotropic turbulence to les of shear flows, Flow Turbul. Combust. **63**, 247 (2000).

[10] J. A. Langford and R. D. Moser, Optimal les formulations for isotropic turbulence, J. Fluid Mech. **398**, 321 (1999).

[11] S. Völker, R. D. Moser, and P. Venugopal, Optimal large eddy simulation of turbulent channel flow based on direct numerical simulation statistical data, Phys. Fluids **14**, 3675 (2002).

[12] J. Smagorinsky, General circulation experiments with the primitive equations, Mon. Weather Rev. **91**, 99 (1963).

[13] M. Germano, U. Piomelli, P. Moin, and W. Cabot, A dynamic subgrid-scale eddy viscosity model, Phys. Fluids **3**, 1760 (1991).

[14] J. Bardina, J. Ferziger, and W. Reynolds, Improved subgrid-scale models for large-eddy

simulation, Technical Report 80-1357, AIAA, 1980.

[15] N. A. Stolz, S. & Adams, An approximate deconvoluton procedure for large-eddy simulation., Physics of Fluids **11**, 1699 (1999).

[16] J. A. Domaradzki and E. M. Saiki, A subgrid-scale model based on the estimation of unresolved scales of turbulence., Physics of Fluids **9**, 1 (1997).

[17] B. J. Geurts, Inverse modeling for large-eddy simulation, Phys. Fluids **9**, 3585 (1997).

[18] S. Ghosal, An analysis of numerical errors in large-eddy simulations of turbulence, J. Comput. Phys. **125**, 187 (1996).

[19] A. G. Kravchenko and P. Moin, On the effect of numerical errors in large eddy simulation of turbulent flows, J. Comput. Phys. **131**, 310 (1997).

[20] D. Carati, G. S. Winckelmans, and H. Jeanmart, On the modelling of the subgrid-scale and filtered-scale stress tensors in large-eddy simulation, J. Fluid Mech. **441**, 119 (2001).

[21] B. Vreman, B. Geurts, and H. Kuerten, Comparison of numerical schemes in large-eddy simulation of the temporal mixing layer, Int. J. for Num. Meth. Fluids **22**, 297 (1996).

[22] B. J. Geurts and J. Fröhlich, A framework for predicting accuracy limitations in large-eddy simulation, Phys. Fluids **14**, L41 (2002).

[23] S. B. Pope, *Turbulent flows*, Cambridge University Press, Cambridge, 2000.

[24] J. Zakin and G. Patterson, editors, *On the role of conditional averages in turbulence theory*, Turbulence in Liquids, Princeton, New Jersey, 1977, Science Press.

[25] R. Adrian and P. Moin, Stochastic estimation of organized turbulent structure: Homogeneous shear flow, J. Fluid Mech. **190**, 531 (1988).

[26] R. Adrian, B. Jones, M. Chung, Y. Hassan, C. Nithianandan, and A. Tung, Stochastic estimation of organized turbulent structure: Homogeneous shear flow, Phys. Fluids **1**, 992 (1989).

[27] J. A. Langford and R. D. Moser, Breakdown of continuity in large-eddy simulation, Phys. Fluids **13**, 1524 (2001).

[28] A. Papoulis and S. U. Pillai, *Probability, random variables and stochastic processes*, McGraw-Hill, New York, 4 edition, 2002.

[29] R. S. Rogallo, Numerical experiments in homogeneous turbulence, Tech. Memo 81315, NASA, 1981.

[30] J. A. Langford, *Toward ideal large-eddy simulation*, PhD thesis, The University of Illinois at

Urbana-Champaign, 2000.

[31] C. Meneveau, Statistics of turbulence subgrid-scale stresses: Necessary conditions and experimental tests, Phys. Fluids **6**, 815 (1994).

[32] R. A. Clark, J. H. Ferziger, and W. C. Reynolds, Evaluation of subgrid scale turbulence models using a fully simulated turbulent flow, J. Fluid Mech. **91**, 1 (1979).

[33] J. H. Ferziger, *Simulation and Modeling of Turbulent Flows*, chapter Large Eddy Simulation, pp. 109–154, Oxford University Press, 1996.

[34] P. Sagaut, *Large Eddy Simulation for Incompressible Flows*, Springer, Berlin, 2nd edition, 2002.

[35] U. Piomelli, P. Moin, and J. H. Ferziger, Model consistency in large eddy simulation of turbulent channel flows, Phys. Fluids **31**, 1884 (1988).

[36] C. M. Rhie and W. L. Chow, Numerical study of the turbulent flow past an airfoil with trailing edge separation, AIAA Journal **14**, 3675 (1983).

[37] J. Boris, F. Grinstein, E. Oran, and R. Kolbe, New insights into large eddy simulation, Fluid Dyn. Res. **10**, 199 (1992).

TABLE I: Relative estimation variations for various finite-volume fluxes. Variations are shown for linear estimates, for estimates with local quadratic products (LQ), and for estimates with nonlocal quadratic products (NLQ) formed from velocities in cells separated by a distance of up to one cell width. Also shown are simplified estimates (†), for which only terms from standard finite-volume approximations are included.

grid arrangement	relative variation			
and estimation type	M_{uw}	M_{ww}	$M_{\partial u/\partial z}$	$M_{\partial w/\partial z}$
collocated linear	0.9983	0.9983	0.4725	0.3170
collocated linear †			0.5065	0.3554
collocated LQ	0.4943	0.4530	0.4720	0.3165
collocated LQ †	0.5341	0.4716		
collocated NLQ	0.4430	0.3530	0.4660	0.3137
collocated NLQ †	0.5040	0.4447		
staggered linear	0.9983	0.9983	0.4622	0.3296
staggered linear †			0.5065	0.3554
staggered NLQ	0.4802	0.4174	0.4588	0.3275
staggered NLQ †	0.5033	0.4494		

TABLE II: Stencils for local models used in the *a posteriori* analysis. † Models with standard terms only. ∗ Models which diverged during simulation.

model	grid type	flux	Stencil dimensions		
			u	v	w
C2 †	collocated	all	1×1×2	-	1×1×2
C4 †	collocated	all	1×1×4	-	1×1×4
C6s † ∗	collocated	all	1×1×6	-	1×1×6
Cws † ∗	collocated	all	3×3×4	-	3×3×4
C6n ∗	collocated	all	1×1×6	1×1×6	1×1×6
Cwn	collocated	all	3×3×4	3×3×4	3×3×4
S2 †	staggered	M_{uw}, $M_{\partial u/\partial z}$	1×1×2	-	2×1×1
		M_{ww}, $M_{\partial w/\partial z}$	-	-	1×1×2
S4 †	staggered	M_{uw}, $M_{\partial u/\partial z}$	1×1×4	-	2×1×1
		M_{ww}, $M_{\partial w/\partial z}$	-	-	1×1×4
S6s †	staggered	M_{uw}, $M_{\partial u/\partial z}$	1×1×6	-	2×1×1
		M_{ww}, $M_{\partial w/\partial z}$	-	-	1×1×6
Sws †	staggered	M_{uw}, $M_{\partial u/\partial z}$	3×3×4	-	4×3×3
		M_{ww}, $M_{\partial w/\partial z}$	-	-	3×3×4
S6n	staggered	M_{uw}, $M_{\partial u/\partial z}$	1×1×6	2×2×2	2×1×1
		M_{ww}, $M_{\partial w/\partial z}$	2×1×1	1×2×1	1×1×6
Swn	staggered	M_{uw}, $M_{\partial u/\partial z}$	3×3×4	4×4×4	4×3×3
		M_{ww}, $M_{\partial w/\partial z}$	4×3×3	3×4×3	3×3×4

TABLE III: *A-priori* relative estimation variation for local estimates, with best global estimates repeated for comparison.

Stencil	M_{uw}	M_{ww}	$M_{\partial u/\partial z}$	$M_{\partial w/\partial z}$
global collocated	0.4430	0.3530	0.4660	0.3137
global staggered	0.4802	0.4174	0.4588	0.3275
C2	0.5794	0.5369	0.5763	0.4636
C4	0.5185	0.4620	0.5160	0.3744
C6s	0.5134	0.4547	0.5089	0.3593
Cws	0.5120	0.4540	0.5137	0.3695
C6n	0.5134	0.4518	0.5089	0.3593
Cwn	0.4590	0.3638	0.4998	0.3289
S2	0.5626	0.5369	0.5763	0.4636
S4	0.5626	0.4620	0.5160	0.3744
S6s	0.5626	0.4547	0.5089	0.3593
Sws	0.5099	0.4575	0.2638	0.3695
S6n	0.4976	0.4566	0.5137	0.3514
Swn	0.2476	0.4422	0.4847	0.3462

TABLE IV: Coefficients for staggered finite-volume models, valid for $Re_\lambda = 164$

Coefficient	Standard second-order FV	Optimal S2	Optimal S4
A	$\nu\,\Delta^{-2}$	$0.314267\Delta^{-1} + 1.37142\nu\Delta^{-2}$	$0.491708\Delta^{-1} + 1.93227\nu\Delta^{-2}$
B	–	–	$-\left(0.0941649\Delta^{-1} + 0.26115\nu\Delta^{-2}\right)$
C	$\nu\,\Delta^{-2}$	$0.130001\Delta^{-1} + 1.24894\nu\Delta^{-2}$	$0.0963195\Delta^{-1} + 2.08884\nu\Delta^{-2}$
D	–	–	$\left(0.0145042\Delta^{-1} - 0.19635\nu\Delta^{-2}\right)$
E	-6$\nu\,\Delta^{-2}$	$-(2A + 4C)$	$-(2(A + B) + 4(C + D))$
F	$0.25\,\Delta^{-1}$	$0.387933\,\Delta^{-1}$	$0.679643\,\Delta^{-1}$
G	$0.5\,\Delta^{-1}$	$0.270394\,\Delta^{-1}$	$0.621382\,\Delta^{-1}$
H	–	–	$0.453439\,\Delta^{-1}$
I	–	–	$0.0917196\,\Delta^{-1}$
J	$0.25\,\Delta^{-1}$	$0.268916\,\Delta^{-1}$	$0.268902\,\Delta^{-1}$

LIST OF CAPTIONS

Fig. 1 Stencils for 1×1×4 and 3×3×4 single velocity stencils are shown. The shaded region identifies the face on which flux is computed. (a) 1×1×4 (b) 3×3×4

Fig. 2 Three-dimensional energy spectrum E(k), a -5/3 power law, and the Nyquist wavenumber associated with the finite-volume filter width.

Fig. 3 Three-dimensional energy spectrum E(k), filtered DNS data compared with *optimal* LES results. (a) Models C2, C4, S2, S4, S6s (b) Models Cwn, S6s, Sws, S6n, Swn

Fig. 4 Third-order structure function $S_3(r)$, filtered DNS data compared with *optimal* LES results. (a) Models C2, C4, S2, S4, S6s (b) Models Cwn, S6s, Sws, S6n, Swn

Fig. 5 Three-dimensional energy spectrum E(k), filtered DNS data compared with *optimal* LES and dynamic Smagorinsky results.

Fig. 6 Third-order structure function $S_3(r)$, filtered DNS data compared with *optimal* LES and dynamic Smagorinsky results.

Fig. 7 Notation for a one-dimensional example problem. The state variables w are averages of some underlying conserved quantity, whose flux across cell boundaries is denoted by M.

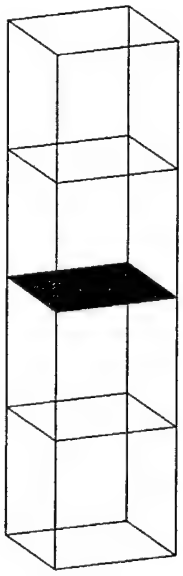

(a)

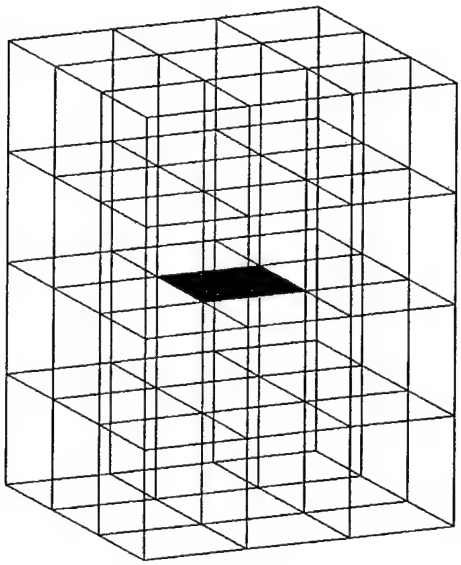

(b)

FIG. 1: Zandonade, Physics of Fluids.

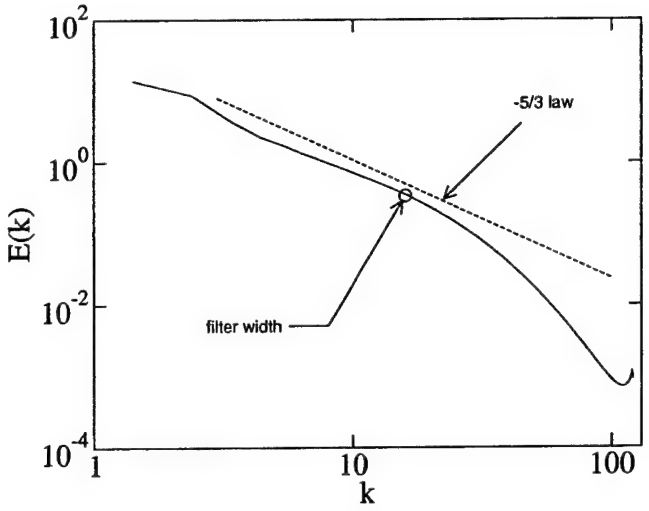

FIG. 2: Zandonade, Physics of Fluids.

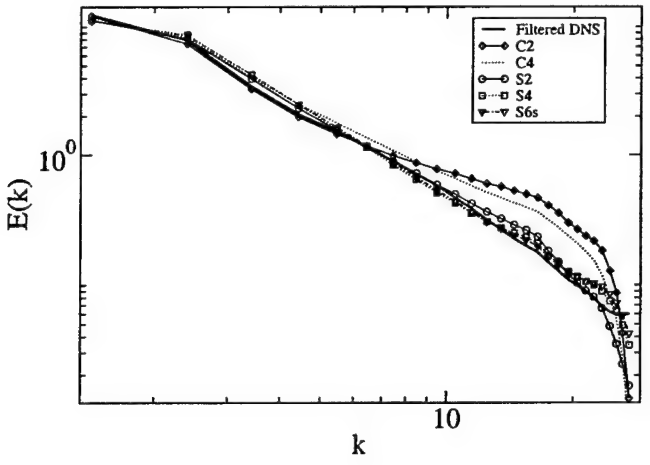

(a)

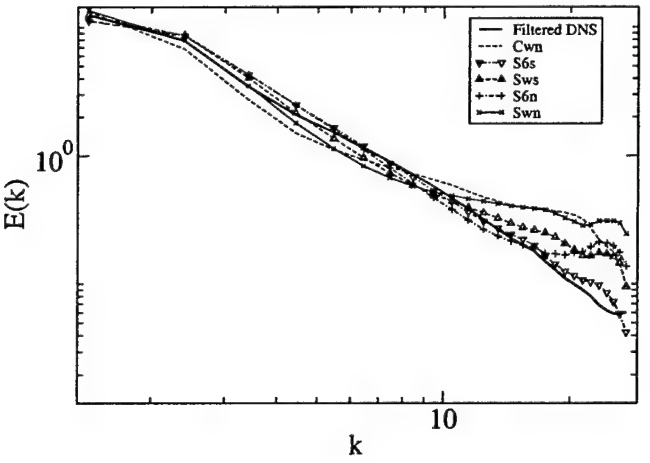

(b)

FIG. 3: Zandonade, Physics of Fluids.

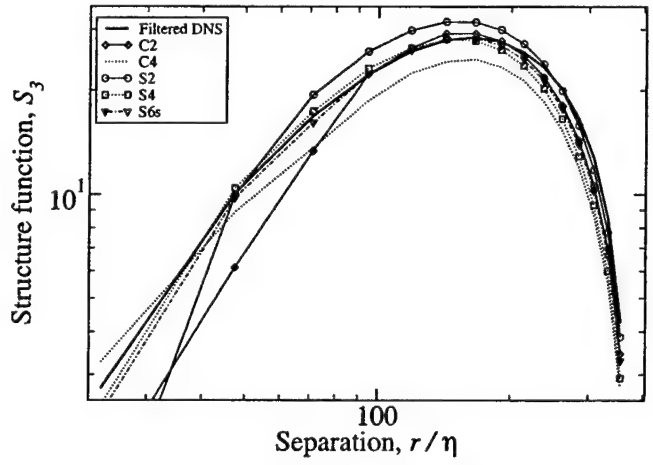

(a)

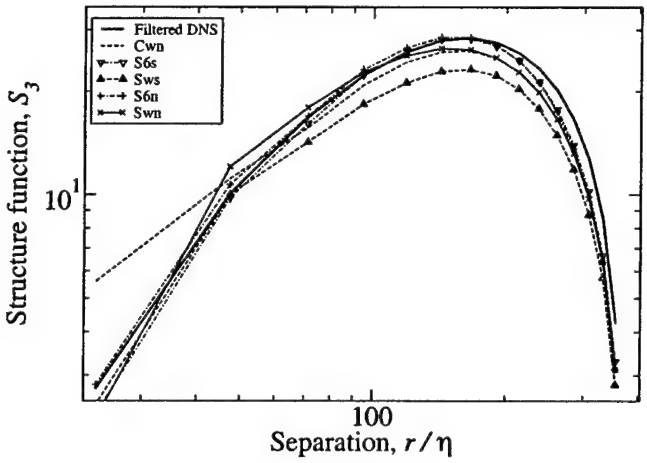

(b)

FIG. 4: Zandonade, Physics of Fluids.

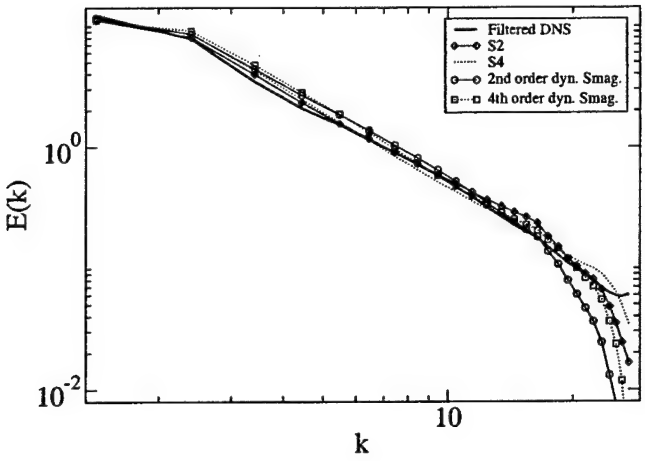

FIG. 5: Zandonade, Physics of Fluids.

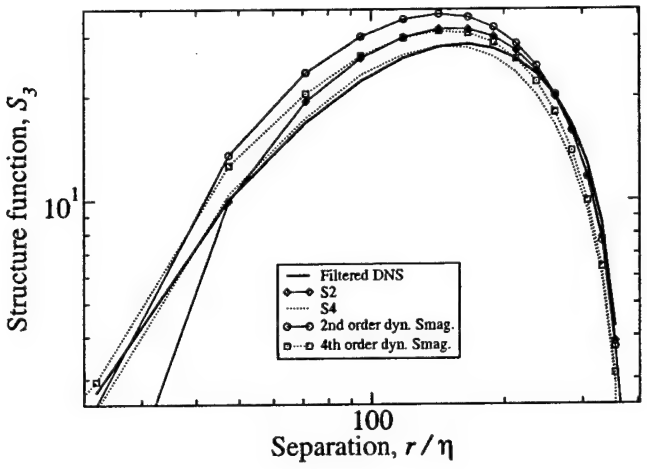

FIG. 6: Zandonade, Physics of Fluids.

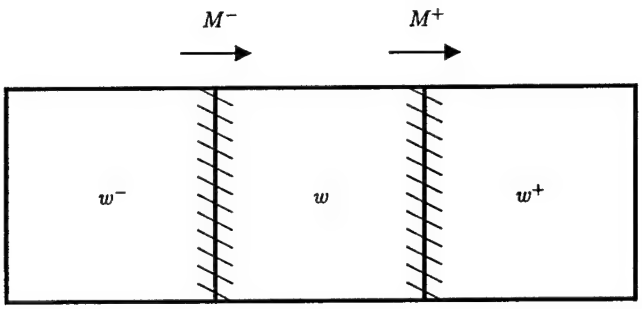

FIG. 7: Zandonade, Physics of Fluids.

APPENDIX B

Preprint of Vedula, P. & Moser, R. D. 2004 On the validity of quasi-normal approximation in turbulent channel flow, submitted to *Phys. of Fluids*.

On the validity of quasi-normal approximation in turbulent channel flow

Prakash Vedula and Robert D. Moser

University of Illinois,
Department of Theoretical and Applied Mechanics,
104 S. Wright Street, Urbana, IL 61801

Abstract

The validity of the quasi-normal approximation, which relates the fourth-order velocity correlations to second-order velocity correlations, is tested using data obtained from direct numerical simulation of turbulent channel flow at $Re_\tau \approx 590$. Our validation study indicates that the quasi-normal approximation is very accurate throughout the channel except for a thin layer near the wall ($y^+ < 50$), where the approximation breaks down for small separations ($r^+ < 150$). This study shows that the quasi-normal approximation can be used as a basis for development of LES models using the optimal LES formulation, in wall bounded flows.

I. Introduction

Several phenomenological and statistical hypotheses have been postulated to enhance our understanding of turbulent flows. One commonly used hypothesis is the Millionshchikov hypothesis, which is also known as the quasi-normal approximation or zero-fourth-cummulant approximation. According to the quasi-normal approximation, the fourth-order velocity cummulants are zero, which allows us to express the fourth-order velocity correlations in terms of second-order velocity correlations (Monin & Yaglom[1]).

The quasi-normal approximation has been used in a variety of contexts in the past. These can be broadly categorized as (a) inference of turbulence statistics from kinematics and phenomenology and (b) dynamical evolution of turbulence structure. In the former category, the quasi-normal approximation was used by Batchelor[2] to deduce the functional behavior of pressure correlations in isotropic turbulence, Limber[3] to obtain the pressure-velocity-velocity correlations and Hill & Wilczack[4] to comment on the scaling of pressure-gradient and acceleration in homogeneous turbulence. In the latter category, the quasi-normal approximation was used by Proudman & Reid[5] and Tatsumi[6] to derive dynamical equations for third-order velocity correlations and Orszag[7] in the development of analytical closure theories (like eddy damped quasi-normal markovian closures).

An experimental justification of the quasi-normal approximation of fourth-order velocity correlations was first provided by Uberoi,[8] who noted the conformity of his results to the quasi-normal approximation, except at the small scales where the approximation breaks down. However, the use of quasi-normal approximation in category (b), was questioned by Ogura[9] who noticed negative values in the energy spectrum after a finite time during the dynamical evolution, a clear violation of realizability constraint. Kraichnan[10] argued that the use of quasi-normal approximation in the Proudman & Reid[5] approach was inconsistent with the equations of motion and that the inconsistency results in a violation of energy conservation. Orszag[7] also noted the pitfalls of the quasi-normal approximation in dynamical evolution equations and attributed the failures to the dynamical properties of the quasi-normal approximation, which include an improper representation of relaxation effects resulting in a violation of realizability. Further attempts to correct these shortcomings led to the development of the eddy-damped quasi-normal Markovian type closures.

Most of the objections to the quasi-normal approximation are in the context of category (b) usages. However, inspite of the experimental justification of quasi-normal approximation (Uberoi[8]), there have been some negatives in category (a) as well. It was noted in Hill & Wilczack[4] and Hill & Thoroddsen,[11] that the quasi-normal approximation (although a good approximation at low Reynolds numbers) underestimates the pressure gradient or acceleration correlation functions (and hence their variances). Since these correlations involve integral relations over both small and large scales, one should attribute the underestimation of these correlations to the failure of quasi-normal approximation at the small scales where intermittency (non-Gaussian) effects are predominant. If one were to consider quasi-normal approximation for physical quantities that do not depend on small scales (i.e. for separations $r >> \eta$) one can expect the approximation to be reasonable.

In this paper, we will examine the validity of this proposition in a turbulent channel flow and quantify the errors due to the quasi-normal approximation using channel flow DNS data at $Re_\tau \approx 590$. The motivation for doing this arises in a different context than has been cited in the literature. Our objective is to develop an *optimal* large eddy simulation (LES) model to simulate high Reynolds number flow. Such a model involves stochastic estimation of the convective acceleration (or momentum flux), which requires the knowledge of fourth-order correlations as inputs. These can then be approximated in terms of second-order correlations using the quasi-normal hypothesis. The channel flow was selected for this study to allow evaluation of the approximation of the quasi-normal approximation in a wall bounded flow, particularly in the log- or overlap region. The limits of applicability of the approximation in nearly homogeneous flows are well understood as described above; these limits need to be established for wall bounded flows, where models for near wall turbulence are one of the primary challenges in LES modeling.

The formulation of the optimal LES approach, is based on the existence of an ideal LES evolution. The large scales of turbulence to be simulated are defined through a spatial filter. The choice of the spatial filter determines the (non-invertible) mapping of the infinite dimensional state space of turbulent Navier-Stokes solutions to a finite-dimensional representation of the large scale field. For any given spatial filter, the best deterministic estimate (in the mean-square sense) of the evolution of the large scale field, is the ideal evolution (Adrian,[12]

Adrian *et al.*,[13] Langford & Moser[14]) which is given by

$$\frac{d\widetilde{w}}{dt} = \left\langle \widetilde{\frac{du}{dt}} \middle| \widetilde{u} = \widetilde{w} \right\rangle \ , \tag{1}$$

where u represents the turbulent field, $\widetilde{w}$ denotes the large scale LES field, and $\widetilde{\cdot}$ denotes the filtering operator. Such an evolution is guaranteed to produce the correct single-time, multi-point statistics (Langford and Moser,[14] Pope[15]). Owing to the huge amount of statistical information embedded in the above conditional average, it is difficult to obtain it directly and hence it is formally approximated using the *optimal* LES approach, which is based on stochastic estimation.[12,16,13]

Earlier, this approach was used for developing optimal sub-grid models in isotropic turbulence (Langford & Moser[14]) and turbulent channel flows (Volker *et al.*[17]), based on spectral filters. More recently, Langford[18] and Zandonade *et al.*[19] developed a finite-volume *optimal* LES technique, wherein discretization and sub-grid effects are treated simultaneously. Besides attempting to address the limitations (e.g. filter definition, treatment of numerical discretization and near-wall modeling) of other LES models, the optimal LES models have also led to very accurate simulations and have the potential of being applicable to the the simulation of flows with complex geometries.

The *optimal* LES models require information regarding multi-point velocity correlations as inputs. Although, these correlations can be obtained from DNS, it is necessary to eliminate the need for DNS data, if optimal models are to be practically useful. We are thus led to replace DNS statistical data with theory based models of the correlations. For instance, among the inputs needed for *optimal* LES models are fourth-order velocity correlations, which may be approximated using the quasi-normal hypothesis. The following sections of this paper explore the validity of the quasi-normal approximation, within the context of *optimal* LES modeling of wall-bounded turbulent flows.

II. Background

In the context of our *optimal* LES models, we need to determine an *optimal* quadratic (stochastic) estimate of the convective acceleration (or flux), which requires the following multi-point correlations (see Sec. 2.2.4 in Zandonade *et al.*[19]) as inputs, for any linear filter:

$$\langle u_i(\mathbf{x}) u_j(\mathbf{x}') \rangle \, , \quad \langle u_i(\mathbf{x}) u_j(\mathbf{x}') u_k(\mathbf{x}'') \rangle \, , \quad \langle u_i(\mathbf{x}) u_j(\mathbf{x}') u_k(\mathbf{x}'') u_l(\mathbf{x}''') \rangle \ . \tag{2}$$

Note that the correlations in Sec. 2.2.4 in Zandonade *et al.*[19] are actually averaged over cell volumes/faces, since an *optimal* convective flux term (averaged over a cell-face) is estimated in terms of volume averaged cell-velocities (up to quadratic term). The volume averaged quantities/correlations appearing in Zandonade *et al.*[19] are a consequence of the filtering operation inherent in the finite-volume formulation, where the filter width is related to the grid spacing. Analogous to the finite-volume optimal LES formulation of Zandonade *et al.*,[19]one can also attempt to construct optimal LES models based purely on finite sampling of the real velocity field (without the use of a conventional filter). Such models, which

represent the "finite-difference" analogue of finite-volume optimal LES, would also require correlations given in (2), as inputs.

In order to reduce the information required as inputs (i.e. in (2)) for obtaining optimal quadratic estimates, we use the quasi-normal hypothesis and express the fourth-order velocity correlations in terms of second-order velocity correlations. The most general form of the fourth-order velocity correlation is given by

$$Q_{i,j,k,l}(\mathbf{x},\mathbf{x}',\mathbf{x}'',\mathbf{x}''') \equiv \langle u_i(\mathbf{x})u_j(\mathbf{x}')u_k(\mathbf{x}'')u_l(\mathbf{x}''')\rangle\,, \tag{3}$$

which can be approximated using the quasi-normal hypothesis as,

$$Q_{i,j,k,l}(\mathbf{x},\mathbf{x}',\mathbf{x}'',\mathbf{x}''') \approx R_{ij}(\mathbf{x},\mathbf{x}')R_{kl}(\mathbf{x}'',\mathbf{x}''') + R_{ik}(\mathbf{x},\mathbf{x}'')R_{jl}(\mathbf{x}',\mathbf{x}''') + R_{il}(\mathbf{x},\mathbf{x}''')R_{jk}(\mathbf{x}',\mathbf{x}''), \tag{4}$$

where $R_{ij}(\mathbf{x},\mathbf{x}') \equiv \langle u_i(\mathbf{x})u_j(\mathbf{x}')\rangle$ denotes the two-point second-order correlation. Note that the quasi-normal hypothesis states that the fourth order moments can be determined as if the underlying probability distribution were Gaussian. However the quasi-normal approximation makes no statement on the behavior of third-order moments or the underlying velocity distribution.

To address the modeling issues of wall-bounded turbulent flows, we use fully developed turbulent channel flow data at $Re_\tau \approx 590$ (Moser *et al.*[20]) as a test case to quantitatively validate the quasi-normal hypothesis. The data was obtained from direct numerical simulation using periodic boundary conditions in the the streamwise, (x) and spanwise, (z) directions, while no slip conditions were used on the two parallel walls. A Fourier spectral representation was used in the streamwise and spanwise directions and a Chebyshev representation was used in the wall-normal, (y) direction.

In order to completely test the quasi-normal approximation in the most general case, one should compare the left and right hand sides of Eq. 4. However, this amounts to evaluating 81 components of the four-point fourth-order tensor at each point in 12-dimensional space. This evaluation is not practical for inhomogeneous flows, inspite of the presence of symmetries.

Noting the statistical homogeneities in the streamwise and spanwise directions, we restrict our attention to a class of two-point fourth order velocity correlations to make the study tractable. This is a degenerate case of Eq. 3, given by

$$Q_{ij,kl}(\mathbf{x},\mathbf{x}') \equiv Q_{i,j,k,l}(\mathbf{x},\mathbf{x},\mathbf{x}',\mathbf{x}') \equiv \langle u_i(\mathbf{x})u_j(\mathbf{x})u_k(\mathbf{x}')u_l(\mathbf{x}')\rangle\,. \tag{5}$$

Further, if the points $\mathbf{x}$ and $\mathbf{x}'$ have the same wall-normal coordinate (i.e. lie in a plane parallel to the walls), we have

$$Q_{ij,kl}(\mathbf{x},\mathbf{x}') = Q_{ij,kl}(\mathbf{0},\mathbf{x}'-\mathbf{x}) = Q_{ij,kl}(\mathbf{r}), \tag{6}$$

due to statistical homogeneity in the streamwise and spanwise directions, where $\mathbf{r} = \mathbf{x}' - \mathbf{x}$. Henceforth, we will test the quasi-normal approximation of $Q_{ij,kl}(\mathbf{r})$ for separation vectors $\mathbf{r}$ parallel to the wall and (a) along the streamwise direction or (b) along the spanwise direction.

In order to quantify the error due to the quasi-normal approximation, we define an error measure[1], $\phi_{ij,kl}(\mathbf{r})$, as,

$$\phi_{ij,kl}(\mathbf{r}) = \frac{Q_{ij,kl}(\mathbf{r}) - QNA}{L(\mathbf{r})}, \tag{7}$$

[1] $\phi_{ij,kl}(y^+,\mathbf{r})$ may be a better definition

where QNA denotes the quasi-normal approximation of the two-point fourth-order velocity correlation tensor, $Q_{ij,kl}(\mathbf{r})$, according to Eq. (4) and $L(\mathbf{r}) \equiv [Q_{ij,kl}(\mathbf{r})\ Q_{ij,kl}(\mathbf{r})]^{1/2}$ is a contraction (summation convention assumed) or invariant of the two-point fourth-order velocity correlation tensor.

The error measure, $\phi_{ij,kl}(\mathbf{r})$, as defined in Eq. (7), quantifies the error due to the quasi-normal approximation, associated with each component of the two-point fourth-order velocity correlation tensor, $Q_{ij,kl}(\mathbf{r})$. Another error measure which quantifies the error over all the components of $Q_{ij,kl}(\mathbf{r})$, can be defined using the same contraction of $\phi_{pq,rs}(\mathbf{r})$ as

$$\Psi(\mathbf{r}) \equiv [\phi_{pq,rs}(\mathbf{r})\phi_{pq,rs}(\mathbf{r})]^{1/2}. \tag{8}$$

This error measure is also relevant to the linear algebra of the stochastic estimation procedure. The relative error in the estimation coefficients due to the quasi-normal approximation is bounded by the condition number of the linear system times $\Psi(\mathbf{r})$.

For separation vectors, normal to the wall, the fourth-order velocity correlations defined in Eq. (5) are functions of two wall-normal coordinates, owing to lack of homogeneity in the wall-normal direction. In this case, the fourth-order velocity correlations are given by,

$$Q_{ij,kl}(\mathbf{x},\mathbf{x}') = Q^{\perp}_{ij,kl}(y,y'), \tag{9}$$

where $\mathbf{x} = (x,y,z)$ and $\mathbf{x}' = (x,y',z)$. Similarly, as in Eq. (7) and Eq. (8), we can define $\phi^{\perp}_{ij,kl}(y,y')$ and $\Psi^{\perp}_{ij,kl}(y,y')$, to quantify the errors associated with the quasi-normal approximation, for separation vectors perpendicular to the wall.

In the next section, the nature of these errors will be explored in the $Re_\tau \approx 590$ channel flow.

III. Results

The normalized error measure for wall normal velocity fluctuations, i.e. $\phi_{22,22}(\mathbf{r})$, as a function of the streamwise separation (in wall units) and distance from the wall (y^+, along the vertical coordinate) is shown in Figure 1a. The separation vectors, $\mathbf{r}$, in this case are along the streamwise direction. The behavior of the error as a function of the spanwise coordinate is shown in Fig. 1b, which is similar to Fig. 1a, except that the separation vectors are chosen along the spanwise direction. The errors are clearly small in these figures, indicating that the quasi-normal approximation is very good for wall normal fluctuations with separations along the spanwise coordinate. The normalized error for spanwise fluctuations ($\phi_{33,33}(\mathbf{r})$) is also very small as shown in figure 2. Although, the data of Moser *et al.*[20] indicate large values of flatness factors of wall-normal (and spanwise) velocity fluctuations near the wall, which significantly differ from the quasi-normal value, the error measure that is relevant for our validation of the quasi-normal approximation for wall-normal (and spanwise) fluctuations within the context of *optimal* LES is $\phi_{22,22}(\mathbf{r})$.

The error measure $\phi_{11,11}(\mathbf{r})$ for streamwise and spanwise separations (similar to Figs. 1a and 1b) are shown in figures 3a and 3b respectively. The contour levels in Fig. 3a indicate that the error is small everywhere except for regions near the wall ($y^+ < 30$) and for small streamwise separations ($\Delta x^+ < 150$), where the error is about 20% . A similar observation

can also be made from Fig. 3b, where the normalized error is small everywhere except in the near-wall region ($y^+ < 50$) and for small spanwise separations ($\Delta z^+ < 100$). The deviation from quasi-normality in a region very near the wall should be expected from the intermittent nature of the near wall flow. Although the quasi-normal approximation breaks down for small streamwise and spanwise separations, our model inputs require fourth correlations approximated by quasi-normal approximation only for streamwise separations that are greater than those in the breakdown region. Typical channel flow *optimal* LES simulations (Volker *et al.* 2002) would require correlations with separations of order $\Delta x^+ > 300$ and $\Delta z^+ > 150$.

To confirm the good accuracy of the quasi-normal approximation described above, a number of other components of the fourth order correlation tensor were checked and found to have small errors due to quasi-normality. Further, the overall error in the representation of the fourth order correlation tensor as measured by $\Psi(\mathbf{r})$, is shown in figure 4. Note that the contours of Ψ shown in figure 4 are similar to those for $\phi_{11,11}$ in figure 3. Thus the error in the quasi-normal approximation in this flow is dominated by the streamwise velocity fluctuation ($\phi_{11,11}$).

For separation vectors in the wall-normal direction, the errors $\phi^{\perp}_{22,22}(y,y')$, $\phi^{\perp}_{33,33}(y,y')$, $\phi^{\perp}_{11,11}(y,y')$ and $\Psi^{\perp}(y,y')$ are shown in figure 5. With the exception of the region very near the wall ($y^+ < 40$, $y'^+ < 40$), the errors are again very small and the overall error as measured by $\Psi^{\perp}(y,y')$ is dominated by the streamwise fluctuations ($\phi_{11,11}$).

IV. Discussion

In this paper, we have used data obtained from direct numerical simulation of turbulent channel flow at $Re_\tau \approx 590$, to test the validity of the quasi-normal approximation of fourth-order velocity correlations (see Eq. (4)). Unlike previous studies (mentioned in Sec. 1), our motivation arises in the context of stochastic estimation of the convective acceleration (or momentum flux) term, in order to develop *optimal* LES models.

The error due to the quasi-normal approximation, of a class of two-point fourth order correlations, was quantified using a component-wise error measure $\phi_{ij,kl}(\mathbf{r})$ and an invariant error measure $\Psi(\mathbf{r})$ for separation vectors in the streamwise, spanwise and wall-normal directions. Our results indicate that the quasi-normal approximation provides an excellent representation of the fourth-order correlation tensor, except in the region very near the wall ($y^+ < 50$) where there are significant errors in the approximation for small separation ($r^+ < 150$). In this region, the error in the representation is dominated by streamwise velocity fluctuations.

Note that the error measures used here are appropriate for evaluating the representation of the correlation tensor as a whole. Because the errors are normalized by a norm of the tensor, small values of a component error measure (e.g. $\phi_{22,22}$) does not imply that the related error in that individual component is necessarily small. For example, $\phi_{22,22}$ is small near the wall, but it is known that the flatness factor of the wall-normal fluctuation u_2, denoted by $\mu_4(u_2) \equiv \langle u_2^4 \rangle / \langle u_2^2 \rangle^2$, is far from the Gaussian value of 3 (according to the data of Moser *et al.*[20]). Thus $\langle u_2^4 \rangle$ is by itself not well represented by the quasi-normal approximation of $3\langle u_2^2 \rangle$ at the wall. The error measure, $\phi_{22,22}$ is small in this case because near the wall

fluctuations of u_2 are insignificant compared to those of u_1 (i.e. streamwise fluctuation), since u_2 goes to zero like y^2 near the wall. Thus near the wall, u_1 fluctuations dominate the norm of the fourth order correlation tensor. These error measures are relevant to our use of the quasi-normal approximation to model statistical quantities for input to optimal LES. The stochastic estimates performed in optimal LES use fourth order correlation components (or their integrals) as elements of the right hand side vector in a linear algebraic equation for the estimation kernels. In this context, the L_2 norm of the error in the quasi-normal approximation will be directly related to the L_2 norm in the resulting estimation kernel, which in turn is directly related to the error due to this approximation in the LES model.

The validity of quasi-normal approximation in wall bounded turbulence, except for a very thin layer near the wall, provides one of several theoretical modeling tools that will be required to make optimal LES a viable, practical modeling paradigm for wall bounded turbulence.

Acknowledgements

We would like to thank R. J. Adrian for helpful discussions. This work was supported by NSF and AFOSR under grants NSF-CTS-001453 and F49620-01-1-0181 respectively.

References

[1]A. S. Monin and A. M. Yaglom, *Statistical Fluid Mechanics: Mechanics of Turbulence* (The MIT Press, ADDRESS, 1975), Vol. 2.

[2]G. K. Batchelor, "Pressure fluctuations in isotropic turbulence," Proc. Cambridge Philos. Soc. **47**, 359 (1951).

[3]D. N. Limber, "Numerical results for pressure-velocity correlations in homogeneous isotropic turbulence," Proc. Nat. Acad. Sci. USA **37**, 230 (1951).

[4]R. J. Hill and J. M. Wilczak, "Pressure structure functions and spectra for locally isotropic turbulence," J. Fluid Mech. **296**, 247 (1995).

[5]I. Proudman and W. H. Reid, "On the decay of a normally distributed and homogeneous turbulent velocity field," Philos. Trans. Royal Soc. London. Series A **247**, 163 (1954).

[6]T. Tatsumi, "The theory of decay of incompressible isotropic turbulence," Proc. Royal Soc. London. Series A **239**, 16 (1957).

[7]S. A. Orszag, "Analytical theories of turbulence," J. Fluid Mech. **41**, 363 (1970).

[8]M. S. Uberoi, "Quadruple velocity correlations and pressure fluctuations in isotropic turbulence," J. Aero. Sci. **20**, 197 (1953).

[9]Y. Ogura, "A consequence of the zero-fourth-cumulant approximation in the decay of isotropic turbulence," J. Fluid Mech. **16**, 33 (1963).

[10]R. H. Kraichnan, "Relation of fourth-order to second-order moments in stationary isotropic turbulence," Phys. Rev. **107**, 1485 (1957).

[11]R. J. Hill and S. T. Thoroddsen, "Experimental evaluation of acceleration correlations for locally isotropic turbulence," Phys. Rev. E **55**, 1600 (1997).

[12]R. J. Adrian, in *Turbulence in liquids*, edited by J. L. Zakin and G. K. Patterson (Science Press, Princeton, NJ, 1977), pp. 323–332.

[13]R. J. Adrian, "Stochastic estimation of subgrid scale motions," Applied Mech. Rev. **43**, S214 (1990).

[14]J. A. Langford and R. D. Moser, "Optimal les formulations for isotropic turbulence," J. Fluid Mech. **398**, 321 (1999).

[15]S. B. Pope, *Turbulent flows* (Cambridge University Press, Cambridge, ADDRESS, 2000).

[16]R. J. Adrian, "Conditional eddies in isotropic turbulence," Phys. Fluids **22**, 2065 (1979).

[17]S. Volker, R. D. Moser, and P. Venugopal, "Optimal large eddy simulation of turbulent channel flow based on direct numerical simulation statistical data," Phys. Fluids **14**, 3675 (2002).

[18]J. A. Langford, *Toward ideal large-eddy simulation* (PhD thesis, The University of Illinois at Urbana-Champaign, ADDRESS, 2000).

[19]P. S. Zandonade, J. A. Langford, and R. D. Moser, "Finite-volume optimal large-eddy simulation of isotropic turbulence," Sumbitted to Phys. Fluids (2003).

[20]R. D. Moser, J. Kim, and N. Mansour, "Direct numerical simulation of turbulent channel flow up to $Re_\tau = 590$," Phys. Fluids **11**, 943 (1999).

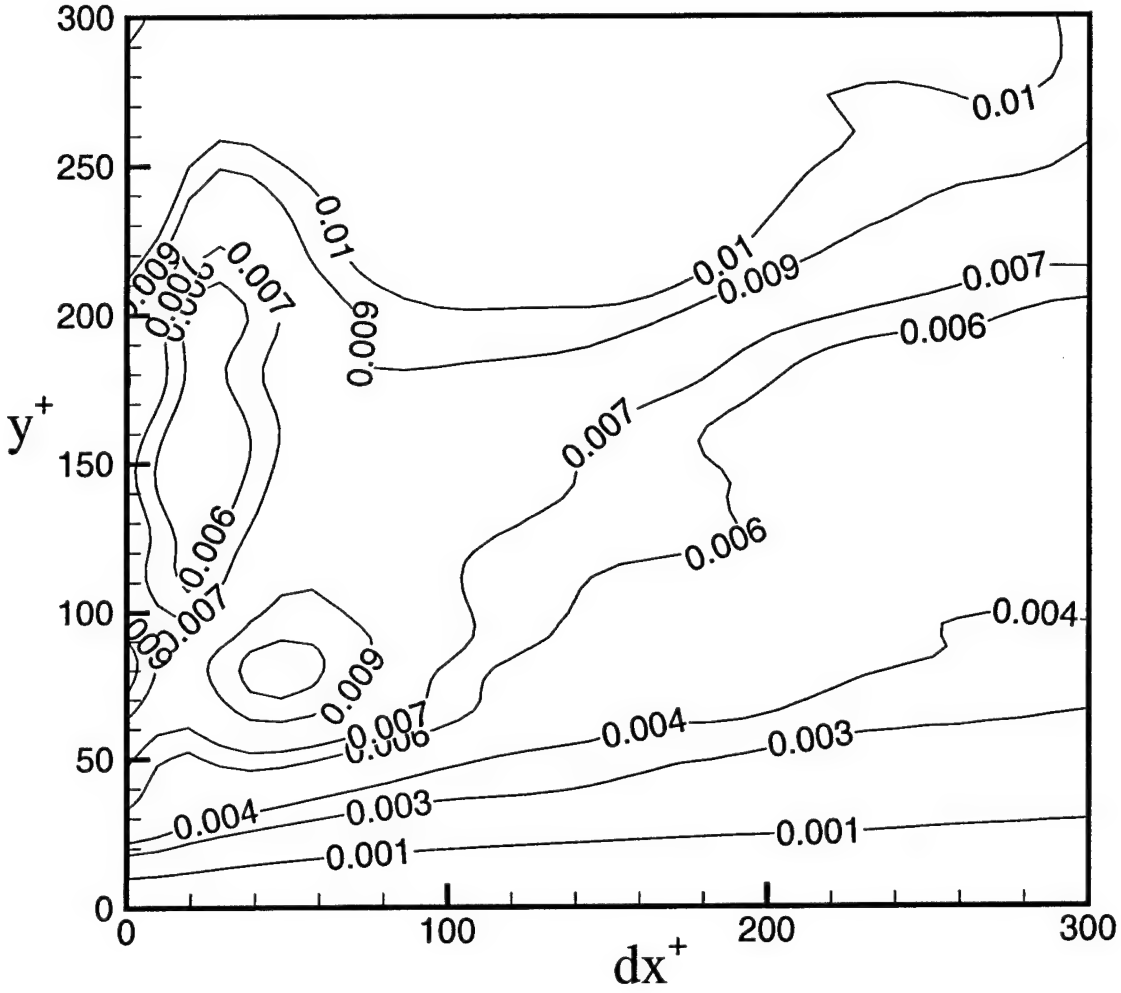

Figure 1a: Countours of normalized error, $\phi_{22,22}(r_1)$, as a function of the streamwise separations (along horizontal coordinate) and wall normal coordinate (vertical coordinate). The axes are scaled by wall units.

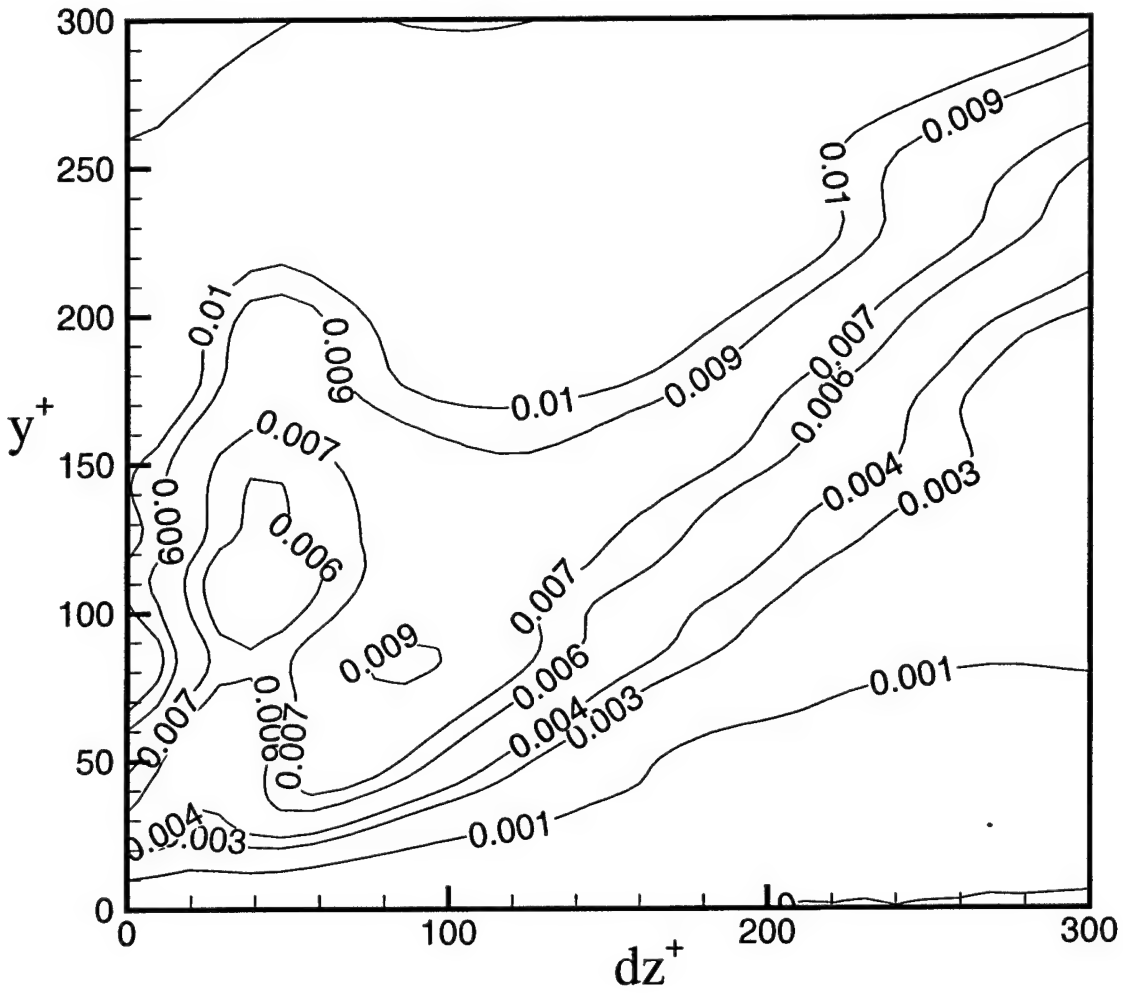

Figure 1b: Contours of $\phi_{22,22}(r_3)$. Same as Figure 1a, but for spanwise separations (along horizontal coordinate)

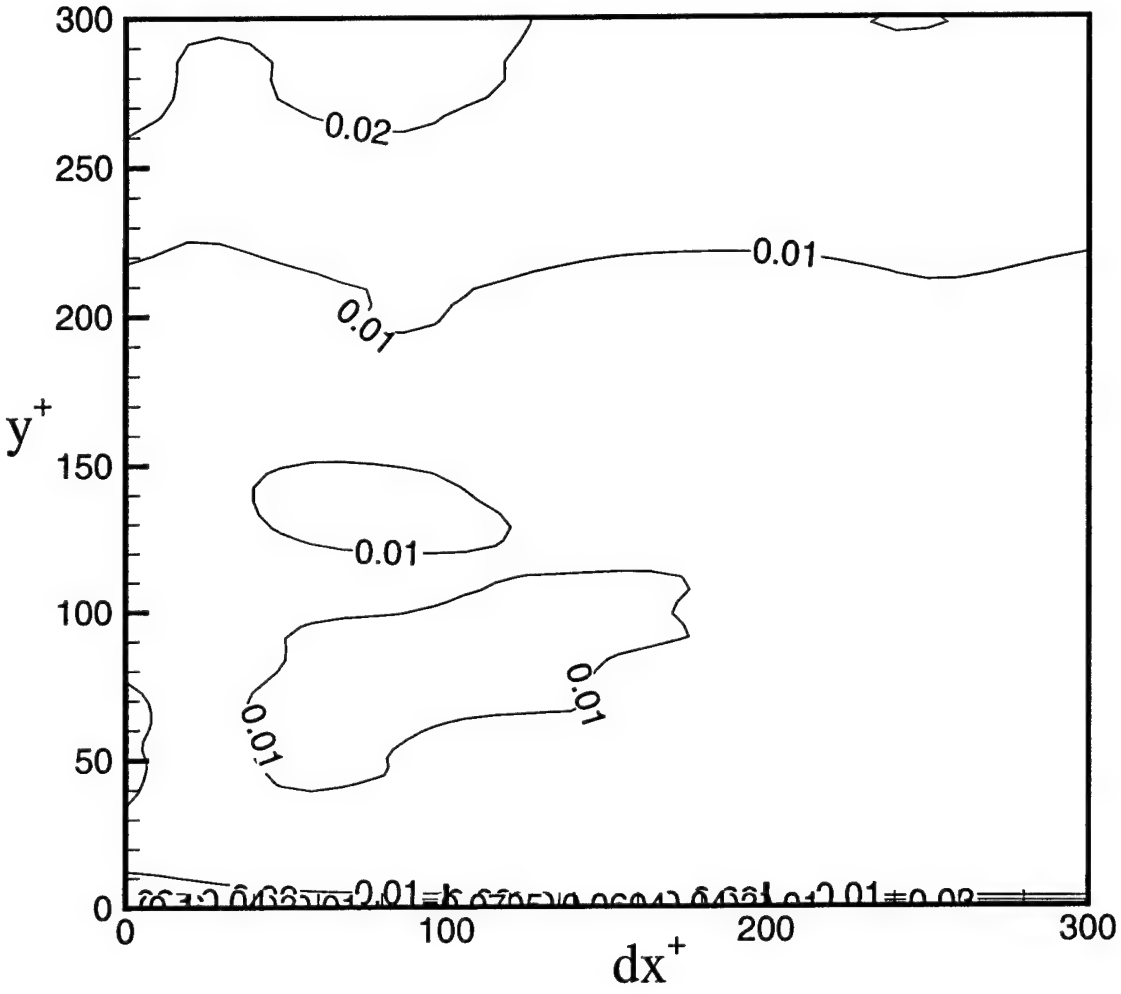

Figure 2: Same as figure 1a, but for the $\phi_{33,33}(r_1)$

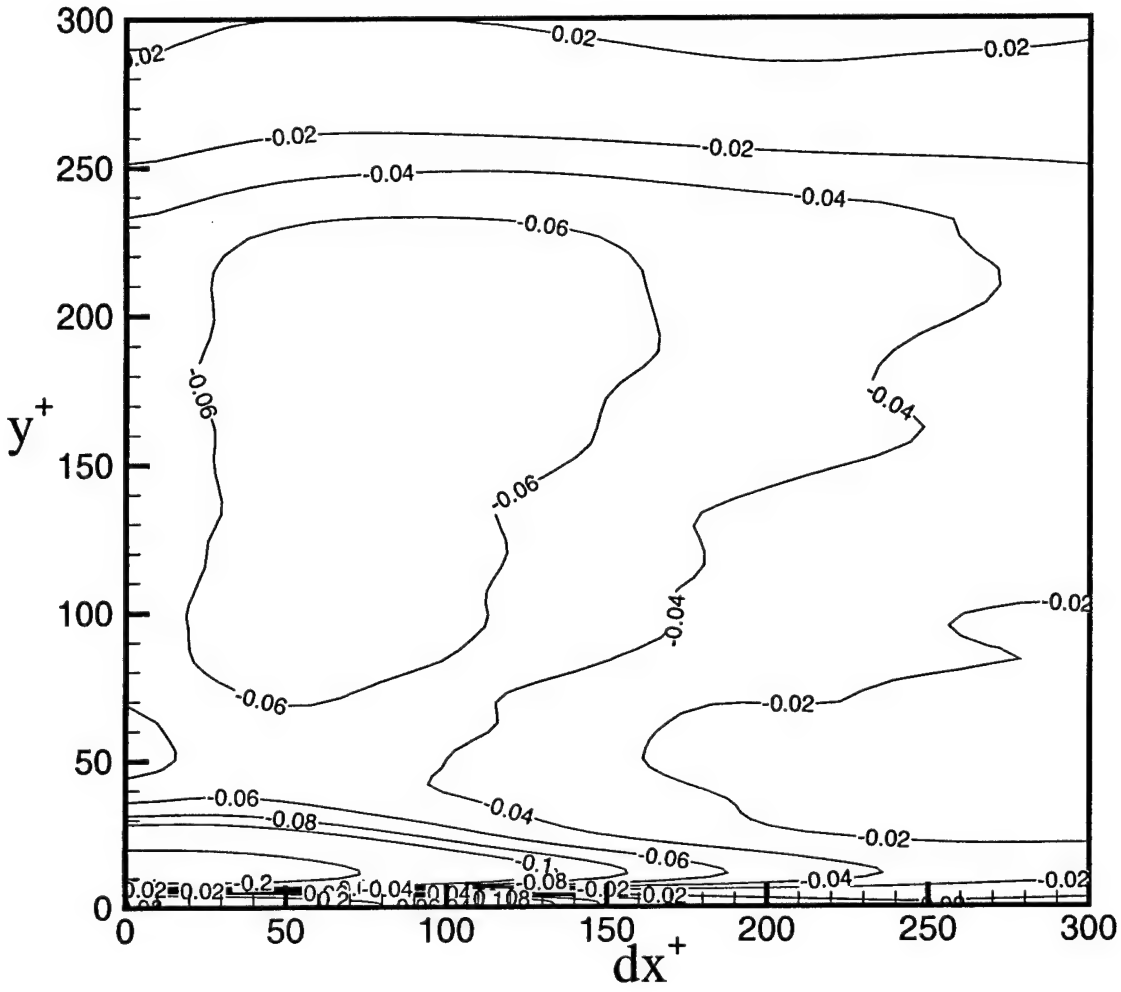

Figure 3a: Same as figure 1a, but for $\phi_{11,11}(r_1)$, with separation vectors aligned along the streamwise direction

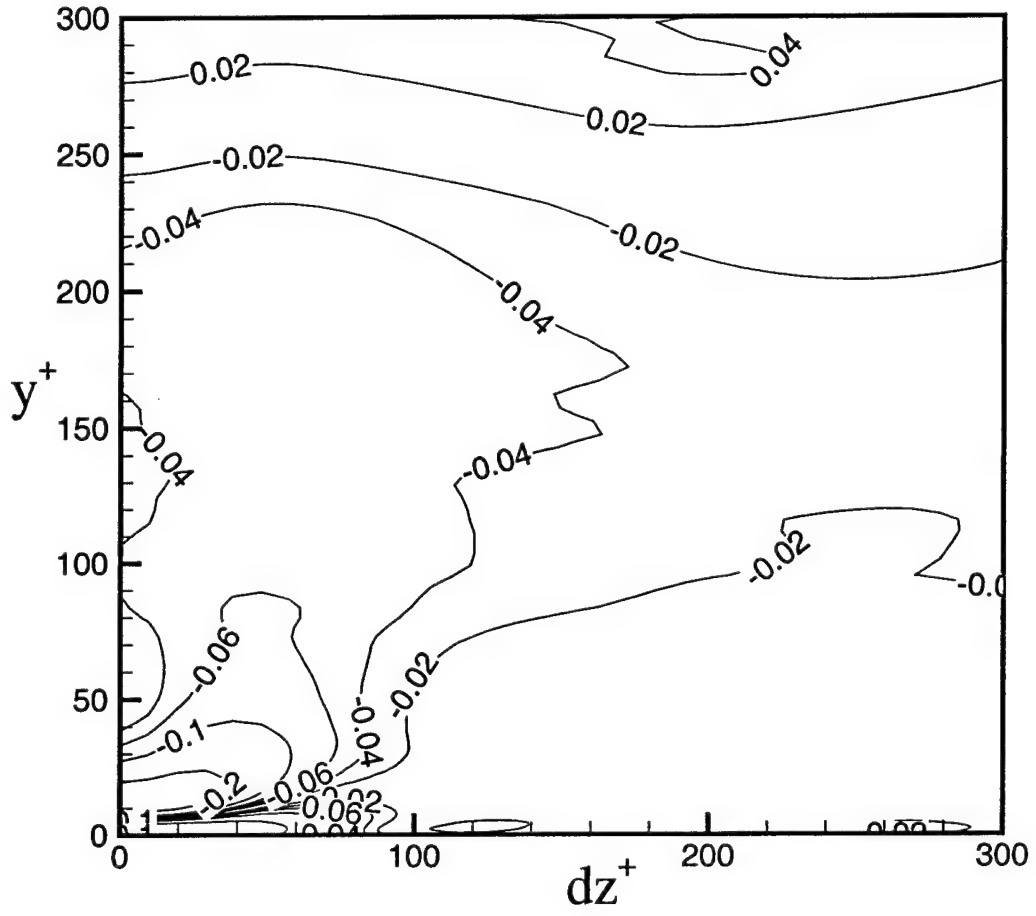

Figure 3b: Same as figure 1b, but for $\phi_{11,11}(r_3)$, with separation vectors aligned along the spanwise direction

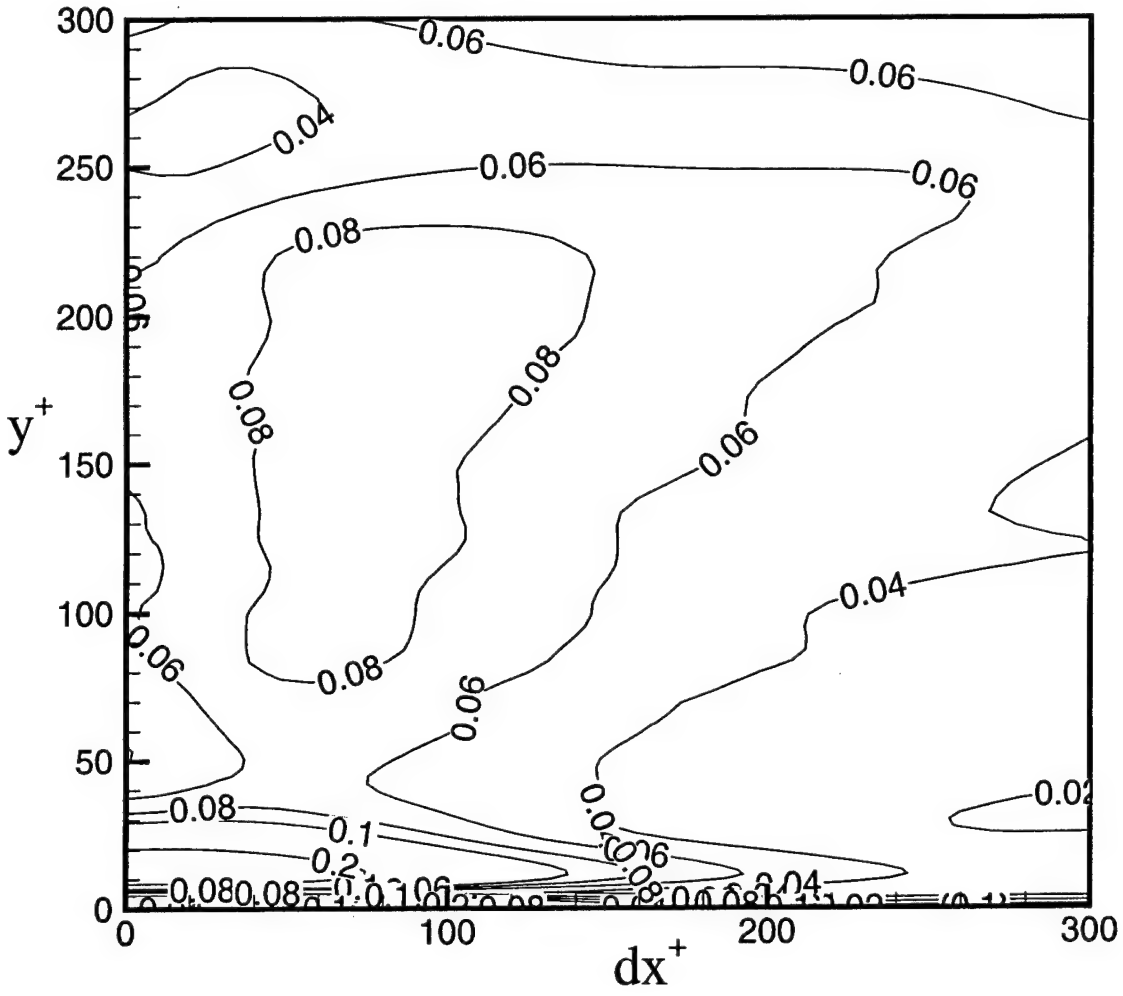

Figure 4a: Contours of the invariant, $\Psi(r_1)$, as a function of streamwise separations and distance from the wall, as in figure 1a

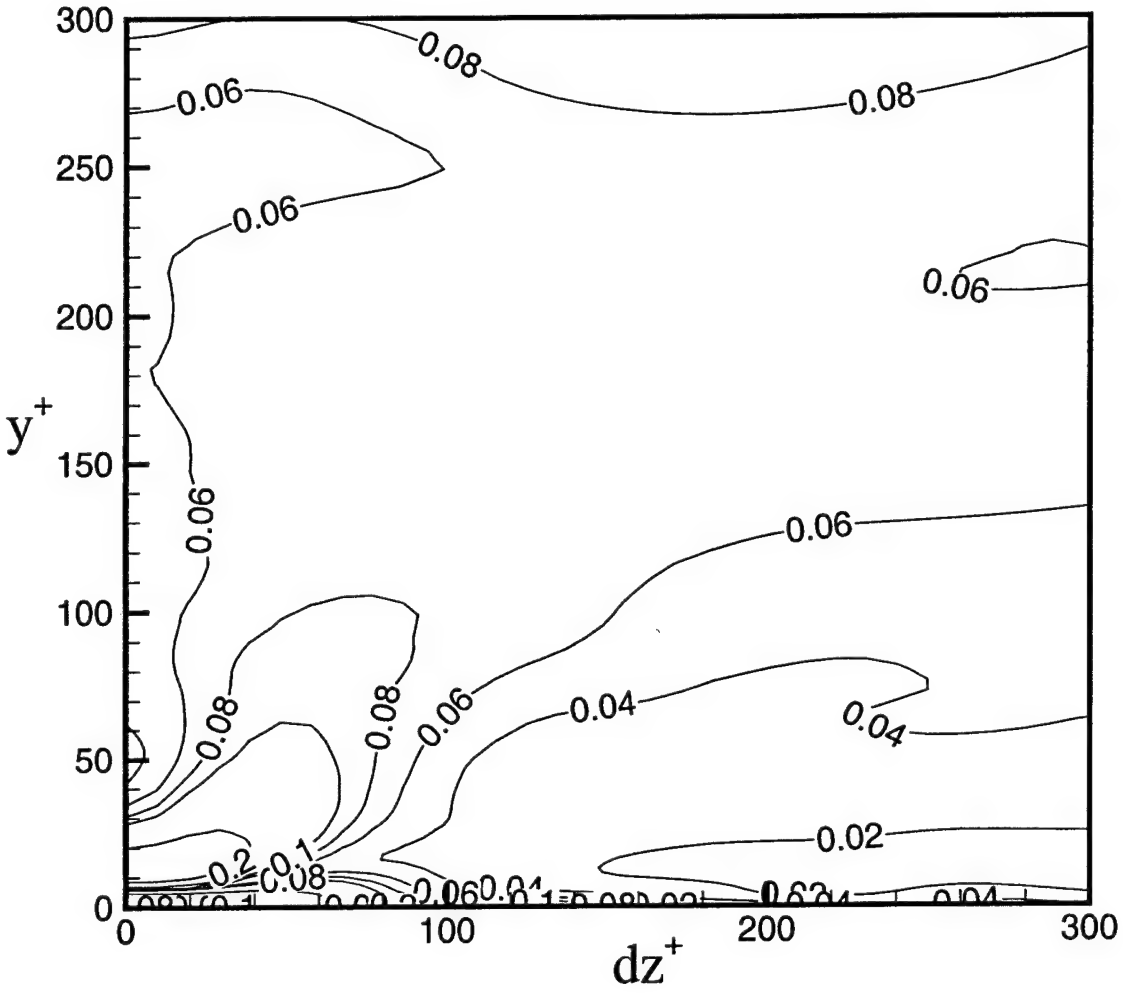

Figure 4b: Contours of the invariant, $\Psi(r_3)$, as function of spanwise separations and distance from the wall, as in figure 1b

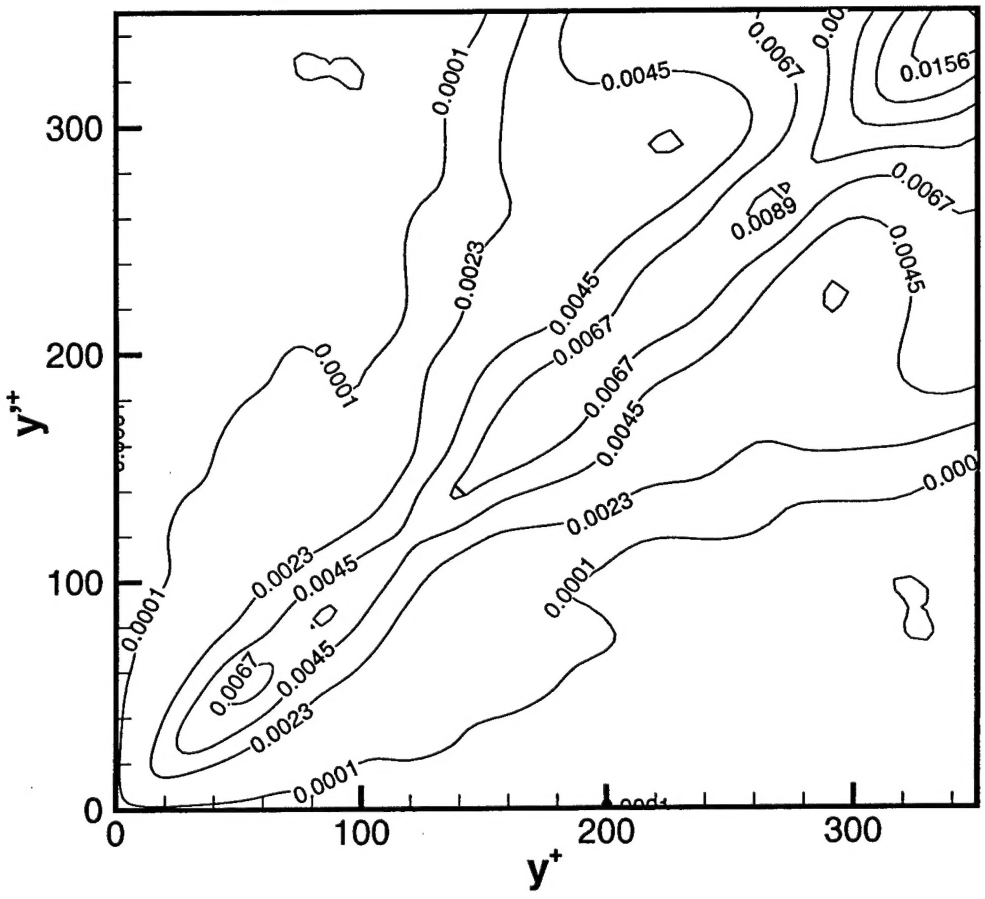

Figure 5a: Contours of $\phi^{\perp}_{22,22}(y, y')$ for separation vectors in the wall-normal direction

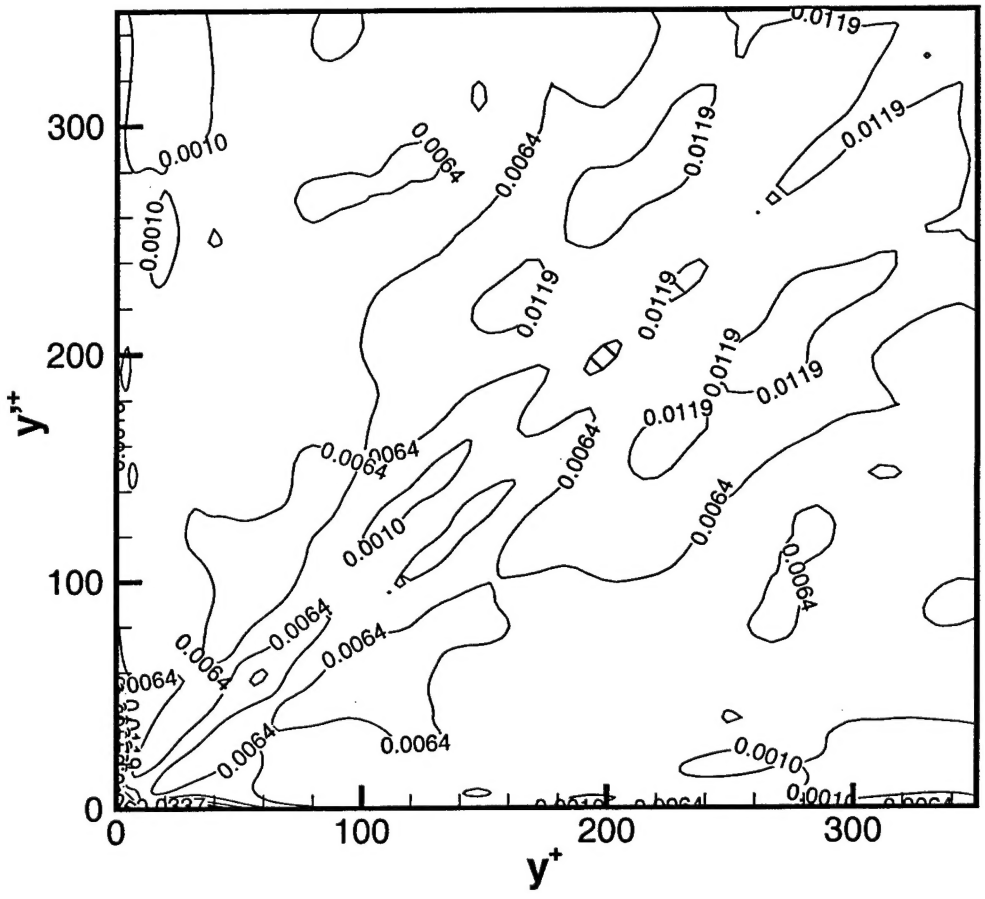

Figure 5b: Contours of $\phi^{\perp}_{33,33}(y, y')$ for separation vectors in the wall-normal direction

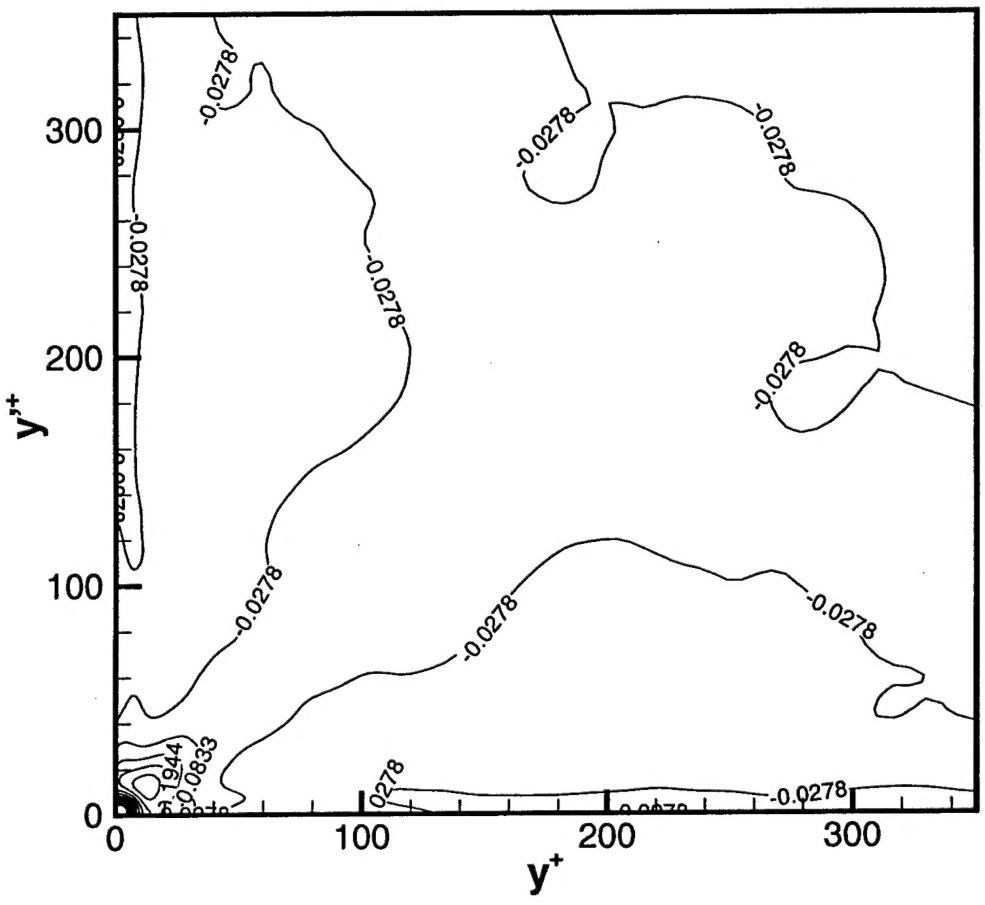

Figure 5c: Contours of $\phi^{\perp}_{11,11}(y, y')$ for separation vectors in the wall-normal direction

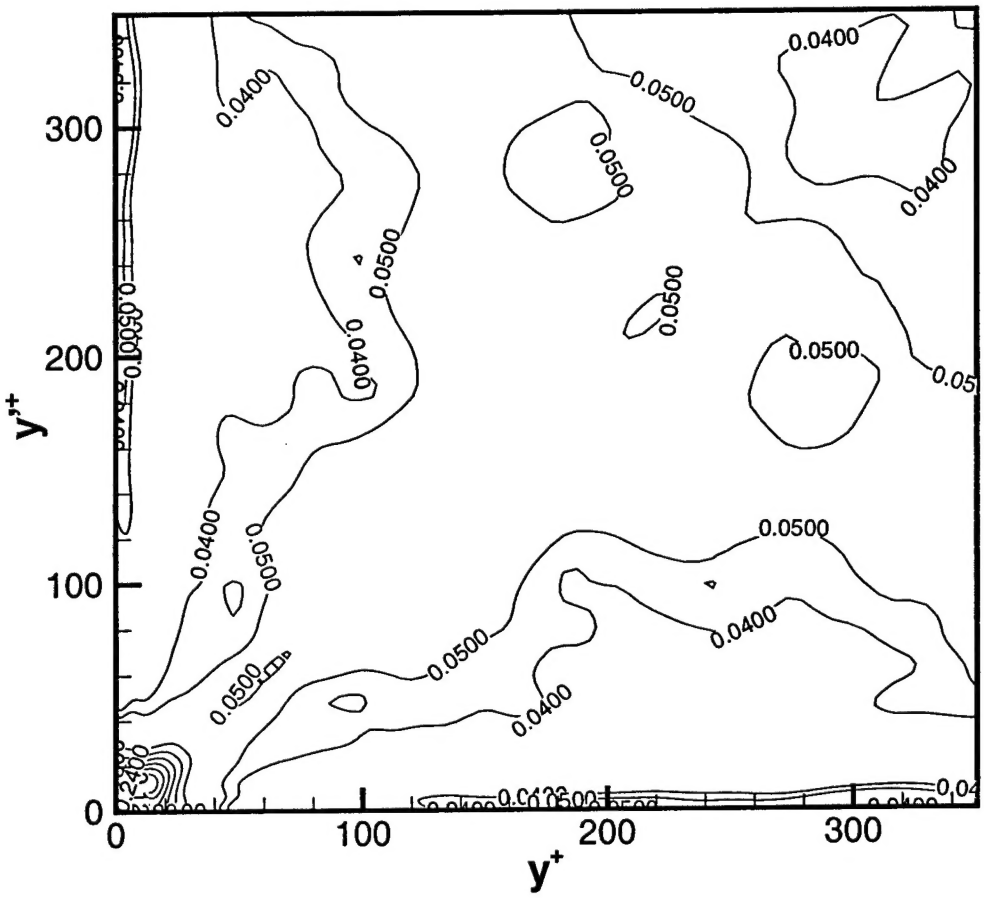

Figure 5d: Contours of the invariant, $\Psi^{\perp}(y, y')$ for separation vectors in the wall-normal direction